University of the Witwatersrand

Heat transfer in a porous radial fin

A thesis submitted in fulfillment of the requirements for the degree of

Doctor of Philosophy

in the School of Computer Science and Applied Mathematics (CSAM)

Faculty of Science.

Author:
Raeesah JOOMA

Supervisor:
Professor Charis HARLEY

Declaration of Authorship

I declare that this thesis titled, "Heat transfer in a porous radial fin" is original except where due references have been made. It has not been submitted before for any degree to any other institution.

R.Jooma

Dedication

I dedicate this thesis to my mother and father.

Acknowledgments

I would like to thank my supervisor, Prof. C.Harley, for all her guidance, support and patience. I would also like to offer my gratitude to the members of the School of Computer Science and Applied Mathematics, especially Prof. D.P. Mason, for all his help and advice.

Publications

Some portions of this thesis have been published in the following article. These portions include figures, tables, algorithms, equations and description of concepts.

1. Jooma, R and Harley, C, *Heat Transfer in a Porous Radial Fin: Analysis of Numerically Obtained Solutions*, 2017, *Adv Math Phys*.
   URL: http://hdl.handle.net/10539/23389.

Heat transfer in a porous radial fin

Raeesah Jooma

School of Computer Science and Applied Mathematics
University of the Witwatersrand
Private Bag 3, Johannesburg, Wits 2050, South Africa.

ABSTRACT

In this thesis, a time dependent nonlinear partial differential equation modelling heat transfer in a porous radial fin is derived. The equation considered is nonlinear in nature due to the presence of two nonlinear terms i.e. the bouyancy/natural convection parameter and the radiation parameter, making obtaining the solution of the equation via analytical methods challenging. As such, we consider semi-analytical and numerical methods for the solution of this problem. A semi-analytical method namely, the Differential Transformation method, is employed to study the behaviour of the heat transfer described by the partial differential equation. By using the Differential Transformation method the nonlinear equations are reduced to recurrence relations and the boundary conditions are transformed into a set of algebraic equations. The solution obtained from the Differential Transformation method is compared to the work of Darvishi et al. [1].

Computational methods such as the Crank-Nicolson scheme with and without the Newton-Raphson and Usmani method as well as the Numerical Well-balancing scheme are used to obtain new numerical solutions which are useful indicators for the exactness of the semi-analytical solution obtained. Lie Symmetry analysis is conducted to derive an appropriate initial condition by means of infinitesimal generators, since the equation under consideration is sensitive to the initial condition when employing the Numerical Well-balancing scheme. These results are then compared to the solution obtained as

per the work of Darvishi et al. [1] and the semi-analytical solution. New physical and mathematical insights are revealed through the numerical methods and steady state solutions found and the comparisons made between them and other already existing solutions.

The findings reveal that the results obtained via the Crank-Nicolson scheme and the Well-balancing scheme match those in the work by Darvishi et al. [1]; the Crank-Nicolson method, incorporating the Newton-Raphson and Usmani method, and the Differential Transformation method do not match these results even though the behaviour observed is appropriate and comparable. In order to engage with the dynamics of this scheme we conduct a dynamical systems analysis. In doing so, we obtain an assessment of the impact of the nonlinear sink terms on the stability of the numerical scheme employed and on the dynamics of the solutions.

Nomenclature

$C_{p,f}$	Specific heat of the ambient fluid
F_{f-a}	Shape factor of radiation heat transfer
Da	Darcy number
g	Acceleration due to gravity
k_{eff}	Effective thermal conductivity of porous fin
k_f	Thermal conductivity of ambient fluid
K_r	Thermal conductivity ratio
$\mathcal{N}_c$	Buoyancy or natural convection parameter
$\mathcal{N}_r$	Radiation parameter
q	Base heat flow
r	Radial coordinate
r_b	Base radius
r_t	Base tip
$\hat{r}$	Dimensionless radius
$\hat{r}^*$	Ratio of tip radius to base radius
s	Fin thickness
T	Local fin temperature
T_a	Ambient temperature
T_b	Base temperature
θ_a	Dimensionless ambient temperature
θ	Non-dimensional temperature
ϵ	Surface emissivity of fin
σ	Stefan-Boltzmann condition
ρ_f	Density of ambient fluid
ν_f	Kinematic viscosity of the ambient fluid
β_f	Volumetric thermal expansion coefficient of the ambient fluid

Table of Contents

List of Figures

List of Tables

Chapter 1

Introduction

A fin is a surface that extends from an object to increase the rate of heat transfer to or from the environment by increasing convection. Extensions on the finned surfaces are used to increase the surface area of the fin in contact with the fluid flowing around it which further increases the rate of heat transfer from the base surface as compared to a fin without the extensions provided [2]. Fins are used to enhance convection heat transfer in a wide range of engineering applications where it is necessary to enhance the heat transfer from a surface to an adjacent coolant so that the fin can perform within the acceptable temperature limits. These engineering applications range from considerably large systems such as industrial heat exchangers to smaller systems such as transistors. These days, fin applications are used in the cooling of computer processors, air conditioning units, refrigerators, air-cooled engines, and oil carrying pipelines [2].

The geometry of the fin has an important role to play with regards to the efficiency of the fin as a heat transfer mechanism. This makes the fin geometry a parameter of importance when we choose to optimize the fin's efficiency. Over the past decades, numerous studies have been conducted on the use of annular fins [3, 4, 5, 6, 7]. Circular annular fins are extensively used to increase the rate of heat transfer from a heat source for a given temperature difference in heat exchange devices or to reduce the temperature difference between the heat source and the given heat flow rate of heat sink [8]. Radial fins have been conventionally used as a coolant for internal combustion engines, heat exchanges, compressors and so forth. Due to these extensive practical applications this is considered a vibrant field of research; this is true even more so since the models that describe these problems are nonlinear and hence not always solvable via analytical techniques.

Many research articles have investigated the use of porous fins. Even though a porous material fin has low thermal conductivity, a vast area of the material comes into contact with the cooling agent enabling the porous fin to have superior performance [1]. A study was conducted by Kiwan and Zeitou [9] to test the performance of rectangular porous fins mounted around the inner cylinder of a cylindrical annulus. It was concluded that in comparison to solid fins, porous fins provided higher transfer rates for similar configurations and that the heat transfer rate from the cylinder equipped with porous fins decreased as the fin inclination increased. Furthermore, Kiwan [10] conducted a thermal analysis of natural convection porous fins by introducing Darcy's model to construct the energy equation governing the distribution of temperature. He further discovered that by choosing a precise value for the thermal conductivity ratio and the fin length to thickness ratio, the performance of the porous fin exceeded the performance of the solid fin. Abu-Hijleh [11] analysed the effects of using permeable fins on the forced convection heat transfer from a horizontal cylinder. The results obtained where similar to results obtained as per Kiwan et al. [9] in terms of the permeable fins providing much higher heat transfer rates. In a similar context, our model takes into account the time rate of change of internal energy, the heat flow due to conduction, as well as the heat due to radiation and convection. For this research, we will model the heat transfer in a porous radial fin.

In order to study the behaviour and performance of heat transfer in the fin as described by a nonlinear partial differential equation, we investigate the use of semi-analytical methods to obtain solutions. Semi-analytical solutions have proved to be successful for authors such as Darvishi et al. [1, 12] where a solution was constructed to describe the thermal performance and the effects of radiation and convective heat transfer in a rectangular porous radial fin. This allowed for natural convection in the fluid saturating the fin and radiation heat loss from the top and bottom surfaces of the fin enabling a solid-fluid interaction to occur. They concluded that in a model containing radiation, more heat is present than in a similar model without radiation. Similarly, this method of solutions also proved to be effective for Aziz and Rahman [13] when examining a fin comprising of functionally graded material and analysing the performance of the radial fin with a continuously increasing thermal conductivity in the radial direction. They discovered that the heat transfer as well as the fin efficiency and effectiveness are at their highest when the thermal conductivity of the fin varies inversely with the square of the radius. To study radial fins, a combination of the Taylor transformation and finite-difference approximations was implemented by Yu and Chen [14, 15]. They further performed a study on the optimization of a circular fin with variable thermal parameters. In the research conducted here, the Differential Transformation Method (DTM) and a Lie Symmetry Analysis are employed to help us overcome certain numerical difficulties and observe the behaviour of the solution.

The Differential Transformation Method (DTM), which was first proposed by Zhou [16], is a numerical semi-analytical method applied to linear and nonlinear systems of ordinary differential equations. This method rapidly provides exact values of the nth derivative of an analytical function at a point in terms of the boundary conditions. This method constructs a semi-analytical solution in the form of a polynomial for differential equations which is different from the high order Taylor series method, which requires symbolic computation of the necessary derivatives of the data functions [17]. The DTM is an iterative procedure used for obtaining Taylor series solutions of differential equations [17]. This method has been successfully implemented in many engineering applications

[18, 19, 20, 21, 22, 23, 24]. Recently, Mohsen et al. [25] analysed the radiative radial fin with temperature-dependent thermal conductivity by implementing the DTM as well as the Boubaker polynomials expansion scheme (BPES). Ndlovu et al. [26] derived approximate analytical solutions for the temperature distribution in a longitudinal rectangular and convex parabolic fin with temperature dependent thermal conductivity and heat transfer coefficients. These authors, for the first time, used a two-dimensional DTM for the transient heat conduction problem. A study of a radial fin in terms of the fin's thickness with convection heating at the base and the convection-radiative cooling at the tip was conducted by Aziz et al. [27]. They conducted an analysis using DTM and verified the results by comparing it to an exact analytical solution. Extensive analytical studies have been done for the solution of problems similar to the one under discussion. However, such studies are at times limited when the problem structure increases in complexity.

In order to introduce the Lie point symmetries method, we will first proceed with the attainment of conditions via Lie point symmetries. Symmetries play an important role in the derivation of exact solutions of both ordinary differential equations (ODEs) and partial differential equations (PDEs) in mathematical physics. The symmetries admitted by a differential equation transforms dependent and independent variables which maps the equation or system of equations onto itself. The Taylor series expansions of the local transformations represented by functions with respect to a parameter in the neighbourhood of $\epsilon = 0$ provides us with infinitesimal transformations. Several advances in the field of symmetry methods (group analysis) of differential equations [28, 29, 30, 31, 32] have been explored since the Lie symmetry is a well-known subject. Lie point symmetry techniques were used to analyze nonlinear heat transfer models in extended fins by Kamogelo [33]. He initially used the method to determine the exact solutions for heat transfer in fins of spherical geometry. They found that the radiation transfers more heat in comparison to a similar model without radiation. In conjuncture with symmetry analysis Ndlovu et al. [34], the same authors of [26], determined the Lie point symmetries associated with the conservation laws for the transient heat conduction problem. Moitsheki and Harley [35] employed symmetry techniques to determine forms of the source, or sink term, for the steady heat transfer through a pin fin. In a similar context the same authors [36] studied the transient heat transfer through a longitudinal fin of various profiles by employing classical Lie point symmetry methods. They observed that for long periods of time the temperature profile becomes unusual for the heat transfer in longitudinal triangular and concave parabolic fins. This was corrected by increasing the value of the thermo-geometric fin parameter. As such, we find that the Differential Transformation Method as well as the Lie point symmetry analysis have been applied to many different problems relating to heat transfer. Since we noticed that the problem under consideration is quite sensitive to the initial condition provided, we attempt to determine initial conditions admitted by the equation under consideration using infinitesimal generators that leave the form invariant.

In cases where semi-analytical methods fail, we rely on numerical techniques to solve specifically complex nonlinear differential equations. The Crank-Nicolson method was developed in the mid 20th century by Crank et al. [37] in order to evaluate numerical solutions for such nonlinear partial differential equations. The Crank-Nicolson method is a finite difference method which can be written as an implicit Runge-Kutta method is implicit time and can lead to unconditionally stable finite different schemes [37]. Gorla and Bakier [38] investigated natural convection and radiation in porous fins by solving a second order non-linear ordinary differential equation using the Runge-Kutta fourth order method. The concept of the Crank-Nicolson scheme combined with the Newton-Raphson method was implemented by Janssen et al. [39]. The Crank-Nicolson scheme was used to transform a system of differential equations into two sets of simultaneous linear equations, which were then solved by applying Gauss's elimination method whereas the Newton-Raphson method was used to implicitly enhance the model's efficiency by improving the poor convergence rate. In a similar context, Qin et al. [40] used this scheme combination to model the heat flux and to estimate the evaporation in applied hydrology and meteorology. The Crank-Nicolson method was used to expand the differential equations whereas the iterative Newton-Raphson method was used to approximate latent heat flux and surface temperatures. In this thesis, we will be employing both these methods in a similar fashion.

Another numerical approach used in this research is the Well-Balancing numerical scheme. It effectively deals with the proper form of the porous radial fin and solves the problem of heat transfer in such a fin. This scheme has been shown to effectively and efficiently obtain results for a rectangular fin profile as per the literature [36, 41, 42]. In the work of Rusgara et al. [43], the Well-Balancing scheme was used to solve a nonlinear partial differential equation modeling the temperature distribution in a triangular fin without requiring any additional assumptions or simplifications of the fin profile. In order to develop this approach, we use a finite volume method to illustrate how it reduces the order of differentiation by one. Thereafter, by using volume averaging and the Taylor series expansion, we establish a numerical balance law. Based on the balance law and information obtained through a consideration of the steady-state equation which in turn is incorporated into the transient heat transfer equation, we obtain a Well-Balancing scheme that maintains steady-state solutions. To the best of the authors knowledge, the Well-Balancing scheme has not previously been used in the literature to solve the problem of heat transfer in a porous radial fin as structured in this thesis.

We mentioned the equation under considered has certain numerical difficulties and is quite sensitive to the initial condition provided. Furthermore, we note that some semi-analytical methods fail due to these difficulties and we have to rely on numerical techniques to solve this complex nonlinear differential equation. As such, we investigate the stability of the partial differential equation using a dynamical system analysis. As far as we know, there has been no or very little work done regarding a dynamical system analysis for the problem presented in this research. For that reason, we will conduct a dynamical system analysis, in an attempt to describe and analyse the limiting behaviour of the scheme and certain physical insights. A dynamical system is a system that evolves over time and space, but their evolution is not random. The system's structure as well as past conditions determines its current state. Hence, the variables used to determine the evolution of the dynamical system are time-indexed [44]. Moitsheki and Harley [36, 45] conducted a small scale dynamical analysis. In order to expand the analysis in [45], Harley [46] employed an in-depth dynamical analysis to specifically monitor the behaviour at the fin tip. This dynamical analysis also served as a means of investigating the role and effect of the thermo-geometric parameter. In this thesis, we will employ a similar methodology, which will prove to be of immense use in classifying the dynamics of specific points of the solution and the engagement between parameters.

A substantial amount of work has been conducted on the steady state case of problems in this field as analytical methods are more suitable for solving these equations. In this research, a time dependent partial differential equation modeling the heat transfer in a porous radial fin will be considered. This thesis is outlined as follows. Chapter 2 provides an overview of the physics and construction of the time dependent partial differential equation. The equation will be derived and nondimensionalised appropriately. In Chapter 3 we employ the semi-analytical approaches namely, the Differential Transformation method as well as the Lie symmetries analysis. These approaches which will be used to study the behaviour of the model and assist in structuring an initial condition respectively. The solutions to these analytical approaches will serve as a means of comparison to the numerical solutions employed. In order to assess the effectiveness of this scheme and its limitations we employ a dynamical systems analysis in Chapter 4; in this manner we are able to engage with the limitations placed on parameter values with regards to obtaining solutions. Chapter 4 further provides insight into the comparative dynamics and stability of the equation obtained via an alternate means of nondimensionalisation. In Chapter 5, the partial differential equation is solved numerically using the Crank-Nicolson scheme combined with the Newton-Raphson method as a predictor corrector to explicitly cater for the model's efficiency when dealing with the nonlinear source terms. Chapter 6 is dedicated to the implementation of the numerical Well-Balancing scheme which is designed to ensure the steadiness of the numerical solution. In the final chapter, Chapter 7, conclusions are drawn from the work done in this thesis.

The importance of this work relates to the detailed analysis of the dynamics of the temperature at the fin tip. Furthermore, we are able to investigate the impact of the nonlinear source terms on the stability of the schemes employed and the solutions that can be obtained. This highlights the care that needs to be taken when choosing to solve equations of this nature, particularly when solving via numerical tools. Parameters of physical importance are shown to have value limitations due to stability requirements of the relevant schemes. Consequently, while numerical solutions may have been obtained here and by other authors it needs to be noted that these do not indicate an ability to obtain solutions for all relevant parameter values, or that it may be assumed that solutions that seemed to have converged are indeed dynamically stable and physically accurate.

Chapter 2

Model Derivation

The work in this Chapter has been published in Advances in Mathematical Physics [47].

In this chapter we derive the partial differential equation pertaining to the physical system of a porous radial fin. The geometry and properties of the porous radial fin are reviewed and a brief theory of constructing the energy balance equation by applying Fourier's law of heat conduction and Darcy's law is presented. This mathematical analysis has been closely followed as per the work done by Darvishi et al. [1] and Aziz et al. [27].

Consider a cylindrical porous radial fin with base radius r_b, tip radius r_t and thickness s as shown in Figure 2.1. The fin is comprised of an effective thermal conductivity porous material k_{eff} and permeability K. It is assumed that the tip of the fin is adiabatic (i.e. a process that occurs without the transfer of heat/matter between the system and its surroundings) and the base of the fin is maintained at a constant temperature T_b. The internal energy per unit volume with the absolute temperature T is denoted by $\rho C_v T$. In accordance with Darcy's law, the fin makes contact with an ambient fluid which infiltrates the fin. The ambient fluid comprises of an effective density of the porous fin ρ_f, a specific heat of the porous fin $C_{p,f}$, the kinematic viscosity of the ambient fluid ν_f, the thermal conductivity of the ambient fluid k_f, and the volumetric thermal expansion coefficient of the ambient fluid β_f. The top and bottom surfaces are presumed to have a constant surface emissivity and emit radiation to the ambient fluid at temperature T_b.

This also serves as the radiation heat sink.

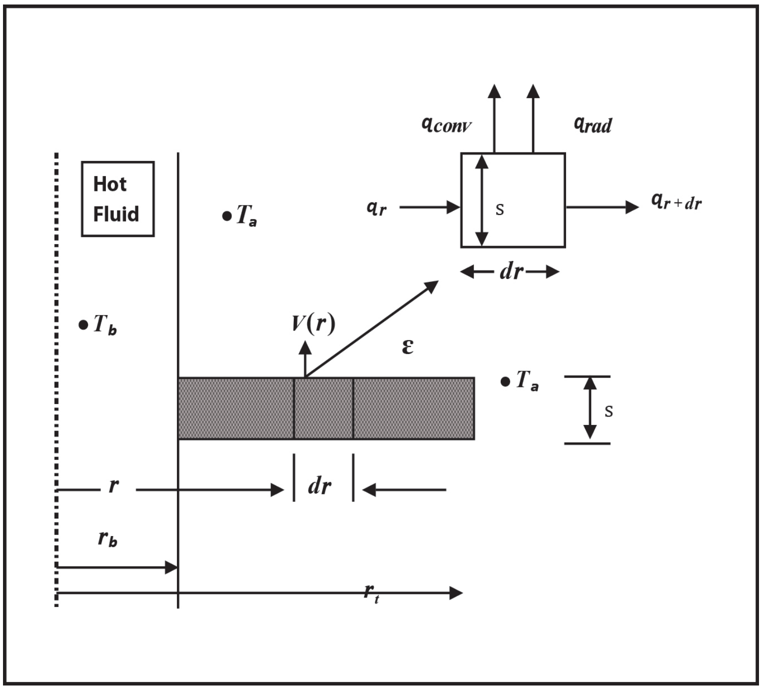

Fig. 2.1: *Porous radial fin geometry incorporating the energy balance of a cylindrical cross section.*

The heat flow into the volume element of thickness s, circumference $2\pi r$, radial width dr at position r is constructed as follows,

$$
\begin{aligned}
&= 2\pi r s q_r - 2q_{r+d_r}\pi(r+dr)s \\
&= -k_{eff}2\pi r s\frac{dT}{dr}(r) + k_{eff}\frac{dT}{dr}(r+dr)2\pi(r+dr)s \\
&= -k_{eff}2\pi r s\frac{dT}{dr}(r) + k_{eff}(2\pi r s + 2\pi dr s)\left[\frac{dT}{dr}(r) + \frac{d^2T}{dr^2}(r)dr\right] \\
&= -k_{eff}2\pi r s\frac{dT}{dr}(r) + k_{eff}\left[2\pi r s\frac{dT}{dr}(r) + 2\pi dr s\frac{dT}{dr} + 2\pi r s\frac{d^2T}{dr^2}(r)dr\right] \\
&= k_{eff}2\pi s\frac{d}{dr}\left(r\frac{dT}{dr}\right)
\end{aligned}
\tag{2.1}
$$

where $q_r = -k_{eff}\frac{dT}{dr}$ is the heat flow per unit area in the r direction.

Constructing the energy balance of a fin element (Figure 2.1), we obtain,

$$q_r - q_{r+dr} - q_{conv} - q_{rad} = I,$$

$$\rightarrow \frac{d}{dr}\big(2\pi rkt\frac{dT}{dr}\big)dr - \rho_f v(r)(2\pi r dr)c_{p,f}(T-T_a) - 2\epsilon\sigma F_{f-a}(2\pi r dr)(T^4 - T_a^4) = \rho C_v 2\pi r s\, dr\frac{dT}{dt}, \tag{2.2}$$

where

$$I = \rho C_v 2\pi r s\, dr\frac{dT}{dt}, \tag{2.3}$$

$$q_r - q_{r+dr} = \frac{d}{dr}\big(2\pi rkt\frac{dT}{dr}\big)dr, \tag{2.4}$$

$$q_{rad} = 2\epsilon\sigma F_{f-a}(2\pi r dr)(T^4 - T_a^4), \tag{2.5}$$

$$q_{conv} = \rho_f v(r)(2\pi r dr)c_{p,f}(T - T_a), \tag{2.6}$$

where Equation (2.3) is the time rate of change of internal energy in the volume element, Equation (2.4) is a basis of the application of Fourier's law of heat conduction, Equation (2.5) denotes the heat loss due to radiation through the top and bottom surfaces of the fin and Equation (2.6) denotes the heat loss due to convection due to Darcy's flow through a porous fin. At any radiation location r, the velocity of the buoyancy driven flow $v(r)$ is obtained by the implementation of Darcy's as follows,

$$v(r) = \frac{g\beta_f(T - T_a)}{v_f}. \tag{2.7}$$

By substituting Equations (2.3) - (2.6) into Equation (2.2),

$$\frac{\partial}{\partial t}\Big[\rho C_v 2\pi r s dr\Big] = k_{eff}2\pi s\frac{\partial}{\partial r}\Big(r\frac{\partial T}{\partial r}\Big) - 2\epsilon\sigma F_{f-a}(2\pi r dr)(T^4 - T_a^4) - \rho_f v(r)(2\pi r dr)c_{p,f}(T - T_a)$$

which implies that,

$$\begin{aligned}\rho C_v 2\pi r s dr \frac{\partial T}{\partial t} = k_{eff} 2\pi s \frac{\partial}{\partial r}\left(r\frac{\partial T}{\partial r}\right) - 2\epsilon\sigma F_{f-a}(2\pi r dr)(T^4 - T_a^4) \\ - \rho_f v(r)(2\pi r dr) c_{p,f}(T - T_a).\end{aligned} \tag{2.8}$$

After multiplying by $\frac{1}{2\pi r s k_{eff} dr}$ and substituting Equation (2.7), the following nonlinear partial differential equation governing the temperature distribution in the fin is obtained,

$$\frac{\rho C_v}{k_{eff}}\frac{\partial T}{\partial t} = \frac{1}{r}\frac{\partial}{\partial r}\left(r\frac{\partial T}{\partial r}\right) - \frac{2\epsilon\sigma F_{f-a}}{k_{eff} s}\left(T^4 - T_a^4\right) - \frac{\rho_f C_{p,f} K g \beta_f}{k_{eff} s V_f}\left(T - T_a\right)^2,$$

$$r_b \leq r \leq r_t, \qquad t \geq 0. \tag{2.9}$$

The boundary conditions are given by,

$$\left.\frac{\partial T}{\partial r}\right|_{r_b} = 0, \qquad T(r_t, t) = T_b. \tag{2.10}$$

The fin is initially kept at the temperature of the fluid (ambient temperature) which is given by,

$$T(r, 0) = T_a. \tag{2.11}$$

We introduce the following dimensionless quantities,

$$\theta = \frac{T - T_a}{T_b - T_a}, \quad \theta_a = \frac{T_a}{T_b - T_a}, \quad \hat{r} = \frac{r - r_t}{r_b - r_t}, \quad \hat{r}^* = \frac{r_b}{r_t}, \quad \tau = \frac{k_{eff} t}{\rho C_v r_t^2},$$

$$\mathcal{N}_c = \frac{\rho_f C_{p,f} K g \beta_f r_t^2 (T_b - T_a)}{V_f k_{eff} s}, \quad \mathcal{N}_r = \frac{2\epsilon\sigma F_{f-a} r_t^2 (T_b - T_a)^3}{k_{eff} s}. \tag{2.12}$$

Firstly, we non-dimensionalise the right hand side of Equation (2.9),

$$\frac{\rho C_v}{k_{eff}}\frac{\partial T}{\partial t} = \frac{\rho C_v}{k_{eff}}\frac{\partial(\theta(T_b - T_a))}{\partial\left(\frac{\tau \rho C_v r_t^2}{k_{eff}}\right)} = \frac{T_b - T_a}{r_t^2}\frac{\partial \theta}{\partial \tau}.$$

We now consider the conserved term on the right hand side,

$$
\begin{aligned}
\frac{1}{r}\frac{\partial}{\partial r}\left(r\frac{\partial T}{\partial r}\right) &= \frac{1}{\hat{r}(r_b-r_t)+r_t}\,\frac{\partial}{\partial(\hat{r}(r_b-r_t)+r_t)}\left((\hat{r}(r_b-r_t)+r_t)\,\frac{\partial(\theta(T_b-T_a)}{\partial(\hat{r}(r_b-r_t)+r_t)}\right),\\
&= \frac{1}{(\hat{r}(r_b-r_t)+r_t)(r_b-r_t)}\,\frac{\partial}{\partial\hat{r}}\left((\hat{r}(r_b-r_t)+r_t)\,\frac{\partial(\theta(T_b-T_a))}{\partial(\hat{r}(r_b-r_t)+r_t)}\right),\\
&= \frac{1}{(\hat{r}(r_b-r_t)+r_t)(r_b-r_t)}\,\frac{\partial}{\partial\hat{r}}\left((\hat{r}(r_b-r_t)+r_t)\,\frac{(T_b-T_a)}{(r_b-r_t)}\frac{\partial\theta}{\partial\hat{r}}\right),\\
&= \frac{(T_b-T_a)}{r_t^2}\left[\frac{1}{\hat{r}(\hat{r}^*-1)+1}\,\frac{\partial}{\partial\hat{r}(\hat{r}^*-1)}\left(\hat{r}(\hat{r}^*-1)+1\,\frac{\partial\theta}{\partial\hat{r}(\hat{r}^*-1)}\right)\right],\\
&= \frac{(T_b-T_a)}{r_t^2}\left[\frac{1}{(\hat{r}(\hat{r}^*-1)+1)(\hat{r}^*-1)}\,\frac{\partial}{\partial\hat{r}}\left(\frac{\hat{r}(\hat{r}^*-1)+1}{(\hat{r}^*-1)}\,\frac{\partial\theta}{\partial\hat{r}}\right)\right].
\end{aligned}
$$

Next, we consider the two nonlinear terms on the right hand side. Firstly,

$$
\begin{aligned}
\frac{\rho_f C_{p,f} K g\beta_f\,(T-T_a)^2}{k_{eff}sV_f} &= \frac{\rho_f C_{p,f} K g\beta_f\,(\theta(T_b-T_a)+\theta_a-(\theta_a(T_b-T_a)))^2}{k_{eff}sV_f},\\
&= \frac{\rho_f C_{p,f} K g\beta_f\,(T_b-T_a)^2(\theta+\theta_a-\theta_a)^2}{k_{eff}sV_f},\\
&= \frac{\rho_f C_{p,f} K g\beta_f\,(T_b-T_a)^2\theta^2}{k_{eff}sV_f}.
\end{aligned}
$$

Secondly,

$$
\begin{aligned}
\frac{2\epsilon\sigma F_{f-a}\,(T^4-T_a^4)}{k_{eff}s} &= \frac{2\epsilon\sigma F_{f-a}\,(\theta(T_b-T_a)+T_a)^4-(\theta_a(T_b-T_a))^4}{k_{eff}s},\\
&= \frac{2\epsilon\sigma F_{f-a}\,(T_b-T_a)^4((\theta+\theta_a)^4-\theta_a^4)}{k_{eff}s}.
\end{aligned}
$$

After multiplying through by $\frac{r_t^2}{T_b-T_a}$, we find that our original Equation (2.9) becomes,

$$
\frac{\partial\theta}{\partial\tau} = \frac{1}{[\hat{r}(\hat{r}^*-1)+1)](\hat{r}^*-1)}\,\frac{\partial}{\partial\hat{r}}\left(\frac{\hat{r}(\hat{r}^*-1)+1}{\hat{r}^*-1}\,\frac{\partial\theta}{\partial\hat{r}}\right)-\mathcal{N}_c\theta^2-\mathcal{N}_r((\theta+\theta_a)^4-\theta_a^4), \quad (2.13)
$$

where $\hat{r}^*$ is defined as $\frac{r_t}{r_b}$ and the parameters $\mathcal{N}_c$ and $\mathcal{N}_r$ are stated as per Equation (2.12).

Employing the non-dimensional transformations given by Equation (2.12) we find that at $\hat{r} = r_b$ we obtain $\hat{r} = 0$ and at r_t we obtain $\hat{r} = 1$. Thus, we now work on the interval $0 \leq \hat{r} \leq 1$ with $\tau \geq 0$.

As such the non-dimensional boundary conditions are given by,

$$\left.\frac{\partial \theta}{\partial \hat{r}}\right|_{\hat{r}_0} = 0, , \qquad \theta(1, \tau) = 1 \tag{2.14}$$

and

$$\theta(\hat{r}, 0) = 0. \tag{2.15}$$

Equation (2.13) is a nonlinear partial differential equation comprising of two nonlinear terms. The first nonlinear term $\mathcal{N}_c$, the coefficient of θ^2, refers to the buoyancy or natural convection transport of energy by the infiltrate whereas the second nonlinear term $\mathcal{N}_r$, the coefficient of $(\theta + \theta_a)^4 - \theta_a^4$, refers to the surface radiative heat transfer from the fin to the ambient fluid. The parameter $\mathcal{N}_c$ is a combination of Rayleigh number R_a, Darcy's number D_a, the thermal conductivity ratio K_r and the ratio of the fin tip radius to fin thickness. The parameter $\mathcal{N}_r$ indicates the role of surface radiation to conduction in the fin. The parameter θ_a is the ratio of the ambient fluid temperature and the difference between the base temperature and the fluid temperature $(T_b - T_a)$.

For the rest of this research we remove the hat on the independent variable r for simplicity. Furthermore, the model employed closely follows the work by Darvishi et al. [1]; in order to compare the results obtained by those authors we use similar parameter values for $r^*, \mathcal{N}_c, \mathcal{N}_r$ and θ_a. The value of $r^* = \frac{r_b}{r_t}$ is however defined as the inverse of the r^* in the investigations of Darvishi et al. [1] (in their work they define this parameter as $R^* = \frac{r_t}{r_b} > 1$). To allow for a means of comparison we prescribe values for r^* as $\frac{1}{R^*}$.

Chapter 3

Steady State Solutions: semi-analytical methods

The work in section 3.2 has been published in Advances in Mathematical Physics [47].

3.1 Introduction

In this chapter, we study the behaviour exhibited by the partial differential equation, Equation (2.13), through the use of analytical solutions. Such solutions are naturally ideal since they can describe the exact behaviour of the heat transfer for a relevant model. Analytical solutions have proved to be effective to authors such as Aziz and Rahman [13] when examining a fin comprising of functionally graded material and analysing the performance on the radial fin with a continuously increasing thermal conductivity in the radial direction. They discovered that the heat transfer as well as the fin efficiency and effectiveness are at their highest when the thermal conductivity of the fin varies inversely with the square of the radius.

In a similar context to the our work, Kiwan [10] conducted a thermal analysis of natural convection porous fins by introducing Darcy's model to construct the energy equation governing the distribution of temperature. He further discovered that, by choosing a precise value for the thermal conductivity ratio and the fin length to thickness ratio, the performance of the porous fin exceeded the performance of the solid fin. Abu-Hijleh

[11] analysed the effects of using permeable fins on the forced convection heat transfer from a horizontal cylinder. The results obtained where similar to results obtained as per Kiwan et al. [9] in terms of the permeable fins providing much higher heat transfer rates.

In the research conducted here, the Differential Transformation Method (DTM), Lie Symmetry Analysis and an asymptotic analysis are employed to help us understand the dynamics of the problem as well as study and observe the behaviour of the solution specifically related to the fin's performance of the partial differential equation.

3.2 Differential Transformation Method

3.2.1 Introduction

In this section, we strive to obtain steady state solutions to Equation 2.13, derived in Chapter 2, modeling the heat transfer in a porous radial fin. The Differential Transformation Method is an approximation method based on the Taylor series expansion that can easily be applied to several linear and nonlinear problems. It constructs an analytical solution in terms of a polynomial and is capable of reducing the size of the computational work.

The predominant advantage of this method is that it can be applied directly to linear and nonlinear ordinary differential equations without requiring linearisation, discretisation or perturbation [48]. This method has been used in a similar manner by Ghasemi et al. [49] to solve the nonlinear temperature distribution equation with temperature dependent internal heat generation in porous and solid longitudinal fins. Furthermore, Fidanoglu et al. [50] used the method to construct a general expression for the heat distribution profile of a fin with spine geometry. Based on the fin effectiveness, entropy values and efficiency, it was found that the cylindrical fin had the highest rate of heat transfer.

In order to implement the method in question, we recall that an arbitrary analytical function $f(x)$ in the domain D can be expanded via the Taylor series about a point $x = 0$ as,

$$f(x) = \sum_{k=0}^{\infty} \frac{x^k}{k!} \left[\frac{d^k f(x)}{dx^k}\right]_{x=0}. \tag{3.2.1.1}$$

The differential transform of $f(x)$ can thus be defined as,

$$F(k) = \frac{1}{k!} \left[\frac{d^k f(x)}{dx^k}\right]_{x=0}, \tag{3.2.1.2}$$

with the inverse differential transform as,

$$f(x) = \sum_{k=0}^{\infty} x^k F(k). \tag{3.2.1.3}$$

The fundamental theorems of the one-dimensional differential transform method - some of which will be implemented in this paper - are given as follows,

Theorem 1 : If $f(x) = g(x) \pm h(x)$, then $F(k) = G(k) \pm H(k)$.

Theorem 2 : If $f(x) = cg(x)$, then $F(k) = cG(k)$, where c is a constant.

Theorem 3 : If $f(x) = \frac{d_n g(x)}{dx^n}$, then $F(k) = \frac{(k+n)!}{k!} G(k+n)$.

Theorem 4 : If $f(x) = g(x)h(x)$, then $F(k) = \sum_{k_1=0}^{k} G(k_1)H(k-k_1)$.

Theorem 5 : If $f(x) = x^n$, then $F(k) = \delta(k-n)$, where $\delta(k-n) = \begin{cases} 1, & k = n \\ 0, & k \neq n \end{cases}$

Theorem 6 : If $f(x) = g_1(x)g_2(x)....g_{n-1}(x)g_n(x)$, then

$$F(k)=\sum_{k_{n-1}=0}^{k}\sum_{k_{n-2}=0}^{k_{n-1}}....\sum_{k_2=0}^{k_3}\sum_{k_1=0}^{k_2}G_2(k_1)G_1(k_2-k_1)\times.....\times G_{n-1}(k_{n-1}-k_{n-2})G_n(k_n-k_{n-1}).$$

3.2.2 Implementation of the Differential Transformation Method

Through the use of these properties of the one-dimensional differential transformation method, we obtain the following iterative procedure for the steady state case of Equation (2.13),

$$\begin{aligned}\Theta[k+2]=&\Big(\frac{-(r^*-1)^2}{(k+1)\,(k+2)}\Big)\Big(\frac{(k+1)\,\Theta[k+1]}{(r^*-1)\,((r^*-1)+1)\,\delta[k-1]}-\mathcal{N}_c*\sum_{k_1=0}^{k}\Theta[k_1]\,\Theta[k-k_1]\\&-\mathcal{N}_r*\Big(\Big(\sum_{k_4=0}^{k}\sum_{k_3=0}^{k_4}\sum_{k_2=0}^{k_3}\sum_{k_1=0}^{k_2}\Theta[k_1]\,\Theta[k_2-k_1]\,\Theta[k_3-k_2]\,\Theta[k_4-k_3]\,\Theta[k-k_4]\Big)\\&+4\,\theta_a\Big(\sum_{k_3=0}^{k}\sum_{k_2=0}^{k_3}\sum_{k_1=0}^{k_2}\Theta[k_1]\,\Theta[k_2-k_1]\,\Theta[k_3-k_2]\,\Theta[k-k_3]\,\Theta[k-k_4]\Big)\\&+6\,\theta_a^2\Big(\sum_{k_2=0}^{k}\sum_{k_1=0}^{k_2}\Theta[k_1]\,\Theta[k_2-k_1]\,\Theta[k-k_2]\Big)+4\,\theta_a^3\,\Theta[k]-\theta_a^4\Big)\Big)\end{aligned}\tag{3.2.2.4}$$

This method requires initial conditions, i.e. we require the values of $\theta(0,\tau)$ and $\frac{\partial\theta(0,\tau)}{\partial r}$ since the equation is of second order. We notice that even though we have an initial value for the first derivative, we do not have a value for θ at $r=0$. Therefore we specify our initial conditions for the iterative procedure (3.2.2.4) as follows,

$$\Theta(0)=\Theta_0,\qquad\qquad \Theta(1)=0\tag{3.2.2.5}$$

where the initial condition for θ is given an assumed value while the first derivative condition becomes $\Theta(1)=0$. Through the use of Equation (3.2.2.4) and the conditions given by Equation (3.2.2.5) we are able to obtain,

$$\begin{aligned}
\Theta(0) &= -(1/2)(-1+r^*)^2(-\Theta_0^2\mathcal{N}_c - \mathcal{N}_r(\Theta_0^5 + 4\Theta_0^4\theta_a + 6\Theta_0^3\theta_a^2 + 4\Theta_0\theta_a^3 - \theta_a^4)),\\
\Theta(1) &= -(1/6)(-1+r^*)^2(\mathcal{N}_r\theta_a^4 - (-1+r^*)(-\Theta_0^2\mathcal{N}_c - \mathcal{N}_r(\Theta_0^5 + 4a^4\theta_a\\
&\quad +6\Theta_0^3\theta_a^2 + 4\Theta_0\theta_a^3 - \theta_a^4))),\\
\Theta(2) &= -(1/12)(-1+r^*)^2(\Theta_0\mathcal{N}_c(-1+r^*)^2(-\Theta_0^2\mathcal{N}_c - \mathcal{N}_r(\Theta_0^5 + 4\Theta_0^4\theta_a + 6\Theta_0^3\theta_a^2\\
&\quad +4\Theta_0\theta_a^3 - \theta_a^4)) - \tfrac{1}{2r^*}((-1+r^*)(\mathcal{N}_r\theta_a^4 - (-1+r^*)(-\Theta_0^2\mathcal{N}_c - \mathcal{N}_r(\Theta_0^5 + 4\Theta_0^4\theta_a\\
&\quad +6\Theta_0^3\theta_a^2 + 4\Theta_0\theta_a^3 - \theta_a^4)))) - \mathcal{N}_r(-\theta_a^4 - 5/2\Theta_0^4(-1+r^*)^2(-\Theta_0^2\mathcal{N}_c - \mathcal{N}_r(\Theta_0^5 + 4\Theta_0^4\theta_a\\
&\quad +6\Theta_0^3\theta_a^2 + 4\Theta_0\theta_a^3 - \theta_a^4)) - 8\Theta_0^3(-1+r^*)^2\theta_a(-\Theta_0^2\mathcal{N}_c - \mathcal{N}_r(\Theta_0^5 + 4\Theta_0^4\theta_a + 6\Theta_0^3\theta_a^2\\
&\quad +4\Theta_0\theta_a^3 - \theta_a^4)) - 9\Theta_0^2(-1+r^*)^2\theta_a^2(-\Theta_0^2\mathcal{N}_c - \mathcal{N}_r(\Theta_0^5 + 4\Theta_0^4\theta_a + 6\Theta_0^3\theta_a^2 + 4\Theta_0\theta_a^3\\
&\quad -\theta_a^4)) - 2(-1+r^*)^2\theta_a^3(-\Theta_0^2\mathcal{N}_c - \mathcal{N}_r(\Theta_0^5 + 4\Theta_0^4\theta_a + 6\Theta_0^3\theta_a^2 + 4\Theta_0\theta_a^3 - \theta_a^4)))),
\end{aligned} \tag{3.2.2.6}$$

which allows us, upon substitution into Equation (3.2.1.3), to obtain,

$$\theta(r) = \sum_{k=0}^{n} (r - r_0)^k \Theta(k) \tag{3.2.2.7}$$

where $r_0 = 0$. However, in order to determine the solution given by Equation (3.2.2.7) we need to first find the value of Θ_0. In order to determine a value for Θ_0, we use the false position method. The boundary condition which has not yet been employed is $\theta(1) = 1$. Thus we substitute the values obtained as per Equation (3.2.2.6) into Equation (3.2.2.7) for $r = 1$. This provides us with the equality $W(\Theta_0) = 1$ where $W(\Theta_0)$ can be written as $\frac{v(\Theta_0)}{u(\Theta_0)}$ and hence we need to solve the equation $Z(\Theta_0) = v(\Theta_0) - u(\Theta_0) = 0$. By plotting $v(\Theta_0)$ and $u(\Theta_0)$ we are able to obtain an interval $[\Theta_0^a, \Theta_0^b]$, where Θ_0^a and Θ_0^b are two guesses to Θ_0, within which the two functions are equal. Using these values we are able to obtain an improved value which satisfies $Z(\Theta_0) = 0$ as follows,

$$\Theta_0^{new} = \frac{\Theta_0^b Z(\Theta_0^b) - \Theta_0^a Z(\Theta_0^a)}{Z(\Theta_0^b) - Z(\Theta_0^a)}. \tag{3.2.2.8}$$

This procedure is iterated until a chosen error tolerance is reached such that $Z(\Theta_0^{new}) \ll \epsilon$. We employed this method as well as `NSolve` in MATHEMATICA as a means of verifying the accuracy of the value. As a brief example, we consider a case where $\mathcal{N}_c = 10$, $\mathcal{N}_r = 1$, $r^* = \frac{1}{1.75}$, $\theta_a = 0.2$ and $n = 3$ for which we would obtain $\Theta_0 = 0.564821$ resulting in,

$$\theta(r) = 0.564821 + 0.311221r^2 + 0.0444111r^3 + 0.0685314r^4 + 0.0110162r^5. \tag{3.2.2.9}$$

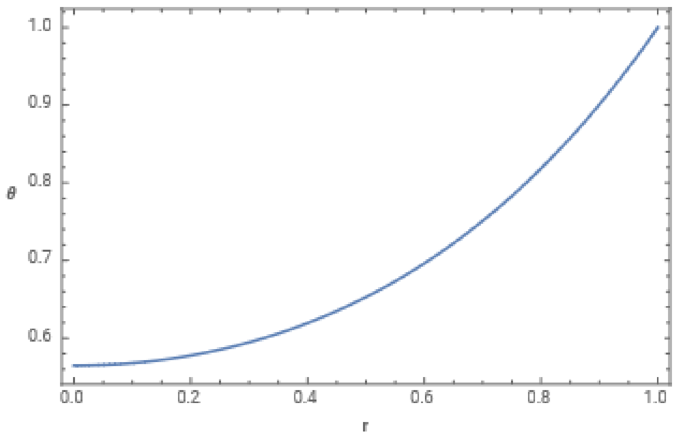

Fig. 3.1: *Plot of solution obtained for DTM with* $\mathcal{N}_c = 10$, $\mathcal{N}_r = 1$, $r^* = \frac{1}{1.75}$, $\theta_a = 0.2$ *and* $n = 3$.

3.2.3 Results and Discussion

Based on the solution obtained, we look at the convergence as well as the validation of the DTM series. The convergence is tested by varying the number of terms of the series whereas the accuracy of the DTM solution is assessed by comparing them with the solution obtained as per the work of Aziz et al. [27].

In this work, we have employed a polynomial of order $n = 10$ as our steady state solution. We are, via this methodology, able to obtain a polynomial of degree $n = 16$ which compares well to the sufficiently accurate solution produced with $n = 15$ as per the work of Aziz et al. [27]. However, for any degree larger we find that limited memory becomes a stumbling block for MATHEMATICA. Furthermore, as seen in Table 3.1, for $n = 10$ we find that our tip temperature $\theta_0 = 0.55725$ whereas for $n = 16$, $\theta_0 = 0.55678$; thus increasing the degree of the polynomial has a minimal effect on the solution in terms of accuracy.

Table 3.1: *Temperatures at the tip of the fin for varied values of n for the DTM solution.*

n	0	1	2	3	4	5	6	7	8
θ_0	0.62034	0.5983	0.56887	0.56482	0.55988	0.55884	0.55778	0.55751	0.55725
n	9	10	11	12	13	14	15	16	
θ_0	0.55717	0.5571	0.55703	0.55697	0.55692	0.55685	0.5580	0.55678	

Parameter values: $\mathcal{N}_c = 10$ $\mathcal{N}_r = 1$ $r^* = \frac{1}{1.75}$ $\theta_a = 0.2$

We can remark here that many terms are likely to be needed in order for the series solution to match solutions obtained in [1]. This discrepancy is also not of extreme concern since this semi-analytical solution is not our only means of comparison to the solutions obtained by Darvishi et al. [1]. The DTM results will be used as a baseline for the numerical schemes methods employed namely; the Crank-Nicolson scheme (CN), the Crank-Nicolson scheme with Newton-Raphson predictor corrector and Usmani method (CN^{NR}) and the Well-Balancing scheme (WBS).

3.3 Lie Symmetry Method

3.3.1 Introduction

We noticed that the problem under consideration is quite sensitive to the initial condition provided when employing numerical schemes, as we will show in subsequent Chapters.

To assist in this regard, we attempt to determine initial conditions admitted by the equation under consideration using infinitesimal generators that leave the form invariant. We will first proceed with the attainment of conditions via Lie point symmetries.

In this section, we propose initial conditions admitted by the equation under consideration using infinitesimal generators that leave the form invariant. Sophus Lie's approach to classical symmetries solves overdetermined systems of linear differential equations for coefficients of vector fields of infinitesimal symmetries by reducing their computation. This computation follows a clear algorithm which may appear simple in structure but sometimes has an enormous volume of calculations with intermediate expressions that contains numerous terms for higher-order partial differential equations [51]. The main use for lie symmetries admitted by a given system of differential equations are:

- To reduce or lower the order of the equation to quadrature in terms of ordinary differential equations and
- To determine the particular solutions also known as "invariant solutions" or to generate new solutions in terms of an ordinary or partial differential equation where a special solution is known.

Lie Symmetry analysis have been used by Moitsheki et al. [52] to determine forms of the arbitrary functions appearing in a steady nonlinear one-dimensional fin problem and by Ali et al. [53] to reduce and obtain exact solutions for a nonlinear fin equation in cylindrical coordinates.

3.3.2 Methodology

In this subsection we will provide an overview of the method to be employed as a means of obtaining an appropriate initial condition for the numerical schemes still to be discussed.

Given the nth order ordinary differential equation,

$$y_n = f(x, y, y_1, \ldots, y_{n-1}) \tag{3.3.2.10}$$

admits the one-parameter Lie group of transformations with the infinitesimal generator,

$$X = \xi(x, y)\frac{\partial}{\partial x} + \eta(x, y)\frac{\partial}{\partial y} \tag{3.3.2.11}$$

if and only if,

$$X^{(n)}[y_n - f(x, y, y_1, \ldots, y_{n-1})] = 0 \tag{3.3.2.12}$$

for,

$$y_n = f(z, x, y, y_1, \ldots, y_{n-1})$$

where,

$$X^{(n)} = \xi(x, y)\frac{\partial}{\partial x} + \eta(x, y)\frac{\partial}{\partial y} + \eta^{(1)}(x, y, y_1)\frac{\partial}{\partial y_1} + \ldots + \eta^{(n)}(x, y, y_1, \ldots, y_n)\frac{\partial}{\partial y_n}$$

is the extended infinitesimal generator of order n for Equation (3.3.2.11). Thus, we can write Equation (3.3.2.12) in the form,

$$\eta^{(n)} = \Big[\xi\frac{\partial f}{\partial x} + \eta\frac{\partial f}{\partial y} + \eta^{(1)}\frac{\partial f}{\partial y_1} + \ldots + \eta^{(n-1)}\frac{\partial f}{\partial y_{n-1}}\Big] = 0 \qquad (3.3.2.13)$$

where $y_n = f(z, x, y, y_1, \ldots, y_{n-1})$. It can be seen that Equation (3.3.2.13) is a polynomial in $y_1, y_2, \ldots, y_{n-1}$ whose coefficients are linear homogeneous in $(\xi(x, y), \eta(x, y))$ and their partial derivative up to order n. Furthermore, we can assign arbitrary values at any fixed point x for each $y_1, y_2, \ldots, y_{n-1}$ for any nth order ODE (3.3.2.13). It follows that the coefficient of each polynomial term in Equation (3.3.2.13) must vanish. Thus, we have a system of linear homogeneous partial differential equations for $(\xi(x, y), \eta(x, y))$. This linear system defines the set of determining equations for the infinitesimals admitted by the nth oder ODE (3.3.2.13). If $n \geq 2$, the set is over-determined since the number of determining equation exceeds two (i.e. the number of unknowns ξ and η).

Suppose that $f(x, y_1, y_2, \ldots, y_{n-1})$ is not a polynomial in $y_1, y_2, \ldots, y_{n-1}$. A corresponding set of determining equations from Equation (3.3.2.13) based on the independence of the variables $y_1, y_2, \ldots, y_{n-1}$ can be derived. It can be shown that the second order ODE admits at most an eight-parameter Lie group on transformations where as an nth order ODE $(n > 2)$ admits at most an $(n+4)-$parameter Lie group of transformations. Now we state some theorems on the forms of infinitesimal generators which can be admitted by ODEs. These theorems simplify the tedious work involved in setting and solving the determining equations for the infinitesimal $(\xi(x, y), \eta(x, y))$.

Theorem 1

Consider an nth order ODE, $n \geq 3$, of the form,

$$y_n = g(x, y, y_1 y_{n-1}) + h(x, y, y_1, \ldots, y_{n-2}). \tag{3.3.2.14}$$

If Equation (3.3.2.14) admits the infinitesimal generator, Equation (3.3.2.11), then

$$\xi_y = 0.$$

Theorem 2

Consider an nth order ODE, $n \geq 3$, of the form,

$$y_n = g(x, y) y_{n-1} + h(x, y, y_1, \ldots, y_{n-2}). \tag{3.3.2.15}$$

If Equation (3.3.2.15) admits the infinitesimal generator, Equation (3.3.2.11), then

$$\xi_y = 0, \qquad \eta_{yy} = 0.$$

Theorem 3

Consider a second order ODE of the form,

$$y_n = g(x, y) y_{n-1} + h(x, y, y_1, \ldots, y_{n-2}). \tag{3.3.2.16}$$

If Equation (3.3.2.16) admits the infinitesimal generator, Equation (3.3.2.11), with $\xi_y = 0$ then

$$\eta_{yy} = 0.$$

3.3.3 Results

We employ this method in MATHEMATICA using the package `"Sym"`, which computes the symmetries of systems of differential equations. We recall that r represents the radial coordinate, r^* the ratio of tip radius to base radius, $\mathcal{N}_r$ the radiation parameter and $\mathcal{N}_c$ the buoyancy or natural convection parameter. In addition, $c_1, c_2, \ldots, c_8$ are arbitrary constants which will be introduced in this section as necessary.

In terms of our nonlinear partial differential equation, we will only consider the cases where either $\mathcal{N}_c \neq 0$ or $\mathcal{N}_r \neq 0$ in order to account for the buoyancy/natural convection transport of energy as well as the surface radiative heat transfer i.e. Case 1, Case 4 and Case 5. Furthermore, we plot the solutions for each case (i.e. 1, 4 and 5) where $\mathcal{N}_c = 0.01$, $\mathcal{N}_r = 0.0001$, $r^* = \frac{1}{1.75}$ and $\theta_a = 0.2$. Thus for the steady state case as per Equation (2.13), we obtain the following classical symmetries from MATHEMATICA:

<u>Case 1</u> : $\mathbf{r^* = 1}$ **and** $\mathcal{N}_\mathbf{r} \neq \mathbf{0}$ **or** $\mathcal{N}_\mathbf{c} = \mathbf{0}$ **and** $\mathcal{N}_\mathbf{r} = \mathbf{0}$ **and** $\mathbf{r^* = 1}$ **or**
$\mathcal{N}_\mathbf{r} = \mathbf{0}$ **and** $\mathbf{r^* = 1}$ **and** $\mathcal{N}_\mathbf{c} \neq \mathbf{0}$

We obtain the infinitesimal generator given by,

$$X = \Big[\theta(c_1 + rc_2) + r^2 c_6 + c_7 + rc_8\Big] \frac{\partial}{\partial r} + \Big[c_3 + rc_4 + \theta(\theta c_2 + c_5 + rc_6)\Big] \frac{\partial}{\partial \theta},$$

with the corresponding coefficients,

$$\xi(r, \theta) = \theta(c_1 + rc_2) + r^2 c_6 + c_7 + rc_8,$$

$$\eta(r, \theta) = c_3 + rc_4 + \theta(\theta c_2 + c_5 + rc_6).$$

which leads to,

$$
\begin{aligned}
X^{[1]} \quad &: \theta \frac{\partial}{\partial r} = 0, \\
X^{[2]} \quad &: \theta r \frac{\partial}{\partial r} + \theta^2 \frac{\partial}{\partial \theta} = 0, \\
X^{[3]} \quad &: \frac{\partial}{\partial \theta} = 0, \\
X^{[4]} \quad &: r \frac{\partial}{\partial \theta} = 0, \\
X^{[5]} \quad &: \theta \frac{\partial}{\partial \theta} = 0, \\
X^{[6]} \quad &: r^2 \frac{\partial}{\partial r} + r\theta \frac{\partial}{\partial \theta} = 0, \\
X^{[7]} \quad &: \frac{\partial}{\partial r} = 0, \\
X^{[8]} \quad &: r \frac{\partial}{\partial r} = 0.
\end{aligned} \tag{3.3.3.17}
$$

Next we solve each characteristic equation for (3.3.3.17) and implement the boundary condition as per Equation (2.14) i.e. $\theta(1) = 1$, such that,

$$
\theta(r) = r. \tag{3.3.3.18}
$$

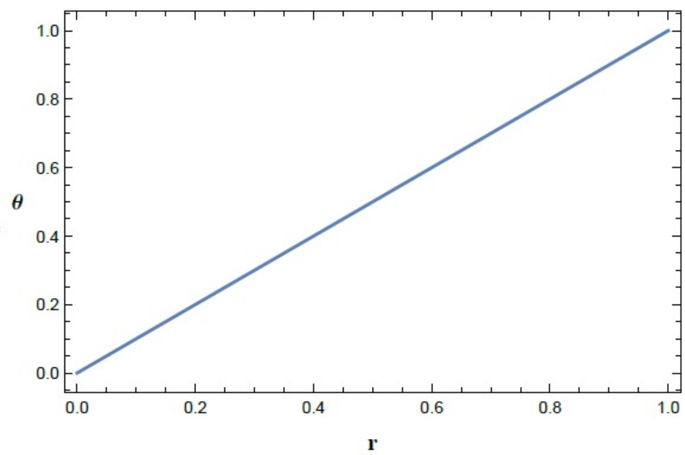

Fig. 3.2: *Plot of the solution of Case 1 obtained via a symmetry analysis.*

The solution obtained for Case 1 is reasonable as the fin temperature is dependent on the radial coordinate which lies within the boundaries of the tip radius and base radius. We observe that for increasing values of r, $\theta(r)$ increases. This means that $\theta(r)$ at the fin base is much larger than at the fin tip, which is to be expected given that heat is introduced at the base.

<u>**Case 2**</u> : $\mathbf{(r^* - 1)(1 - r + rr^*) \neq 0}$ **and** $\mathcal{N}_\mathbf{c} = \mathbf{0}$ **and** $\mathcal{N}_\mathbf{r} = \mathbf{0}$

We obtain the infinitesimal generator given by,

$$\begin{aligned} X =&(1+r(r^*-1))\Big[\theta c_5 + c_7 + (\theta c_6 + c_8)\mathrm{Log}(1+r(r^*-1)) + \frac{c_1 \mathrm{Log}(1+r(r^*-1))^2}{(r^*-1)^2}\Big]\frac{\partial}{\partial r} \\ &+ \frac{(r^*-1)(\theta c_2 + c_4 + (r^*-1)\theta^2 c_6) + (\theta c_1 + c_3)\mathrm{Log}(1+r(r^*-1))}{r^*-1}\frac{\partial}{\partial \theta}. \end{aligned}$$

where the appropriate coefficients have been calculated as follows,

$$\xi(r,\theta) = (1+r(r^*-1))\Big[\theta c_5 + c_7 + (\theta c_6 + c_8)\mathrm{Log}(1+r(r^*-1)) + \frac{c_1 \mathrm{Log}(1+r(r^*-1))^2}{(r^*-1)^2}\Big],$$

$$\eta(r,\theta) = \frac{(r^*-1)(\theta c_2 + c_4(r^*-1)\theta^2 c_6) + (\theta c_1 + c_3)\mathrm{Log}(1+r(r^*-1))}{r^*-1}.$$

which leads to,

$$\begin{aligned} X^{[1]} &: \tfrac{(1+r(r^*-1))\mathrm{Log}(1+r(r^*-1))^2}{(r^*-1)^2}\tfrac{\partial}{\partial r} + \tfrac{\theta \mathrm{Log}(1+r(r^*-1))}{r^*-1}\tfrac{\partial}{\partial \theta} = 0, \\ X^{[2]} &: \theta\tfrac{\partial}{\partial \theta} = 0, \\ X^{[3]} &: \tfrac{\mathrm{Log}(1+r(r^*-1))}{r^*-1}\tfrac{\partial}{\partial \theta} = 0, \\ X^{[4]} &: \tfrac{\partial}{\partial \theta} = 0, \\ X^{[5]} &: (1+r(r^*-1))\theta\tfrac{\partial}{\partial r} = 0, \\ X^{[6]} &: (1+r(r^*-1))\theta \mathrm{Log}(1+r(r^*-1))\tfrac{\partial}{\partial r} + \theta^2\tfrac{\partial}{\partial \theta} = 0, \\ X^{[7]} &: (1+r(r^*-1))\tfrac{\partial}{\partial r} = 0, \\ X^{[8]} &: (1+r(r^*-1))\mathrm{Log}(1+r(r^*-1))\tfrac{\partial}{\partial r} = 0. \end{aligned} \tag{3.3.3.19}$$

Next we solve each characteristic equation for (3.3.3.19) and implement the boundary condition as per Equation (2.14) i.e. $\theta(1) = 1$, such that,

$$\theta(r) = \frac{[(1 + r(r^* - 1)^2)(r^* - 1)^3]^2}{[(1 + (r^* - 1)^2)(r^* - 1)^3]^2} \tag{3.3.3.20}$$

Although we are able to obtain a solution for Case 2, we will omit this solution from our research. The reason for this is that we want a solution that takes into account the nonlinear terms i.e. the buoyancy/natural convection transport of energy by the infiltrate $\mathcal{N}_c$ and the surface radiative heat transfer $\mathcal{N}_r$.

Case 3 : $\boldsymbol{\mathcal{N}_c = 0}$ **and** $\boldsymbol{-\mathcal{N}_r\theta_a + r\mathcal{N}_r\theta_a + r^*\mathcal{N}_r\theta_a - 2rr^*\mathcal{N}_r\theta_a + rr^{*2}\mathcal{N}_r\theta_a \neq 0}$ **or** $\boldsymbol{\mathcal{N}_c\,\mathcal{N}_r(r^* - 1)(1 - r + rr^*) \neq 0}$

We obtain the infinitesimal generator given by,

$$X = 0,$$

with the corresponding coefficients,

$$\xi(r, \theta) = 0,$$

$$\eta(r, \theta) = 0.$$

Unfortunately, for Case 3, we cannot construct a solution and the buoyancy/natural convection transport of energy $\mathcal{N}_c = 0$. Hence, we omit such a solution in this thesis.

<u>**Case 4**</u> : $\mathbf{(r^* - 1)(1 - r + rr^*) \neq 0}$ **and** $\mathcal{N}_\mathbf{r} \neq \mathbf{0}$ **and** $\mathcal{N}_\mathbf{c} = \mathbf{0}$ **and** $\theta_\mathbf{a} = \mathbf{0}$

We obtain the infinitesimal generator given by,

$$X = \Big[(1 + r(r^* - 1))c_1\Big] \frac{\partial}{\partial r} + \Big[-\frac{2}{3}(r^* - 1)\theta c_1\Big] \frac{\partial}{\partial \theta}$$

with the corresponding coefficients,

$$\xi(r, \theta) = (1 + r(r^* - 1))c_1,$$

$$\eta(r, \theta) = -\frac{2}{3}(r^* - 1)\theta c_1.$$

By solving the characteristic equations and implementing the boundary condition as per Equation (2.14) i.e. $\theta(1) = 1$, we obtain,

$$\theta(r) = r^{*\frac{3}{2(r^*-1)}} [1 + r(r^* - 1)]^{\frac{3}{2(1-r^*)}}. \qquad (3.3.3.21)$$

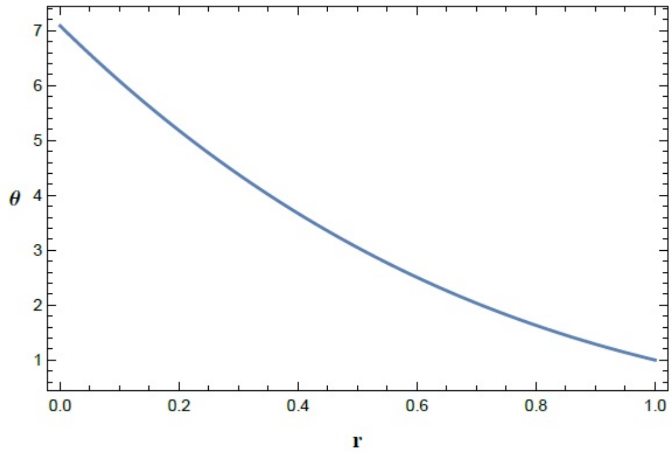

Fig. 3.3: *Plot of the solution of Case 4 obtained via a symmetry analysis.*

The solution obtained for Case 4 shows that as r increases, the temperature in the fin θ decreases. This solution is inconsistent with the physical dynamics of the problem and does not make sense. Hence, this is not a reasonable initial guess and will be excluded from this thesis.

<u>Case 5</u> : $\mathbf{(r^* - 1)(1 - r + rr^*) \neq 0}$ **and** $\mathbf{\mathcal{N}_c \neq 0}$ **and** $\mathbf{\mathcal{N}_r = 0}$

We obtain the infinitesimal generator given by,

$$X = \Big[(1 + r(r^* - 1))c_1\Big] \frac{\partial}{\partial r} + \Big[-2(r^* - 1)\theta c_1\Big] \frac{\partial}{\partial \theta}$$

with the corresponding coefficients,

$$\xi(r, \theta) = (1 + r(r^* - 1))c_1,$$

$$\eta(r, \theta) = -2(r^* - 1)\theta c_1.$$

By solving the characteristic equations and implementing the boundary condition as per Equation (2.14) i.e. $\theta(1) = 1$, such that

$$\theta(r) = r^{*\frac{1}{2(r^*-1)}} [1 + r(r^* - 1)]^{\frac{1}{2(1-r^*)}}. \tag{3.3.3.22}$$

The solution obtained for Case 5 is similar to the solution obtained in Case 4 which illustrates that as r increases, the temperature in the fin θ steadily decreases. Hence, this is not a reasonable solution.

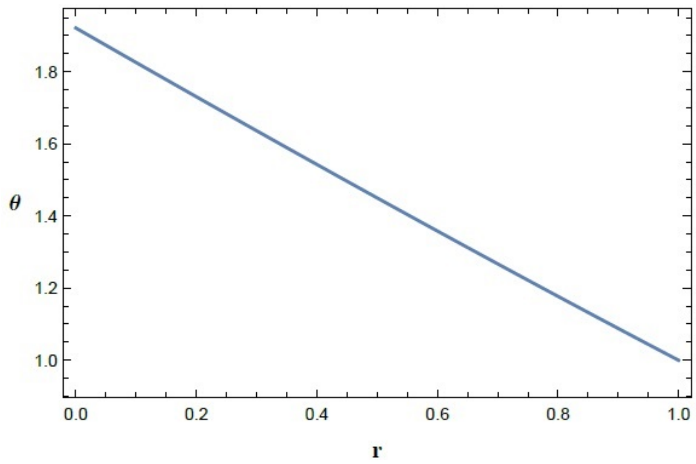

Fig. 3.4: *Plot of the solution of Case 5 obtained via a symmetry analysis.*

3.3.4 Concluding Remarks

In an attempt to overcome the boundary value problem and cater for the nonlinear terms i.e. the buoyancy/natural convection transport of energy by the infiltrate $\mathcal{N}_c$ and the surface radiative heat transfer $\mathcal{N}_r$ which impacts the scheme's stability, we have shown how the Lie group method provides a useful tool for obtaining initial conditions.

The solution obtained for Case 1, shows that the fin temperature is dependent on the radial coordinate which lies between the tip base and tip radius. We observe that the $\theta(r)$ increases with increasing values of r. In terms of Case 2, the solution produced will not be considered for this research as the solution does not depend on the nonlinear terms. For Case 3, we are unable to obtain a solution based on the characteristic equations; hence, we omit such a solution.

The solutions produced for Case 4 and Case 5 illustrates that the temperature in the fin decreases as the values of r increases. These solutions are inconsistent with the physical dynamics of the problem and does not make sense. Based on the results in Section

3.3.3, we can see that only Case 1 provides initial value solutions. This solution may prove to be useful in terms of a starting value or initial condition for the analytical and numerical approaches to follow.

3.4 Asymptotic Analysis

3.4.1 Introduction

In an attempt to describe and analyse the limiting behaviour of the physical system, we will employ an asymptotic analysis. An asymptotic analysis is a useful mathematical tool which provides analytical insight and numerical information about the solutions of complicated problems [54]. In some cases obtaining asymptotic estimates are straightforward, but in other cases it can be quite challenging and may involve a fair amount of ad-hoc analysis. There is generally a relatively large diversity of asymptotic methods. A general strategy used to derive asymptotics is to rely on some explicit formulas in order to approximate the solution of the problem, in some regions of the space of variables.

Based on the use of an asymptotic analysis, Kimura et al. [55] found three distinctive regimes depending on the magnitude of the permeability ratio K for the natural convection heat transfer and flow structure in an anisotropic porous medium. The first regime stipulates that when the permeability ratio $K = 1$, the Nusselt number (i.e. the ratio of convection to conduction heat transfer across the boundary) and the fluid velocity are scaled with $(KRa)^{\frac{1}{2}}$ when either K or the Rayleigh number Ra varies [55]. As $K \to 0$, the heat transfer across the cavity approaches the conductive state and the convecting velocity is scaled with (KRa). Lastly, as $K \to \infty$, the average Nusselt number and the fluid velocity are scaled with Ra which is independent of K [55]. Through the construction of multi-scale asymptotic expansions for computing temperature fields for the transient heat conduction problem, Yang et al. [56] obtained explicit convergence rates which were termed feasible and valid for predicting the heat transfer performance of period porous materials. Given the important results obtained in [55] and [56], the method is a feasible means of investigating the problem under discussion.

3.4.2 Methodology

In this section we consider the steady state case of Equation (2.13). We will assume that nonlinear terms $\ll \epsilon$; i.e the bouyancy/natural convection transport of energy by the infiltrate ($\mathcal{N}_c$) and the surface radiative heat transfer from the fin ($\mathcal{N}_c$) are much smaller than some small parameter ϵ. This will allow us to investigate the nature of the solutions of the steady state case of (2.13) under particular circumstances.

We assume a solution of the form $\theta(r) = \theta_0(r) + \epsilon\theta_1(r) + \epsilon^2\theta_2(r)$ where $\epsilon \to 0$ and consider a case where $r^* = \frac{1}{1.75}$ and $\theta_a = 0.2$ to obtain,

$$\mathcal{N}_c \left(\theta_0(r) + \epsilon\left(\theta_1(r) + \epsilon\theta_2(r)\right)\right)^2 - \mathcal{N}_r \left(\left(\frac{1}{5} + \theta_0(r) + \epsilon\left(\theta_1(r) + \epsilon\theta_2(r)\right)\right)^4 - \frac{1}{625}\right) =$$

$$\frac{49\left(\theta_0'(r) + \epsilon\left(\theta_1'(r) + \epsilon\theta_2'(r)\right)\right)}{-21 + 9r} + \frac{49}{9}\left(\theta_0''(r) + \epsilon\left(\theta_1''(r) + \epsilon\theta_2''(r)\right)\right). \qquad (3.4.2.23)$$

We expand Equation (3.4.2.23) using a series expansion allowing us to separate Equation (3.4.2.23) according to powers of ϵ and obtain the following system of equations:

$$
\begin{aligned}
O(\epsilon^0):\quad & -\tfrac{4}{125}\mathcal{N}_r\theta_0(r) - \mathcal{N}_c\theta_0(r)^2 - \tfrac{6}{25}\mathcal{N}_r\theta_0(r)^2 - \tfrac{4}{5}\mathcal{N}_r\theta_0(r)^3 - \mathcal{N}_r\theta_0(r)^4 \\
& + \tfrac{49\theta_0'(r)}{-21+9r} + \tfrac{49}{9}\theta_0''(r), \\
O(\epsilon^1):\quad & -\tfrac{4}{125}\mathcal{N}_r\theta_1(r) - 2\mathcal{N}_c\theta_0(r)\theta_1(r) - \tfrac{12}{25}\mathcal{N}_r\theta_0(r)\theta_1(r) - \tfrac{12}{5}\mathcal{N}_r\theta_0(r)^2\theta_1(r) \\
& -4\mathcal{N}_r\theta_0(r)^3\theta_1(r) + \tfrac{49\theta_1'(r)}{-21+9r} + \tfrac{49}{9}\theta_1''(r), \\
O(\epsilon^2):\quad & -\mathcal{N}_c\theta_1(r)^2 - \tfrac{6}{25}\mathcal{N}_r\theta_1(r)^2 - \tfrac{12}{25}\mathcal{N}_r\theta_0(r)\theta_1(r)^2 - 6\mathcal{N}_r\theta_0(r)^2\theta_1(r)^2 \\
& -\tfrac{4}{125}\mathcal{N}_r\theta_2(r) - 2\mathcal{N}_c\theta_0(r)\theta_2(r) - \tfrac{12}{25}\mathcal{N}_r\theta_0(r)\theta_2(r) - \tfrac{12}{5}\mathcal{N}_r\theta_0(r)^2\theta_2(r) \\
& -4\mathcal{N}_r\theta_0(r)^3\theta_2(r) + \tfrac{49\theta_2'(r)}{-21+9r} + \tfrac{49}{9}\theta_2''(r),
\end{aligned}
$$

$$
\begin{aligned}
O(\epsilon^3):\quad & -\tfrac{4}{5}\mathcal{N}_r\theta_1(r)^3 - 4\mathcal{N}_r\theta_0(r)\theta_1(r)^3 - 2\mathcal{N}_c\theta_1(r)\theta_2(r) - \tfrac{12}{25}\mathcal{N}_r\theta_1(r)\theta_2(r) \\
& -\tfrac{24}{5}\mathcal{N}_r\theta_0(r)\theta_1(r)\theta_2(r) - 12\mathcal{N}_r\theta_0(r)^2\theta_1(r)\theta_2(r), \\
O(\epsilon^4):\quad & -\mathcal{N}_r\theta_1(r)^4 - \tfrac{12}{5}\mathcal{N}_r\theta_1(r)^2\theta_2(r) - 12\mathcal{N}_r\theta_0(r)\theta_1(r)^2\theta_2(r) - \mathcal{N}_c\theta_2(r)^2 \\
& -\tfrac{6}{25}\mathcal{N}_r\theta_2(r)^2 - \tfrac{12}{5}\mathcal{N}_r\theta_0(r)\theta_2(r)^2 - 6\mathcal{N}_r\theta_0(r)^2\theta_2(r)^2, \\
O(\epsilon^5):\quad & -4\mathcal{N}_r\theta_1(r)^3\theta_2(r) - \tfrac{12}{5}\mathcal{N}_r\theta_1(r)\theta_2(r)^2 - 12\mathcal{N}_r\theta_0(r)\theta_1(r)\theta_2(r)^2, \\
O(\epsilon^6):\quad & -6\mathcal{N}_r\theta_1(r)^2\theta_2(r)^2 - \tfrac{4}{5}\mathcal{N}_r\theta_2(r)^3 - 4\mathcal{N}_r\theta_0(r)\theta_2(r)^3.
\end{aligned} \tag{3.4.2.24}
$$

Next, we use `NDSolve` in MATHEMATICA to obtain the values of θ_0, θ_1 and θ_2 in order to obtain the relevant solution.

3.4.3 Results and Discussion

The solutions obtained for the equation under consideration interpolate polynomials and as such cannot be displayed here. Figure 3.5 represents the solution obtained for $\mathcal{N}_c = 0.01, \mathcal{N}_r = 0.0001, r^* = \frac{1}{1.75}$ and $\theta_a = 0.2$.

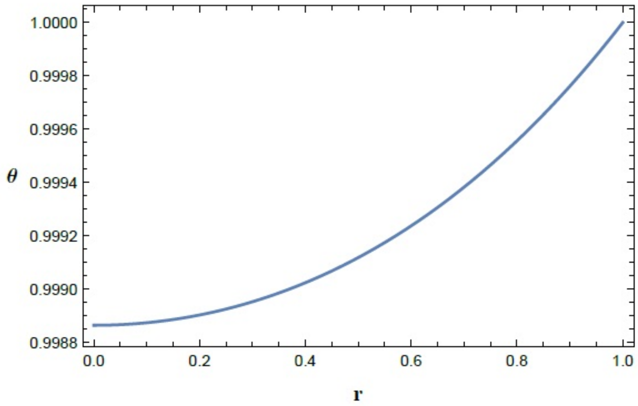

Fig. 3.5: *Plot of the temperature obtained via an asymptotic solution.*

The solution derived for the problem was not deemed useful in terms of providing deeper insight into the dynamics observed. The solution provides appropriate behaviour only but the value at the origin is not accurate. This is likely due to the assumption that the nonlinear terms have minimal impact, represented by the assumptions that $\mathcal{N}_r \to 0$ and $\mathcal{N}_c \to 0$.

Chapter 4

Dynamical Systems Analysis

The work in this chapter has been published in Advances in Mathematical Physics [47].

4.1 Introduction

In order to ascertain whether a simple linearisation of the steady state equation may be used as a means of analysing the dynamics of the nonlinear system, we need to determine what this linearised system and the relevant equilibrium points are. It must be noted that we consider the case where $r = 0$; this is due to the physical relevance placed on the dynamics at the fin tip. In an attempt to investigate the stability; that is whether or not a system is stable or will be stable if perturbed; of the partial differential equation we consider in this thesis, especially with respect to the initial condition, we conduct a local analysis of solutions in the vicinity of what are called critica points. To do this however, we use a linearisation approach in order to investigate the impact of the nonlinear terms on the nonlinear non-autonomous system.

4.2 Consideration of viability of the linearised system

In this section, we expand our stability analysis to consider the nonlinear terms and the degree to which they impact the scheme's stability. This analysis has been used by Mojtabi et al. [57] in the study of Soret-driven convection in a horizontal porous layer.

Furthermore, Patel et al. [58] performed a stability analysis via the fixed point theorem method when solving a solid and porous fin with temperature dependent internal heat generation while solving the problem via the Adomian decomposition sumudu transformation method.

As explained in [59], we restructure our steady state partial differential equation into a system of ordinary differential equations as follows,

$$\dot{\underline{\theta}} = \mathbf{f}(\underline{\theta}, r) \tag{4.2.1}$$

so that

$$\dot{\theta}_1 = \theta_2$$

and

$$\dot{\theta}_2 = \frac{(1-r^*)\theta_2}{r(r^*-1)+1} + \mathcal{N}_r(r^*-1)^2((\theta_1+\theta_a)^4 - \theta_a^4) + \mathcal{N}_c(r^*-1)^2\theta_1^2. \tag{4.2.2}$$

We can use a linearisation approach to study the linear stability of this nonlinear non-autonomous system [60]. In order to do so we consider a Taylor series expansion of $\mathbf{f}[\bullet]$ near the equilibrium point $\underline{\theta} \approx \underline{0}$ (the reason for considering this equilibrium point will become apparent later in this thesis). This may be constructed as follows,

$$\begin{aligned}
\dot{\theta}(t)\Big|_{\underline{\theta}\approx 0} &= \mathbf{f}(\underline{\theta}, r) \\
&= \mathbf{f}(\underline{\theta}, r) + \frac{\partial \mathbf{f}(\underline{\theta}, r)}{\partial \underline{\theta}}\Bigg|_{\underline{\theta}\approx 0} \underline{\theta} + \text{higher order terms.}
\end{aligned}$$

where we need to ensure that the higher order terms $(h.o.t.)$ are small enough for $\underline{\theta}$

close to 0, the equilibrium point, and for all r. A commonly used criteria based on the L_2-norm is,

$$\sup \left. \frac{||\mathbf{f}_{h.o.t.}(\underline{\theta}, r)||}{||\underline{\theta}||} \right|_{|x| \to 0} \approx \underline{0} \quad \text{for all } r \tag{4.2.3}$$

which specifies that the higher order terms ($h.o.t.$) of the Taylor series expansion are approximated by zero at the relevant equilibrium point; this allows us to approximate the nonlinear non-autonomous system by a linearised system.

In order to consider the higher order terms we recall that,

$$f^i(x) = f^i(x_0) + \left. \frac{\partial f^i}{\partial x_j} \right|_{x=x_0} + \frac{1}{2} \left. \frac{\partial^2 f^i}{\partial x_j \partial x_k} \right|_{x=x_0} (x_j - x_0)(x_k - x_0) + \cdots \tag{4.2.4}$$

which for our system (4.2.2) provides us with the following higher order terms $\frac{1}{2!}\underline{\theta}^T \mathbf{H} \underline{\theta} + \cdots$ where $\mathbf{H}$ is the Hermian matrix,

$$H(f_1) = \begin{bmatrix} \frac{\partial^2 f_1}{\partial \theta_1^2} & \frac{\partial^2 f_1}{\partial \theta_1 \partial \theta_2} \\ \frac{\partial^2 f_1}{\partial \theta_2 \partial \theta_1} & \frac{\partial^2 f_1}{\partial \theta_2^2} \end{bmatrix} = \begin{bmatrix} 0 & 0 \\ 0 & 0 \end{bmatrix}$$

$$H(f_2) = \begin{bmatrix} \frac{\partial^2 f_2}{\partial \theta_1^2} & \frac{\partial^2 f_2}{\partial \theta_1 \partial \theta_2} \\ \frac{\partial^2 f_2}{\partial \theta_2 \partial \theta_1} & \frac{\partial^2 f_2}{\partial \theta_2^2} \end{bmatrix} = \begin{bmatrix} 12\mathcal{N}_r(r^* - 1)^2(\theta_1 + \theta_a)^2 + 2\mathcal{N}_c(r^* - 1)^2 & 0 \\ 0 & 0 \end{bmatrix}. \tag{4.2.5}$$

Now as $|\underline{\theta}| \to 0$, we have,

$$\begin{bmatrix} 12\mathcal{N}_r(r^* - 1)^2\theta_a^2 + 2\mathcal{N}_c(r^* - 1)^2 & 0 \\ 0 & 0 \end{bmatrix} \tag{4.2.6}$$

which implies that, $12\mathcal{N}_r(r^* - 1)^2\theta_a^2 + 2\mathcal{N}_c(r^* - 1)^2 = (r^* - 1)^2[12\mathcal{N}_r\theta_a^2 + 2\mathcal{N}_c]$ should tend to 0 or be approximately 0 in order for us to consider the dynamics of the linear system as a guide for those of the nonlinear non-autonomous system. Thus, given that

$r^* \neq 1$ we need $12\mathcal{N}_r U_a^2 + 2\mathcal{N}_c \approx 0$ such that,

$$\mathcal{N}_r \approx -\frac{\mathcal{N}_c}{6\theta_a^2} \tag{4.2.7}$$

which is unrealistic. The only manner in which (4.2.7) could hold is if both parameters were to approximate zero, i.e. $\mathcal{N}_c, \mathcal{N}_r \approx 0$. Thus, we conclude that the higher order terms have an influence on the stability of the system and cannot be ignored. Were we to choose to engage with the linear system as a means of analysis then we can only do so for small values of $\mathcal{N}_c$ and $\mathcal{N}_r$. It is for this reason that the phase portraits presented are for $\mathcal{N}_c = 0.01, 0.1$ and $\mathcal{N}_r = 1$. In the next section we consider the system with these points in mind.

4.3 Nonlinear dynamical systems analysis

It must be noted that we consider the case where $r = 0$; this is due to the physical relevance placed on the dynamics at the fin tip.

Firstly, as per [59], we restructure our steady state partial differential equation into a system of ordinary differential equations as follows,

$$\dot{\underline{\theta}} = \mathbf{f}(\underline{\theta}, r) \tag{4.3.8}$$

so that,

$$\dot{\theta}_1 = \theta_2$$

and

$$\dot{\theta}_2 = \frac{(1-r^*)\theta_2}{r(r^*-1)+1} + \mathcal{N}_r(r^*-1)^2((\theta_1+\theta_a)^4 - \theta_a^4) + \mathcal{N}_c(r^*-1)^2\theta_1^2. \tag{4.3.9}$$

We now turn to equilibrium solutions with the intention of investigating the dynamics of the system [61]. In the case of this nonlinear, non-autonomous system the fixed points (or equilibrium points) are defined by the vanishing of the vector field; that is,

$$\mathbf{f}(\underline{\theta}, r) = \underline{0}. \tag{4.3.10}$$

Theorems for the stability of fixed points of the system,

$$\dot{\underline{\theta}} = A\underline{\theta} + \mathbf{f}(\underline{\theta}, r) \tag{4.3.11}$$

are presented by Coddington and Levinson [62], where A is a constant matrix (upon substitution of the relevant equilibrium points and parameter values) and the vector function $\mathbf{f}$ is continuous in $\underline{\theta}$ and r. In order to employ these theorems we write our system of Equations (4.3.9) in the form (4.3.11),

$$\dot{\underline{\theta}} = \begin{bmatrix} 0 & 1 \\ 4\mathcal{N}_r(r^* - 1)^2(\theta_1 + \theta_a)^3 + 2\mathcal{N}_c(r^* - 1)^2\theta_1 & 0 \end{bmatrix} \underline{\theta} + \begin{bmatrix} 0 & 0 \\ 0 & \frac{1-r^*}{r(r^*-1)+1}. \end{bmatrix} \tag{4.3.12}$$

As per equation (4.3.12) we obtain the equilibrium points (θ_1, θ_2),

$$(0, 0) \tag{4.3.13}$$

and

$$\left(\frac{\sqrt[3]{18\mathcal{N}_c\mathcal{N}_r^2\theta_a - 10\mathcal{N}_r^3\theta_a^3 + 5.19615\sqrt{\mathcal{N}_c^3\mathcal{N}_r^3 + 14\mathcal{N}_c^2\mathcal{N}_r^4\theta_a^2 - 12\mathcal{N}_c\mathcal{N}_r^5\theta_a^4 + 4\mathcal{N}_r^6\theta_a^6}}}{3\mathcal{N}_r} \right.$$

$$\left. - \frac{3\mathcal{N}_c\mathcal{N}_r + 2\mathcal{N}_r^2\theta_a^2}{3\mathcal{N}_r\sqrt[3]{18\mathcal{N}_c\mathcal{N}_r^2\theta_a - 10\mathcal{N}_r^3\theta_a^3 + 5.19615\sqrt{\mathcal{N}_c^3\mathcal{N}_r^3 + 14\mathcal{N}_c^2\mathcal{N}_r^4\theta_a^2 - 12\mathcal{N}_c\mathcal{N}_r^5\theta_a^4 + 4\mathcal{N}_r^6\theta_a^6}}} - \frac{4\theta_a}{3}, 0 \right). \tag{4.3.14}$$

In considering the eigenvalues of A from Equation (4.3.12), we can write them with general parameter values as follows,

$$\lambda_1 = -\sqrt{2}(r^* - 1)\sqrt{\mathcal{N}_c\theta_1 + 2\mathcal{N}_r\theta_1^3 + 6\mathcal{N}_r\theta_1^2\theta_a + 6\mathcal{N}_r\theta_1\theta_a^2 + 2\mathcal{N}_r\theta_a^3},$$

$$\lambda_2 = \sqrt{2}(r^* - 1)\sqrt{\mathcal{N}_c\theta_1 + 2\mathcal{N}_r\theta_1^3 + 6\mathcal{N}_r\theta_1^2\theta_a + 6\mathcal{N}_r\theta_1\theta_a^2 + 2\mathcal{N}_r\theta_a^3},$$

to be evaluated at the equilibrium points in order to classify them. From the form they take we can see two possible cases (depending on whether the term inside the square root is positive or negative): a saddle point or a centre.

Case 1: Equilibrium point (4.3.13)

The eigenvalues of A at equilibrium point (4.3.13) are

$$\lambda_1 = -2\sqrt{\mathcal{N}_r}(r^* - 1)\theta_a^{3/2}, \quad \lambda_2 = 2\sqrt{\mathcal{N}_r}(r^* - 1)\theta_a^{3/2}.$$

We can see that this equilibrium point (given the ranges for the relevant parameter values) represents a saddle point which is unstable - see the plot on the right of Figure 4.1.

Coddington and Levinson [62] have shown that if at least one eigenvalue of A has a real part which is positive, then upon $\mathbf{f}(\underline{\theta}, r)$ satisfying the requirement that given any $\epsilon > 0$, there exists a δ and T such that,

$$\mathbf{f}(\underline{\theta}, r) \leqq \epsilon|\underline{\theta}| \quad (|\underline{\theta}| \leqq \delta, t \geqq T) \tag{4.3.15}$$

then the solution $\underline{\theta} = \underline{0}$ of (4.3.11) is not stable. In our case, we find that for the equilibrium point $(0,0)$ at least one eigenvalue of A is positive and furthermore,

$$\mathbf{f}(\underline{\theta}, r) = \begin{bmatrix} 0 & 0 \\ 0 & \frac{1-r^*}{r(r^*-1)+1} \end{bmatrix} \begin{bmatrix} \theta_1 \\ \theta_2 \end{bmatrix}. \tag{4.3.16}$$

We need to show that $\left|\frac{1-r^*}{r(r*-1)+1}\theta_2\right| \leqq \epsilon|\theta_2|$. In an attempt to do so, we maximise the term on the left of the inequality, i.e. we consider $r = 0$ such that,

$$\left|\frac{1-r^*}{r(r^*-1)+1}\theta_2\right| \leqq \left|\frac{1-r^*}{r(r^*-1)+1}\right| |\theta_2| \leqq |1-r^*|\,|\theta_2| = \epsilon\,|\theta_2|$$

where, given that $0 < 1 - r^* < 1$ we define $0 < \epsilon < 1$. This proves our requirement (4.3.15), confirming that the equilibrium point (4.3.13) is not stable.

Case 2: Equilibrium point (4.3.14)

The eigenvalues of A at this equilibrium point are lengthy for arbitrary values of $\mathcal{N}_c, \mathcal{N}_r, r^*$ and θ_a. However, as pointed out above, the second case needs to be for $\mathcal{N}_c\theta_1 + 2\mathcal{N}_r\theta_1^3 + 6\mathcal{N}_r\theta_1^2\theta_a + 6\mathcal{N}_r\theta_1\theta_a^2 + 2\mathcal{N}_r\theta_a^3 < 0$. A variety of values were considered for the parameters $\mathcal{N}_c, \mathcal{N}_r, r^*$ and θ_a, all leading to eigenvalues of the form expected, which are,

$$\lambda_1 = \mu i, \quad \lambda_2 = -\mu i, \quad \text{where} \quad i^2 = -1,$$

providing us with a stable centre - see the plot on the left of Figure 4.1. At this stage we note that this case requires $\theta_1 = \theta < 0$ which is not physically relevant.

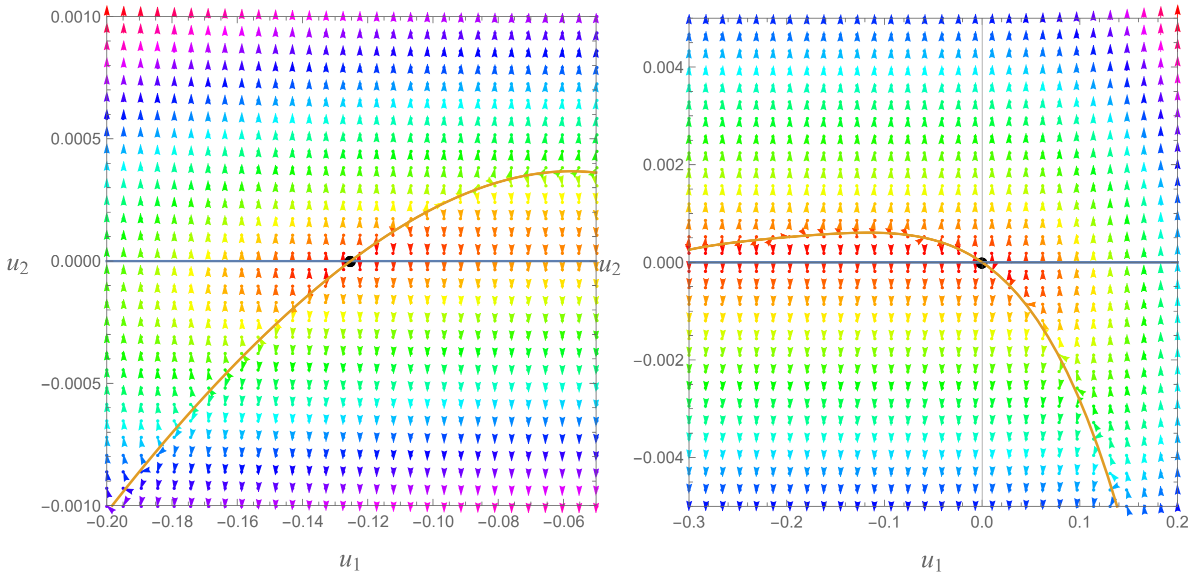

Fig. 4.1: *Phase plots indicating the trajectories around the equilibrium points (4.3.13) and (4.3.14) for* $\theta_a = 0.2$, $r^* = \frac{1}{1.75}$ *and* $\mathcal{N}_r = 1$. *The plot on the left has* $\mathcal{N}_c = 0.1$ *whereas the plot on the right has* $\mathcal{N}_c = 0.01$. *The plot on the left is a closer view of the second equilibrium point.*

4.3.1 Conclusion

We find that for $\theta_1 = \theta_2 = 0$, equilibrium point (4.3.13), we are in fact referring to the point where $\theta = \theta' = 0$, which is a point that would be located at the origin $r = 0$ (see the boundary conditions). We find that as $\mathcal{N}_r \to \infty$ that $\theta \to 0$ at the point where $\theta'(0) = 0$. Thus as $\mathcal{N}_r$ increases we would have a situation which reflects this equilibrium point; albeit a rare case.

This behaviour of the solution makes physical sense since $\mathcal{N}_r$ serves as the radiative sink and as such large values thereof would mean that the surface radiation heat transfer is large which decreases the temperature unrealistically. Thus, the instability of the equilibrium point $(0, 0)$ is confirmed by our numerical results. In fact, our results from the previous subsection with relation to the higher order terms are confirmed: only if we assume that $\mathcal{N}_r$ (and also $\mathcal{N}_c$ in fact) is small, will the linear system approximate the nonlinear system.

4.4 Steady State Analysis: Alternate Nondimensionalization

In order to support our findings in the sections above, we consider the nondimensionalisation introduced in Darvishi et al. [1]. We employ a similar analysis, and show that our results are consistent irrespective of the construction of the dimensionless equation. Of interest, would be any additional insights which we may obtain.

The nondimensionalisation employed in Darvishi et al. [1] is given as follows,

$$\theta = \frac{T}{T_b}, \quad \theta_a = \frac{T_a}{T_b}, \quad \hat{r} = \frac{r}{r_b}, \quad \hat{r}^* = \frac{r_t}{r_b}, \quad \mathcal{N}_c = \frac{\rho_f C_{p,f} K g \beta_f r_b^2 T_b}{V_f k_{eff} s}, \quad \mathcal{N}_r = \frac{2\epsilon\sigma F_{f-a} r_b^2 T_b^3}{k_{eff} s}. \tag{4.4.17}$$

Given that we are considering the time dependent case we also incorporate,

$$\tau = \frac{k_{eff} t}{\rho C_v r_b^2}$$

providing the following equation for consideration,

$$\frac{\partial \theta}{\partial \tau} = \frac{1}{r}\frac{\partial}{\partial r}\left(r\frac{\partial \theta}{\partial r}\right) - \mathcal{N}_c \left(\theta - \theta_a\right)^2 - \mathcal{N}_r \left(\theta^4 - \theta_a^4\right), \tag{4.4.18}$$

where $\hat{r}^* > 1$ is defined as $\frac{r_t}{r_b}$ and the parameters $\mathcal{N}_c$ and $\mathcal{N}_r$ are stated as per Equation (4.4.17).

Employing the non-dimensional transformations given by equation (4.4.17) we obtain the following boundary conditions,

$$\theta(1) = 1, \qquad \left.\frac{d\theta}{dr}\right|_{r=r^*} = 0. \tag{4.4.19}$$

4.5 Dynamical System Analysis: Alternate Nondimensionalization

In order to consider the dynamics of the system we structure the equations as before,

$$\dot{\theta}_1 = \theta_2,$$

$$\dot{\theta}_2 = -\frac{\theta_2}{r} + \mathcal{N}_c(\theta_1 - \theta_a)^2 + \mathcal{N}_r\left(\theta_1^4 - \theta_a^4\right). \tag{4.5.20}$$

It must be noted that we consider the case where $r = r^*$; this is due to the physical relevance placed on the dynamics at the fin tip. We now structure this system as per the work of Coddington and Levinson [62],

$$\dot{\underline{\theta}} = A\underline{\theta} + \mathbf{f}(\underline{\theta}, r) \tag{4.5.21}$$

so that we may employ theorems for the stability of fixed points of the system by considering the eigenvalues of A. We obtain the equilibrium points (θ_1, θ_2):

$$(\theta_a, 0) \tag{4.5.22}$$

and

$$\left(\frac{2^{/3}\sqrt[3]{5.19615\sqrt{\mathcal{N}_c^3\mathcal{N}_r^3 + 14.\mathcal{N}_c^2\mathcal{N}_r^4\theta_a^2 - 12.\mathcal{N}_c\mathcal{N}_r^5\theta_a^4 + 4.\mathcal{N}_r^6\theta_a^6} + 18.\mathcal{N}_c\mathcal{N}_r^2\theta_a - 10.\mathcal{N}_r^3\theta_a^3} - \left(3.\mathcal{N}_c\mathcal{N}_r + 2.\mathcal{N}_r^2\theta_a^2\right)}{3\mathcal{N}_r\ {}^{1/3}\sqrt[3]{5.19615\sqrt{\mathcal{N}_c^3\mathcal{N}_r^3 + 14.\mathcal{N}_c^2\mathcal{N}_r^4\theta_a^2 - 12.\mathcal{N}_c\mathcal{N}_r^5\theta_a^4 + 4.\mathcal{N}_r^6\theta_a^6} + 18.\mathcal{N}_c\mathcal{N}_r^2\theta_a - 10.\mathcal{N}_r^3\theta_a^3}} - \frac{\theta_a}{3}, 0\right). \tag{4.5.23}$$

In considering the eigenvalues of A from Equation (4.5.21), we can write them with general parameter values as follows,

$$\lambda_1 = -\sqrt{2}\sqrt{\mathcal{N}_c\theta_1 + 2\mathcal{N}_r\theta_1^3 - \mathcal{N}_c\theta_a},$$

$$\lambda_2 = \sqrt{2}\sqrt{\mathcal{N}_c\theta_1 + 2\mathcal{N}_r\theta_1^3 - \mathcal{N}_c\theta_a},$$

to be evaluated at the equilibrium points we want to classify. Again as per the work conducted above we have two cases: a saddle point or a centre.

Case 1: Equilibrium point (4.5.22)

The eigenvalues of A at equilibrium point (4.5.22) are,

$$\lambda_1 = -2\sqrt{\mathcal{N}_r}\theta_a^{3/2}, \quad \lambda_2 = 2\sqrt{\mathcal{N}_r}\theta_a^{3/2},$$

which represent an unstable saddle point - see the plot on the right of Figures 4.2 and 4.3 corresponding to the saddle point obtained for the equilibrium point $(0, 0)$ for the previous nondimensionalisation.

Next, we consider the impact of the higher order terms as done before. We obtain the following

$$H(f_1) = \begin{bmatrix} \frac{\partial^2 f_1}{\partial\theta_1^2} & \frac{\partial^2 f_1}{\partial\theta_1\partial\theta_2} \\ \frac{\partial^2 f_1}{\partial\theta_2\partial\theta_1} & \frac{\partial^2 f_1}{\partial\theta_2^2} \end{bmatrix} = \begin{bmatrix} 0 & 0 \\ 0 & 0 \end{bmatrix},$$

$$H(f_2) = \begin{bmatrix} \frac{\partial^2 f_2}{\partial\theta_1^2} & \frac{\partial^2 f_2}{\partial\theta_1\partial\theta_2} \\ \frac{\partial^2 f_2}{\partial\theta_2\partial\theta_1} & \frac{\partial^2 f_2}{\partial\theta_2^2} \end{bmatrix} = \begin{bmatrix} 12\mathcal{N}_r\theta_1^2 + 2\mathcal{N}_c & 0 \\ 0 & 0 \end{bmatrix}. \tag{4.5.24}$$

Now as $|\underline{\theta}| \to (\theta_a, 0)$, we have,

$$H(f_2) = \begin{bmatrix} 12\mathcal{N}_r\theta_a^2 + 2\mathcal{N}_c & 0 \\ 0 & 0 \end{bmatrix}, \tag{4.5.25}$$

which means that for the linear system to approximate the nonlinear dynamics of the system we now require $\mathcal{N}_c \approx 0$ and either $\mathcal{N}_r$ or θ_a to ≈ 0.

Given the fact that we obtained an unstable saddle point at this equilibrium value, we can now via the analysis conducted here, confirm that for this problem structure there are certain values of θ_a for which limitations are placed upon $\mathcal{N}_c$, $\mathcal{N}_r$ in order to obtain solutions. We note here, that the behaviour of this equilibrium point matches that of (4.3.13) considered for the original nondimensionalisation. Once more, it comments on unstable behaviour at the fin tip under very specific values of θ and θ'.

Case 2: Equilibrium point (4.3.14)

The eigenvalues of A at this equilibrium point are lengthy for arbitrary values of $\mathcal{N}_c, \mathcal{N}_r, r^*$ and θ_a. However, as before we realise that the eigenvalues would have the form,

$$\lambda_1 = \mu i, \qquad \lambda_2 = -\mu i, \qquad \text{where} \qquad i^2 = -1,$$

providing us with a stable centre - see the plot on the left of Figurse 4.2 and 4.3. In this instance we find that since $\theta_1 = \theta > 0$ we indeed have a physically relevant equilibrium point. We can in this fashion confirm that the boundary dynamics at the fin tip, i.e. for $\theta < 1$ and $\theta' = 0$, we indeed have stability.

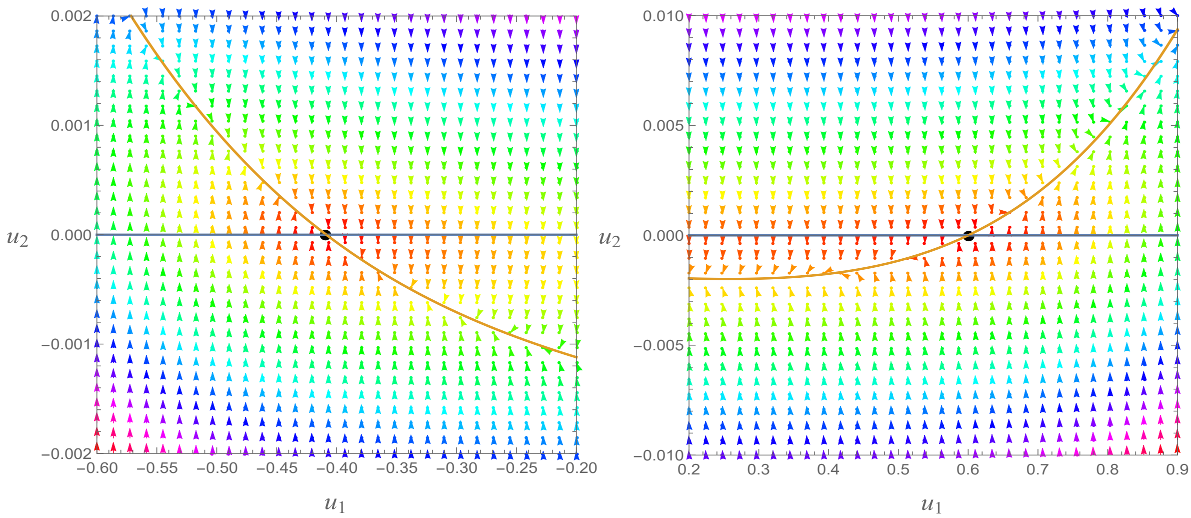

Fig. 4.2: *Phase plots indicating the trajectories around the equilibrium points (4.5.23) for $\theta_a = 0.6$, $r^* = 1.75$, $\mathcal{N}_c = 0.001$ and $\mathcal{N}_r = 0.1$. On the left is a closer view of the second equilibrium point for the alternate nondimensionalisation.*

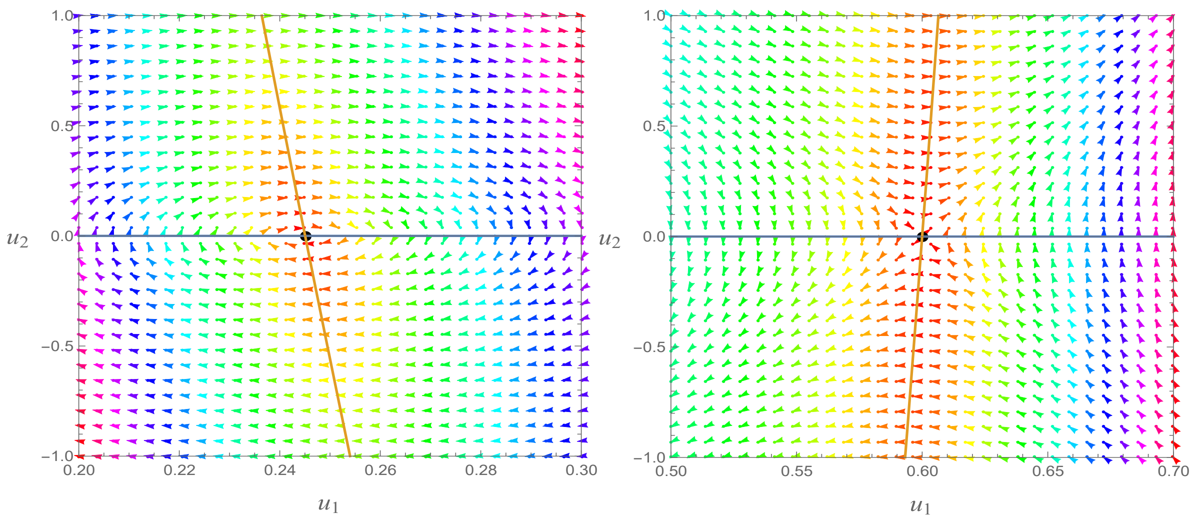

Fig. 4.3: *Phase plots indicating the trajectories around the equilibrium points (4.5.23) for $\theta_a = 0.6$, $r^* = 1.75$, $\mathcal{N}_c = 100$ and $\mathcal{N}_r = 100$. On the left is a closer view of the second equilibrium point for the alternate nondimensionalisation.*

4.5.1 Conclusion

This comparison to the equilibrium point $(0, 0)$ obtained is important given the numerical solutions we obtain for certain values of θ_a. While for the initial nondimensionalised equation considered, we were able to obtain solutions (whose behaviour provided sensible insight into the problem) for a range of values of θ_a, we were unable to do so in this instance. For $\theta_a > 0.4$ we found that the numerical solutions blew up numerically.

Next, we find that once we have defined the nonlinear parameters i.e. $\mathcal{N}_c$ and $\mathcal{N}_r$, to be relatively small we were able to obtain solutions for the equation under consideration (4.4.18) without any difficulty. In fact for the case $\mathcal{N}_c \leq 5$, we were able to obtain solutions for all values of the other parameters. Once $\theta_a > 0.4$, we found that there were values for $\mathcal{N}_c$ and $\mathcal{N}_r$ for which we could not obtain solutions.

In particular we noticed that as $\mathcal{N}_c \to \infty$, we needed $\mathcal{N}_r$ and θ_a to decrease in value in a comparative fashion: for $\mathcal{N}_c = 100$ with $\mathcal{N}_r = 0.5$, we could not obtain a solution to $\theta_a = 0.8$ but we could do so for $\theta_a = 0.1$. As such, rather than $\mathcal{N}_r$ being the dominant influencing factor with regards to instability as in the previous case of nondimensionalisation, we find that the value of $\mathcal{N}_c$ plays a more prominent role. It must also be noted that the intricate interaction between these three parameters makes it difficult to always isolate whether solutions can be obtained or not, unless they are all chosen to be small.

4.6 Conclusion

Upon investigating the dynamics of the system, we find that the equilibrium point $(0, 0)$ is an unstable saddle point, a result which also matches the behaviour of our numerical solutions. We find that for $\theta_1 = \theta_2 = 0$ we are in fact referring to the point where $\theta = \theta' = 0$, which is a point that would be located at the origin $r = 0$ (see the boundary conditions). We find that as $\mathcal{N}_r \to \infty$ that $\theta \to 0$ at the point where $\theta'(0) = 0$. Thus as $\mathcal{N}_r$ increases we would have a situation which reflects this equilibrium point. The numerical solutions to both schemes verify the instability of this equilibrium point, which only occurs for $\mathcal{N}_r \to \infty$: both schemes' solutions blow up numerically, producing negative temperature values at the origin and exaggerated negative temperature values at $r = 1$. As such, the impact of the nonlinear sink terms, in particular the term for which $\mathcal{N}_r$ is a coefficient, are not negligible.

Furthermore, via our analysis, we could ascertain the impact of $\mathcal{N}_r$, showing that as $\mathcal{N}_r \to \infty$ we observe erratic and unstable behaviour at the equilibrium point in question ($\theta \to 0$, $\theta'(0) = 0$) which represents the fin tip. This is sensible given that the relevant sink term in structure can lead to blow up were either the temperature in the fin or the ambient temperature to increase too drastically. The dynamics at the fin tip can be said to be stable in general however, since this instance would rarely occur.

We also compared the dynamics between the nondimensionalised equation introduced here and that considered in [1]. Considering the second form of nondimensionalisation, the equilibrium point $(\theta_a, 0)$ is found to be unstable as well. This case would correspond to an instance where the tip temperature is equated to the ambient temperature (to compare to the alternate case: we previously had an ambient temperature which corresponded to zero so this equilibrium point is equivalent to the one mentioned in the paragraph above). As such the dynamics at the fin tip can again be considered to be unstable under certain circumstances. We found that the buoyancy force had a more dominant role to play in the scheme's ability to obtain solutions. This seems reasonable given the nature of the higher order terms obtained where the terms tend to zero or are approximately 0.

The interesting additional insight with regards to the latter nondimensionalisation was that since $\theta_1 = \theta > 0$ we obtained a second physically relevant equilibrium point. The dynamical analysis conducted assisted us in confirming that the boundary dynamics at the fin tip, i.e. for $\theta < 1$ and $\theta' = 0$, are indeed stable. Given the other equilibrium point, it would seem however that for cases where $\theta = \theta_a$ we would revert to unstable behaviour at the fin tip. An interesting finding to note is that since in the latter nondimensionalised equation θ_a engages with both the buoyancy force/convection parameter and the radiation parameter in the equation, the dynamics are more intricate. As the convection increases, small values of the radiation parameter lead to no solution. Then as the latter increases the solution will achieve the ambient temperature at the fin tip.

As $\mathcal{N}_c \to \infty$ with small values of $\mathcal{N}_r$ leads to no solution. As $\mathcal{N}_r$ increases the tip temperature hits the ambient temperature. More complex dynamics since the θ_a and $\mathcal{N}_r$ engage in the situation for case 1; in the second Case $\mathcal{N}_r$ and $\mathcal{N}_c$ are both related to terms with θ_a. As such the values of θ_a has an impact creating a more intricate relationship. For both nondimensionalised equations we discovered that under certain circumstances there could be unstable behaviour at the fin tip; the convection and radiation parameter as well as the ambient temperature have a role to play regarding the stability and effectiveness of the numerical scheme employed. Future research will aim to establish the distinct manner in which these parameters interact, so that we may more fully understand the impact of the parameters on solution accuracy and stability.

Chapter 5

Crank-Nicolson Method

The work in this Chapter has been published in Advances in Mathematical Physics [47].

5.1 Introduction

Most differential equations cannot be analytically solved as these solutions are obtained through the simplification of the model, which are often physically unreasonable. Under such circumstances, we turn to numerical techniques to solve these differential equations. In the numerical investigation conducted here, we employ an efficient, accurate, extensively validated and unconditionally stable Crank-Nicolson method. This method was developed in the mid 20th century by Crank et al. [37] in order to evaluate numerical solutions for nonlinear partial differential equations. This method is implicit in time, often provides unconditional stability and has a high order of accuracy. The complexity of our problem lies in the nonlinear source terms and this will affect not only the stability of the scheme, but also the order of accuracy that the scheme can achieve.

We will then extend the scheme through the incorporation of a Newton-Raphson corrector given the pesence of the nonlinear sink terms. The concept of the Crank-Nicolson scheme combined with the Newton-Raphson method was implemented by Janssen et al. [39]. The Crank-Nicolson scheme was used to transform a system of differential equations into algebraic equations whereas the Newton-Raphson method was used to implicitly enhance the model's efficiency by improving the poor convergence rate. In a similar context, Qin et al. [40] used this scheme combination to model the heat flux and to estimate the evaporation in applied hydrology and meteorology. The Crank-Nicolson method was used to expand the differential equations whereas the iterative Newton-Raphson method was used to approximate latent heat flux and surface temperatures. Both these methods proved to be successful.

5.2 Crank-Nicolson Scheme

In all numerical solutions, the partial differential equation is replaced with a discrete approximation which is a finite number of points in the physical domain. Based on our partial different equation under consideration, we will reduce our problem to a discrete problem which we are able to solve by approximating all the derivatives using finite differences. We divide the domain in space using a mesh $r_0, r_1, r_2, \ldots, r_N$ and in time using a mesh $\tau_0, \tau_1, \tau_2, \ldots, \tau_m$. First, we assume a uniform partition both in space and time, so that the difference between two consecutive space points will be Δr and between two consecutive time points will be $\Delta\tau$ i.e.,

$$r_i = r_0 + i\Delta r \qquad i = 0, 1, \ldots, N;$$

$$\tau_j = \tau_0 + j\Delta\tau \qquad j = 0, 1, \ldots, m.$$

In terms of the finite difference schemes, we approximate $\frac{\partial\theta}{\partial\tau}$ using the forward time difference approximation at τ_m which gives,

$$\frac{\partial\theta}{\partial\tau} \approx \frac{\theta_n^{m+1} - \theta_n^m}{\Delta\tau}, \tag{5.2.1}$$

where $\Delta\tau$ is the step size in the time domain $\tau \geq 0$. Furthermore, we approximate the spatial terms $\frac{\partial\theta}{\partial r}$ and $\frac{\partial^2\theta}{\partial r^2}$ using the central difference approximations at r_n giving,

$$\frac{\partial\theta}{\partial r} \approx \frac{\theta_{n+1}^m - \theta_{n-1}^m}{2\Delta r}, \tag{5.2.2}$$

and,

$$\frac{\partial^2\theta}{\partial r^2} \approx \frac{\theta_{n+1}^m - 2\theta_n^m + \theta_{n-1}^m}{\Delta r^2}, \tag{5.2.3}$$

respectively, where Δr is the step size in the spatial domain $r \in [0, 1]$.

The Crank-Nicolson scheme makes use of approximations to values halfway between nodes by taking averages over two time points. Thus the finite difference approximations on the spatial terms are given by,

$$\frac{\partial\theta}{\partial r} \approx \frac{\theta_{n+1}^{m+1} - \theta_{n-1}^{m+1}}{4\Delta r} + \frac{\theta_{n+1}^m - \theta_{n-1}^m}{4\Delta r}, \tag{5.2.4}$$

and,

$$\frac{\partial^2\theta}{\partial r^2} \approx \frac{\theta_{n+1}^{m+1} - 2\theta_n^{m+1} + \theta_{n-1}^{m+1}}{2\Delta r^2} + \frac{\theta_{n+1}^m - 2\theta_n^m + \theta_{n-1}^m}{2\Delta r^2}. \tag{5.2.5}$$

Given our non-dimensional boundary conditions (2.14) and the finite difference approximation given by Equation (5.2.1) we find that,

$$\left.\frac{\partial\theta}{\partial r}\right|_{r_0=0} \implies \theta_1^m = \theta_{-1}^m \quad \forall m, \tag{5.2.6}$$

and,

$$\theta(1,\tau) = 1 \implies \theta_N^m = 1 \quad \forall m \quad \text{where} \quad r_N = 1. \tag{5.2.7}$$

The initial condition is given as,

$$\theta_n^0 = 0 \quad \forall n. \tag{5.2.8}$$

Having employed the Crank-Nicolson scheme on spatial terms and a forward difference approximation for the time derivative on Equation (2.13), we have,

$$\begin{aligned}\frac{\theta_n^{m+1} - \theta_n^m}{\Delta\tau} &= \frac{1}{(r_n(r^*-1)+1)(r^*-1)}\left[\frac{\theta_{n+1}^{m+1} - \theta_{n-1}^{m+1}}{4\Delta r} + \frac{\theta_{n+1}^{m} - \theta_{n-1}^{m}}{4\Delta r}\right] \\ &+ \frac{1}{(r^*-1)^2}\left[\frac{\theta_{n+1}^{m+1} - 2\theta_n^{m+1} + \theta_{n-1}^{m+1}}{2\Delta r^2} + \frac{\theta_{n+1}^{m} - 2\theta_n^{m} + \theta_{n-1}^{m}}{2\Delta r^2}\right] \\ &- \mathcal{N}_c\,(\theta_n^m)^2 - \mathcal{N}_r\,((\theta_n^m + \theta_a)^4 - \theta_a^4).\end{aligned} \tag{5.2.9}$$

It should be noticed that we have not applied the Crank-Nicolson method to the non-linear terms. At present, this is for simplicity sake, however this will be revisited in the next subsection. From Equation (5.2.9) we obtain,

$$\begin{aligned}\theta_n^{m+1} - \theta_n^m &= \frac{\Delta\tau}{(r_n(r^*-1)+1)(r^*-1)(4\Delta r)}\left[\theta_{n+1}^{m+1} - \theta_{n-1}^{m+1} + \theta_{n+1}^{m} - \theta_{n-1}^{m}\right] \\ &+ \frac{\Delta\tau}{2\Delta r^2(r^*-1)^2}\left[\theta_{n+1}^{m+1} - 2\theta_n^{m+1} + \theta_{n-1}^{m+1}\theta_{n+1}^{m} - 2\theta_n^{m} + \theta_{n-1}^{m}\right] \\ &- \Delta\tau\mathcal{N}_c\,(\theta_n^m)^2 - \Delta\tau\mathcal{N}_r\,((\theta_n^m + \theta_a)^4 - \theta_a^4).\end{aligned} \tag{5.2.10}$$

For the sake of simplicity we define,

$$\gamma_n = \frac{1}{(r_n(r^*-1)+1)(r^*-1)}.$$

Thus the partial differential equation can now be written as,

$$\begin{aligned}\theta_n^{m+1} - \theta_n^m = \frac{\Delta\tau\gamma_n}{4\Delta r}\left[\theta_{n+1}^{m+1} - \theta_{n-1}^{m+1} + \theta_{n+1}^{m} - \theta_{n-1}^{m}\right] + \frac{\Delta\tau}{2\Delta r^2(r^*-1)^2}\Big[\theta_{n+1}^{m+1} - 2\theta_n^{m+1} + \theta_{n-1}^{m+1} \\ + \theta_{n+1}^{m} - 2\theta_n^{m} + \theta_{n-1}^{m}\Big] - \Delta\tau\mathcal{N}_c\,(\theta_n^m)^2 - \Delta\tau\mathcal{N}_r\,((\theta_n^m + \theta_a)^4 - \theta_a^4),\end{aligned} \tag{5.2.11}$$

For further simplification we define,

$$\alpha_n = \frac{\Delta\tau\gamma_n}{4\Delta r} + \frac{\Delta\tau}{2\Delta r^2(r^*-1)^2}, \qquad \sigma = \frac{\Delta\tau}{\Delta r^2(r^*-1)^2}, \qquad \beta_n = -\frac{\Delta\tau\gamma_n}{4\Delta r} + \frac{\Delta\tau}{2\Delta r^2(r^*-1)^2},$$

which allows us to write Equation (5.2.11) as follows,

$$\begin{aligned}&-\alpha_n\,\theta_{n+1}^{m+1} \;+\; (1+\delta)\,\theta_n^{m+1} - \beta_n\,\theta_{n-1}^{m+1}\\ &= \alpha_n\,\theta_{n+1}^{m} \;+\; (1-\delta)\,\theta_n^{m} + \beta_n\,\theta_{n-1}^{m} - \Delta\tau\mathcal{N}_c\,(\theta_n^m)^2 - \Delta\tau\mathcal{N}_r\,((\theta_n^m+\theta_a)^4 - \theta_a^4).\end{aligned} \tag{5.2.12}$$

This equation can be given in the following matrix notation,

$$\begin{bmatrix} (1+\delta) & -\alpha_0-\beta_0 & 0 & 0 & \dots & 0\\ -\beta_1 & (1+\delta) & -\alpha_1 & 0 & \dots & 0\\ 0 & -\beta_2 & (1+\delta) & -\alpha_2 & \ddots & 0\\ \vdots & \ddots & \ddots & \ddots & \ddots & \vdots\\ 0 & \ddots & \ddots & -\beta_{N-2} & (1+\delta) & -\alpha_{N-2}\\ 0 & \ddots & \ddots & \ddots & -\beta_{N-1} & (1+\delta) \end{bmatrix} \begin{bmatrix} \theta_0^{m+1}\\ \theta_1^{m+1}\\ \theta_2^{m+1}\\ \vdots\\ \theta_{N-2}^{m+1}\\ \theta_{N-1}^{m+1} \end{bmatrix}$$

$$= \begin{bmatrix} (1-\delta) & \alpha_0+\beta_0 & 0 & 0 & \dots & 0\\ \beta_1 & (1-\delta) & \alpha_1 & 0 & \dots & 0\\ 0 & \beta_2 & (1-\delta) & \alpha_2 & \ddots & 0\\ \vdots & \ddots & \ddots & \ddots & \ddots & \vdots\\ 0 & \ddots & \ddots & \beta_{N-2} & (1-\delta) & \alpha_{N-2}\\ 0 & \ddots & \ddots & \ddots & \beta_{N-1} & (1-\delta) \end{bmatrix} \begin{bmatrix} \theta_0^{m}\\ \theta_1^{m}\\ \theta_2^{m}\\ \vdots\\ \theta_{N-2}^{m}\\ \theta_{N-1}^{m} \end{bmatrix}$$

$$+\begin{bmatrix} -\Delta\tau\,\mathcal{N}_r((\theta_0^m+\theta_a)^4-\theta_a^4)-\Delta\tau\,\mathcal{N}_c\,(\theta_0^m)^2 \\ -\Delta\tau\,\mathcal{N}_r((\theta_1^m+\theta_a)^4-\theta_a^4)-\Delta\tau\,\mathcal{N}_c\,(\theta_1^m)^2 \\ -\Delta\tau\,\mathcal{N}_r((\theta_2^m+\theta_a)^4-\theta_a^4)-\Delta\tau\,\mathcal{N}_c\,(\theta_2^m)^2 \\ \vdots \\ \vdots \\ -\Delta\tau\,\mathcal{N}_r((\theta_{N-2}^m+\theta_a)^4-\theta_a^4)-\Delta\tau\,\mathcal{N}_c\,(\theta_{N-2}^m)^2 \\ -\Delta\tau\,\mathcal{N}_r((\theta_{N-1}^m+\theta_a)^4-\theta_a^4)-\Delta\tau\,\mathcal{N}_c\,(\theta_{N-1}^m)^2-2\alpha_{N-1} \end{bmatrix}.$$

5.3 Crank-Nicolson scheme: Newton-Raphson and Usmani Method

In numerical computation, a predictor-corrector method is an algorithm that implements two steps. First, the prediction step calculates a rough approximation of the desired quantity whereas the second step refines the initial approximation using other means. The Crank-Nicolson with the Newton-Raphson method has been used to determine the solution of a nonlinear diffusion equation by Kouhia [63], which proved to be efficient as per the numerical results obtained. Furthermore, Habibi et al. [64] used the numerical method to model the electron heat transfer process in laser inertial fusion for the energy transport mechanism from the region of energy decomposition into the ablation surface.

In this research we will require such a technique given the presence of the nonlinear sink terms, known as the Newton-Raphson method. In this manner the nonlinear term on the $m+1^{th}$ level will be dealt with through an implementation of the Newton method [65] in an iterative fashion as done by Britz et al. [66] and discussed in [67]. This method has been known for its fast convergence to the root as well as its dependence on the initial condition. Furthermore, in order to find the explicit inverse of a general tridiagonal matrix, we shall implement Usmani's method [68].

5.3.1 Implementation

In this section we employ the Crank-Nicolson method for the nonlinear source terms as well. As such we rewrite our scheme Equation (2.13) as follows,

$$\begin{aligned}
\frac{\theta_n^{m+1}-\theta_n^m}{\Delta\tau} &= \frac{1}{(r_n(r^*-1)+1)(r^*-1)}\Big[\frac{\theta_{n+1}^{m+1}-\theta_{n-1}^{m+1}}{4\Delta r}+\frac{\theta_{n+1}^{m}-\theta_{n-1}^{m}}{4\Delta r}\Big] \\
&+\frac{1}{(r^*-1)^2}\Big[\frac{\theta_{n+1}^{m+1}-2\theta_n^{m+1}+\theta_{n-1}^{m+1}}{2\Delta r^2}+\frac{\theta_{n+1}^{m}-2\theta_n^{m}+\theta_{n-1}^{m}}{2\Delta r^2}\Big] \\
&-\frac{\mathcal{N}_c}{2}\left(((\theta_n^{m+1})^2)+(\theta_n^m)^2\right)-\frac{\mathcal{N}_r}{2}\left((\theta_n^{m+1}+\theta_a)^4-\theta_a^4+(\theta_n^m+\theta_a)^4-\theta_a^4\right).
\end{aligned} \tag{5.3.1.13}$$

Again we define the following,

$$\gamma_n = \frac{1}{(r_n(r^*-1)+1)(r^*-1)}, \qquad \alpha_n = \frac{\Delta\tau\gamma_n}{4\Delta r}+\frac{\Delta\tau}{2\Delta r^2(r^*-1)^2},$$

$$\sigma = \frac{\Delta\tau}{\Delta r^2(r^*-1)^2}, \qquad \beta_n = -\frac{\Delta\tau\gamma_n}{4\Delta r}+\frac{\Delta\tau}{2\Delta r^2(r^*-1)^2}.$$

Thus the partial differential equation reduces to,

$$\begin{aligned}
&-\alpha_n\,\theta_{n+1}^{m+1} + (1+\delta)\,\theta_n^{m+1}-\beta_n\,\theta_{n-1}^{m+1}+\frac{\Delta\tau\mathcal{N}_c}{2}\left((\theta_n^{m+1})^2\right)+\frac{\Delta\tau\mathcal{N}_r}{2}\left((\theta_n^{m+1}+\theta_a)^4-\theta_a^4\right) \\
&=\alpha_n\,\theta_{n+1}^{m} + (1-\delta)\,\theta_n^{m}+\beta_n\,\theta_{n-1}^{m}-\frac{\Delta\tau\mathcal{N}_c}{2}\left((\theta_n^{m})^2\right)-\frac{\Delta\tau\mathcal{N}_r}{2}\left((\theta_n^{m}+\theta_a)^4-\theta_a^4\right).
\end{aligned} \tag{5.3.1.14}$$

In matrix notation,

$$
\begin{bmatrix}
(1+\delta) & -\alpha_0-\beta_0 & 0 & 0 & \dots & 0 \\
-\beta_1 & (1+\delta) & -\alpha_1 & 0 & \dots & 0 \\
0 & -\beta_2 & (1+\delta) & -\alpha_2 & \ddots & 0 \\
\vdots & \ddots & \ddots & \ddots & \ddots & \vdots \\
0 & \ddots & \ddots & -\beta_{N-2} & (1+\delta) & -\alpha_{N-2} \\
0 & \ddots & \ddots & \ddots & -\beta_{N-1} & (1+\delta)
\end{bmatrix}
\begin{bmatrix}
\theta_0^{m+1} \\ \theta_1^{m+1} \\ \theta_2^{m+1} \\ \vdots \\ \theta_{N-2}^{m+1} \\ \theta_{N-1}^{m+1}
\end{bmatrix}
$$

$$
+\begin{bmatrix}
\frac{\Delta\tau\,\mathcal{N}_r}{2}((\theta_0^{m+1}+\theta_a)^4-\theta_a^4)+\frac{\Delta\tau\,\mathcal{N}_c}{2}\,((\theta_0^{m+1})^2) \\
\frac{\Delta\tau\,\mathcal{N}_r}{2}((\theta_1^{m+1}+\theta_a)^4-\theta_a^4)+\frac{\Delta\tau\,\mathcal{N}_c}{2}((\theta_1^{m+1})^2) \\
\frac{\Delta\tau\,\mathcal{N}_r}{2}((\theta_2^{m+1}+\theta_a)^4-\theta_a^4)+\frac{\Delta\tau\,\mathcal{N}_c}{2}\,((\theta_2^{m+1})^2) \\
\vdots \\
\vdots \\
\frac{\Delta\tau\,\mathcal{N}_r}{2}((\theta_{N-2}^{m+1}+\theta_a)^4-\theta_a^4)+\frac{\Delta\tau\,\mathcal{N}_c}{2}\,((\theta_{N-2}^{m+1})^2) \\
\frac{\Delta\tau\,\mathcal{N}_r}{2}((\theta_{N-1}^{m+1}+\theta_a)^4-\theta_a^4)+\frac{\Delta\tau\,\mathcal{N}_c}{2}\,((\theta_{N-1}^{m+1})^2)
\end{bmatrix}
$$

$$
=\begin{bmatrix}
(1-\delta) & \alpha_0+\beta_0 & 0 & 0 & \dots & 0 \\
\beta_1 & (1-\delta) & \alpha_1 & 0 & \dots & 0 \\
0 & \beta_2 & (1-\delta) & \alpha_2 & \ddots & 0 \\
\vdots & \ddots & \ddots & \ddots & \ddots & \vdots \\
0 & \ddots & \ddots & \beta_{N-2} & (1-\delta) & \alpha_{N-2} \\
0 & \ddots & \ddots & \ddots & \beta_{N-1} & (1-\delta)
\end{bmatrix}
\begin{bmatrix}
\theta_0^{m} \\ \theta_1^{m} \\ \theta_2^{m} \\ \vdots \\ \theta_{N-2}^{m} \\ \theta_{N-1}^{m}
\end{bmatrix}
$$

$$
+\begin{bmatrix}
-\frac{\Delta\tau\,\mathcal{N}_r}{2}((\theta_0^m+\theta_a)^4-\theta_a^4)-\frac{\Delta\tau\,\mathcal{N}_c}{2}\,((\theta_0^m)^2) \\
-\frac{\Delta\tau\,\mathcal{N}_r}{2}((\theta_1^m+\theta_a)^4-\theta_a^4)-\frac{\Delta\tau\,\mathcal{N}_c}{2}((\theta_1^m)^2) \\
-\frac{\Delta\tau\,\mathcal{N}_r}{2}((\theta_2^m+\theta_a)^4-\theta_a^4)-\frac{\Delta\tau\,\mathcal{N}_c}{2}\,((\theta_2^m)^2) \\
\vdots \\
\vdots \\
-\frac{\Delta\tau\,\mathcal{N}_r}{2}((\theta_{N-2}^m+\theta_a)^4-\theta_a^4)-\frac{\Delta\tau\,\mathcal{N}_c}{2}\,((\theta_{N-2}^m)^2) \\
-\frac{\Delta\tau\,\mathcal{N}_r}{2}((\theta_{N-1}^m+\theta_a)^4-\theta_a^4)-\frac{\Delta\tau\,\mathcal{N}_c}{2}\,((\theta_{N-1}^m)^2)+2\alpha_{N-1}
\end{bmatrix}.
$$

We obtain an approximation for the nonlinear vector at the $(m+1)^{th}$ time level in an iterative fashion as done by Britz et al. [67]. The system $\mathbf{J}\delta\mathbf{u}=-\mathbf{F}(\mathbf{u})$ given by,

$$
\begin{bmatrix}
\begin{matrix}(1+\delta)+\Delta\tau\mathcal{N}_c\theta_0^{m+1}\\+2\Delta\tau\mathcal{N}_r(\theta_0^{m+1}-\theta_a)^3\end{matrix} & -\alpha_0-\beta_0 & 0 & \cdots & 0 \\
-\beta_1 & \begin{matrix}(1+\delta)+\Delta\tau\mathcal{N}_c\theta_1^{m+1}\\+2\Delta\tau\mathcal{N}_r(\theta_1^{m+1}-\theta_a)^3\end{matrix} & -\alpha_1 & \cdots & 0 \\
\vdots & \ddots & \ddots & \ddots & \vdots \\
0 & \ddots & \ddots & \begin{matrix}(1+\delta)+\Delta\tau\mathcal{N}_c\theta_{N-2}^{m+1}\\+2\Delta\tau\mathcal{N}_r(\theta_{N-2}^{m+1}-\theta_a)^3\end{matrix} & -\alpha_{N-2} \\
0 & \ddots & \ddots & -\beta_{N-1} & \begin{matrix}(1+\delta)+\Delta\tau\mathcal{N}_c\theta_{N-1}^{m+1}\\+2\Delta\tau\mathcal{N}_r(\theta_{N-1}^{m+1}-\theta_a)^3\end{matrix}
\end{bmatrix}
\begin{bmatrix}
\delta S_0 \\ \delta S_1 \\ \delta S_2 \\ \vdots \\ \delta S_{N-2} \\ \delta S_{N-1}
\end{bmatrix}
$$

$$
=\begin{bmatrix}
(\alpha_0+\beta_0)\;\theta_1^m\;+\;(1-\sigma)\;\theta_0^m-\frac{\Delta\tau\mathcal{N}_c}{2}\;(\theta_0^m)^2-\frac{\Delta\tau\mathcal{N}_r}{2}\;((\theta_0^m+\theta_a)^4-\theta_a^4) \\
\alpha_1\;\theta_2^m\;+\;(1-\sigma)\;\theta_1^m+\beta_1\;\theta_0^m-\frac{\Delta\tau\mathcal{N}_c}{2}\;(\theta_1^m)^2-\frac{\Delta\tau\mathcal{N}_r}{2}\;((\theta_1^m+\theta_a)^4-\theta_a^4) \\
\vdots \\
\vdots \\
\alpha_{N-2}\;\theta_{N-1}^m\;+\;(1-\sigma)\;\theta_{N-2}^m+\beta_{N-2}\;\theta_{N-3}^m-\frac{\Delta\tau\mathcal{N}_c}{2}\;(\theta_{N-2}^m)^2-\frac{\Delta\tau\mathcal{N}_r}{2}\;((\theta_{N-2}^m+\theta_a)^4-\theta_a^4) \\
(1-\sigma)\;\theta_{N-1}^m+\beta_{N-1}\;\theta_{N-2}^m-\frac{\Delta\tau\mathcal{N}_c}{2}\;(\theta_{N-1}^m)^2-\frac{\Delta\tau\mathcal{N}_r}{2}\;((\theta_{N-1}^m+\theta_a)^4-\theta_a^4)+2\alpha_{N-1}
\end{bmatrix},
$$

is solved where $\mathbf{F}$ is the set of difference equations created as per Equation (5.3.1.14) such that $\mathbf{F}(\mathbf{u})=0$. The starting vector at $t=0$ is chosen as per the initial condition

(5.2.8) such that $\mathbf{u} = 0$. The Newton iteration converges within 2-3 steps given that changes are usually relatively small.

The computational time required for the convergence of the Crank-Nicolson method incorporating the Newton-Raphson method was found to be extremely slow, making the method impracticable and infeasible. We discovered that this was due to the fact that the Jacobian $\mathbf{J}$ is either close to being singular or badly scaled. As such, we decided to implement Usmani's method, which is a simple algorithm for finding the explicit inverse of a general Jacobi tridiagonal matrix [68]. This provided the results which we expected, however we still found that the computational time taken by the method to reach convergence proved inefficient.

5.4 Results

In Section 5.4.1, we compare the results we obtained via our two numerical methods i.e. the Crank-Nicolson scheme (CN) and the Crank-Nicolson scheme incorporating the Newton-Raphson predictor corrector and Usmani method (CN^{NR}). The results obtained via these two numerical schemes is also compared to the solution obtained as per the work of Darvishi et al. [1] and the Differential Transformation Method discussed in Section 5.4.2.

5.4.1 Comparison of numerical schemes

It is important to note that in comparison to the solution observed in Darvishi et al. [1], only the Crank-Nicolson scheme matches the results and behaviour obtained of the solution. The Crank-Nicolson scheme with the Newton-Raphson and Usmani method provides appropriate behaviour, however, the value at the origin cannot be accurately evaluated so as to compare to [1]; this inability is attributed to the length of computational time required for convergence. We provide values which indicate that the method can converge appropriately, but in conclusion the second method is not efficient in terms of running time.

In order to make a comparison between the two numerical schemes we have employed, we allow our numerical schemes to iterate for large time - termed T - so that we allow for convergence to a steady state. In this instance we find that convergence has occurred for the Crank-Nicolson scheme at $T = 1$, however this is not the case for the Crank-Nicolson method with predictor corrector. To maintain our CFL number as less than one for stability purposes, we choose $\triangle r = 0.1$ and $\triangle t = 0.0001$. As can be surmised, the consequence of this is that the Crank-Nicolson scheme, which employs the Newton-Raphson method as a means of updating the nonlinear terms, requires a lot of computational time.

The two numerical schemes produce solutions similar in shape and behaviour but there are discrepancies when we consider the errors between the methods. The temperature at the origin, i.e. $\theta(0)$, is often not the same across the two methods - see Tables 5.1 - 5.4. Taking into consideration the temperature at the fin tip, we find that the solutions do not converge to the same value of θ_0 for set parameter values, nor do these solutions converge at the same rate. In the figures which follow we employ the Crank-Nicolson method without the predictor corrector method due to the speed with which it is able to reach convergence, and its accuracy upon comparison with the work by Darvishi et al. [1].

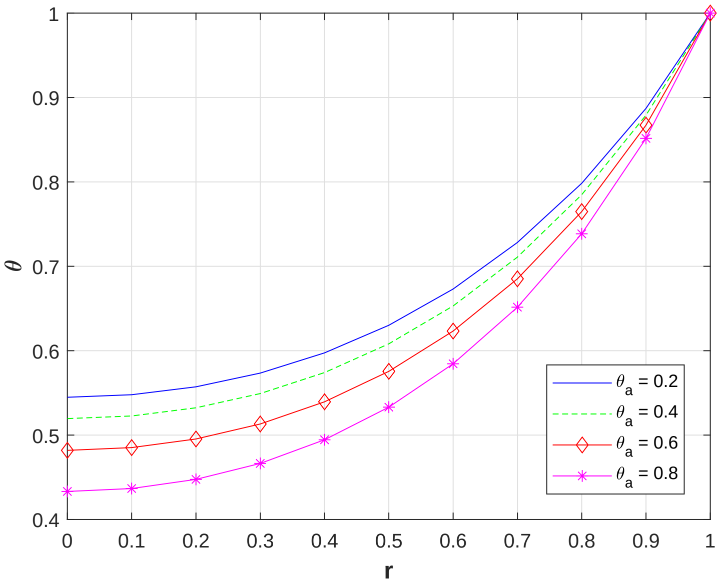

Fig. 5.1: *Plot of the temperature with* $\mathcal{N}_r = 1$*,* $\mathcal{N}_c = 10$ *and* $r^* = \frac{1}{1.75}$ *for* $T = 1$ *and varied values of* θ_a*.*

Table 5.1: *Maximum error computed between the respective numerical solutions obtained, where* $\mathcal{E} = Max\left|CN_{sol} - CN_{sol}^{NR}\right|$ *and their respective temperatures at the tip of the fin for varied values of* θ_a*.*

θ_a	$\mathcal{E}$	θ_0^{CN}	θ_0^{NR}
0.2	0.12845	0.54482	0.67327
0.4	0.13031	0.51860	0.64891
0.6	0.16803	0.48088	0.61438
0.8	0.13723	0.43321	0.57044
Parameter values: $\mathcal{N}_c = 10$	$\mathcal{N}_r = 1$	$r^* = \frac{1}{1.75}$	$T = 1$

While there are discrepancies we can see behaviour patterns emerging from the different solutions. In Figure 5.1 as well as Table 5.1 we observe that an increase in the dimensionless ambient temperature, leads to a decrease in the tip temperature; however this can be misleading. We note, as before, that the dimensionless ambient temperature θ_a is defined as $\frac{T_a}{T_b}$ in the work of Darvishi et al. [1]. In this work we altered our nondimensionalisation to define θ_a as $\frac{T_a}{T_b - T_a}$, as above. This change in ratio impacts on the behaviour observed by the solution with regards to changes in the value of θ_a. Instead of a linear relationship between T_a and θ_a we have a nonlinear one given by $T_a = \frac{\theta_a T_b}{1+\theta_a}$, such that the behaviour inversely corresponds to that of Darvishi et al. [1]. Hence, our results are consistent with the physical dynamics of the problem.

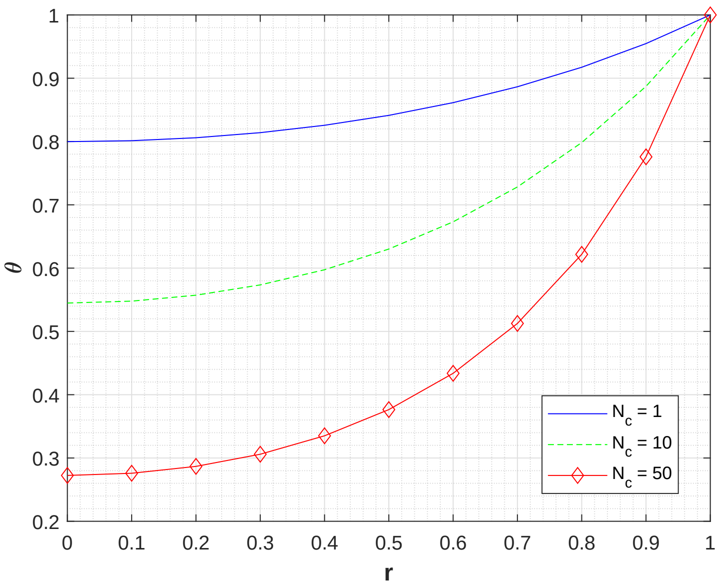

Fig. 5.2: *Plot of the temperature with* $\theta_a = 0.2$, $r^* = \frac{1}{1.75}$ *and* $\mathcal{N}_r = 1$ *for* $T = 1$ *and varied values of* $\mathcal{N}_c$.

Table 5.2: *Maximum error computed between the respective numerical solutions obtained, where* $\mathcal{E} = Max\left|CN_{sol} - CN_{sol}^{NR}\right|$ *and their respective temperatures at the tip of the fin for varied values of* $\mathcal{N}_c$.

$\mathcal{N}_c$	$\mathcal{E}$	θ_0^{CN}	θ_0^{NR}
1	0.07624	0.79980	0.87604
10	0.12845	0.54482	0.67327
50	0.11453	0.27244	0.38697
Parameter values: $\theta_a = 0.2$	$\mathcal{N}_r = 1$	$r^* = \frac{1}{1.75}$	$T = 1$

A consideration of Figure 5.2 and Table 5.2 shows the effect of the natural convection heat loss ($\mathcal{N}_c$) on the temperature distribution in the fin for set parameter values. As the buoyancy effect increases, i.e. $\mathcal{N}_c$, the local temperature in the fin θ decreases.

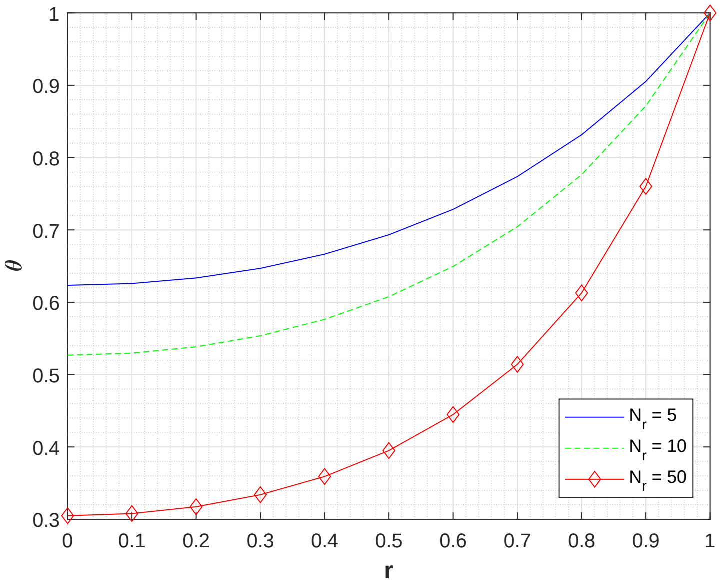

Fig. 5.3: *Plot of the temperature with* $\theta_a = 0.2$, $r^* = \frac{1}{1.75}$ *and* $\mathcal{N}_c = 1$ *for* $T = 100$ *and varied values of* $\mathcal{N}_r$.

Table 5.3: *Maximum error computed between the respective numerical solutions obtained, where* $\mathcal{E} = Max\left|CN_{sol} - CN_{sol}^{NR}\right|$ *and their respective temperatures at the tip of the fin for varied values of* $\mathcal{N}_r$.

$\mathcal{N}_r$		$\mathcal{E}$	θ_0^{CN}	θ_0^{NR}
5		0.10318	0.62343	0.72661
10		0.10698	0.52686	0.63384
50		0.09496	0.30490	0.39982
Parameter values: $\theta_a = 0.2$		$r^* = \frac{1}{1.75}$	$\mathcal{N}_c = 1$	$T = 100$

Similarly, for Figure 5.3 and Table 5.3 the increasing surface radiative heat transfer from the fin to the ambient fluid, i.e. $\mathcal{N}_r$, leads to a decrease in the local fin temperature θ. This in indicative of the effect of natural convective heat loss on the temperature distribution in the fin when the radiation heat loss, the environment temperature, and the ratio of inner to outer radius are kept fixed. Since buoyancy is principally a macro scale effect we see that the buoyancy force ($\mathcal{N}_c$) influences the velocity and temperature fields. Furthermore, the impact of radiation ($\mathcal{N}_r$) influences the temperature field by increasing the heat transfer rates from the surface. We find that when the convection parameter ($\mathcal{N}_c$) and the radiation parameter ($\mathcal{N}_r$) are allowed to vary, the local fin temperature decreases because of the increasing strength of radiative heat exchange between the exposed surface of the fin and the ambient [1].

Table 5.4: *Maximum error computed between the respective numerical solutions obtained, where* $\mathcal{E} = Max\left|CN_{sol} - CN_{sol}^{NM}\right|$, *and their respective temperatures at the tip of the fin, given as* θ_0, *for varied values of* r^*.

r^*	$\mathcal{E}$	θ_0^{CN}	θ_0^{NR}
0.2	0.10849	0.27903	0.38752
0.4	0.12751	0.40088	0.52840
0.6	0.12615	0.57382	0.69998
0.8	0.07434	0.81944	0.89379
Parameter values: $\theta_a = 0.2$	$\mathcal{N}_r = 1$	$\mathcal{N}_c = 10$	$T = 1$

Table 5.4 displays the heat transfer rates versus the ambient temperature with the ratio of the tip radius to base radius (r^*) as a parameter. We observe that the heat transfer increases with increasing (r^*) which is due to the increased heat transfer area as (r^*) increases. Furthermore, it should be noted that as the ambient temperature increases, the heat transfer rate decreases. This is expected as the driving force for the heat transfer decreases as θ_a increases.

5.4.2 Comparison of the numerical results to semi-analytical solution

In this section, we compare the results we obtained via our two numerical methods against the series solution obtained for the steady state. We calculate a polynomial of degree $n = 10$ via the DTM, and also consider the work in [1] to be a benchmark. We find that all three solutions perform well, however only the Crank-Nicolson scheme performs as accurately and efficiently as required.

Table 5.5: *Numerical solutions obtained for DTM and the maximum error computed between the DTM solution and the respective numerical solutions obtained, where* $\mathcal{E}^{CN} = Max\left|CN_{sol} - DTM_{sol}\right|$ *and* $\mathcal{E}^{NR} = Max\left|CN_{sol}^{NR} - DTM_{sol}\right|$ *for varied values of* $\mathcal{N}_c$.

θ_a	θ_0^{DTM}	$\mathcal{E}^{CN}$	$\mathcal{E}^{NR}$
0.2	0.55725	0.01284	0.11602
0.4	0.54037	0.02087	0.10919
0.6	0.51752	0.03561	0.09758
0.8	0.49348	0.06028	0.07696
Parameter values: $\mathcal{N}_c = 10$	$\mathcal{N}_r = 1$	$r^* = \frac{1}{1.75}$	$T = 5$

It can be seen in Table 5.5, for increasing θ_a, that both the DTM solution and the error produced between the DTM and the Crank-Nicolson scheme increases, whereas the error between DTM and the Crank-Nicolson with the Newton-Raphson predictor corrector decreases.

Table 5.6: *Numerical solutions obtained for DTM and the maximum error computed between the respective numerical solutions obtained, where* $\mathcal{E}^{CN} = Max\left|CN_{sol} - DTM_{sol}\right|$ *and* $\mathcal{E}^{NR} = Max\left|CN_{sol}^{NR} - DTM_{sol}\right|$ *and their respective temperatures at the tip of the fin for varied values of* $\mathcal{N}_c$.

$\mathcal{N}_c$	θ_0^{DTM}	$\mathcal{E}^{CN}$	$\mathcal{E}^{NR}$
1	0.81615	0.01635	0.05989
10	0.55725	0.01284	0.11602
50	0.27747	0.01177	0.10950
Parameter values: $\theta_a = 0.2$	$\mathcal{N}_r = 1$	$r^* = \frac{1}{1.75}$	$T = 5$

Table 5.7: *Numerical solutions obtained for DTM and the maximum error computed between the respective numerical solutions obtained, where* $\mathcal{E}^{CN} = Max\left|CN_{sol} - DTM_{sol}\right|$ *and* $\mathcal{E}^{NR} = Max\left|CN_{sol}^{NR} - DTM_{sol}\right|$ *and their respective temperatures at the tip of the fin for varied values of* $\mathcal{N}_c$.

$\mathcal{N}_r$	θ_0^{DTM}	$\mathcal{E}^{CN}$	$\mathcal{E}^{NR}$
1	0.81615	0.016720	0.04911
5	0.66993	0.047281	0.03450
10	0.59043	0.06465	0.01524
Parameter values: $\theta_a = 0.2$	$r^* = \frac{1}{1.75}$	$\mathcal{N}_c = 1$	$T = 100$

Tables 5.6 indicates that the temperature at the tip of the fin for both the Crank-Nicolson and the Crank-Nicolson with the Newton-Raphson method agree to the first

decimal place only. Furthermore, it can be seen that for increasing values of $\mathcal{N}_c$, the error between the DTM and the Crank-Nicolson method decreases when $T = 5$; in turn Table 5.7 indicates that for increasing values of $\mathcal{N}_r$ at $T = 100$ we obtain an increase in the error. These relationships are inverted when considering the comparison between the semi-analytical solution and the Crank-Nicolson scheme with the predictor corrector: it increases for increasing values of $\mathcal{N}_c$ at $T = 5$ and decreases for increasing values of $\mathcal{N}_r$ at $T = 100$.

Table 5.8: *Numerical solutions obtained for DTM and the maximum error computed between the respective numerical solutions obtained, where* $\mathcal{E}^{CN} = Max\,|CN_{sol} - DTM_{sol}|$ *and* $\mathcal{E}^{NR} = Max\,\left|CN_{sol}^{NR} - DTM_{sol}\right|$ *and their respective temperatures at the tip of the fin, given as* θ_0*, for varied values of* r^**.*

r^*	θ_0^{DTM}	$\mathcal{E}^{CN}$	$\mathcal{E}^{NR}$
0.2	0.30038	0.05459	0.07799
0.4	0.41843	0.02504	0.09325
0.6	0.58528	0.01230	0.08572
0.8	0.82286	0.00361	0.02814
Parameter values: $\theta_a = 0.2$	$\mathcal{N}_r = 1$	$\mathcal{N}_c = 10$	$T = 100$

It can be seen in Table 5.8, for increasing r^*, that the DTM solution increases but the error produced between the DTM and the Crank-Nicolson scheme decreases. The error between DTM and the Crank-Nicolson with the Newton-Raphson predictor corrector initially increases for $r^* = 0.2, 0.4$ but thereafter decreases for $r^* = 0.6, 0.8$.

5.5 Conclusion

We employed the Crank-Nicolson method via the Usmani method, with and without the Newton-Raphson predictor corrector, to solve a model describing the heat transfer in a porous radial fin. We compared the results we obtained via the two numerical schemes, and also contrasted them with the steady state solution. Furthermore, we show that the results obtained match those in the work by Darvishi et al.[1]; the Crank-

Nicolson method, incorporating the Newton-Raphson and Usmani method, does not match these results even though the behaviour observed is appropriate and comparable. As mentioned, this is due to the fact that the Jacobian required for the predictor-corrector method is heavily influenced since it is close to singular or badly scaled.

Given the solutions obtained in Darvishi et al. [1] the error we obtained when comparing our numerical solutions to the DTM may be due to a poor approximation of this series solution. Due to computational limitations we are able to obtain a limited number of terms before a lack of memory becomes an issue; $n = 10$ are very few terms if one considers the work of other authors such as Darvishi et al. [1] and Aziz et al. [27] for instance.

The results obtained by Darvishi et al. [1] confirm that the Crank-Nicolson scheme produces accurate solutions efficiently. Unfortunately the addition of a Newton-Raphson predictor corrector slows the scheme down excessively. By increasing T one can see that the scheme does tend to the values obtained by the Crank-Nicolson method alone however, in terms of computational efficiency, the Crank-Nicolson with Newton-Raphson predictor corrector has shown itself inappropriate.

Chapter 6

Numerical Well-Balancing Scheme

6.1 Introduction

By making use of numerical schemes as a solution method, it is crucial to identify that the proper numerical treatment of the source terms may eliminate possible spurious steady-sate numerical solutions. In this chapter we will focus on the appropriate treatment of the source terms and provide a numerical approach that effectively deals with the proper form of the porous radial fin and solve, via the Well-Balancing numerical scheme, the problem of heat transfer in such a fin. In order to develop this approach, we use a finite volume method to illustrate how it reduces the order of differentiation by one. Thereafter, by using volume averaging and the Taylor series expansion, we establish a numerical balance law. Based on the balance law and information obtained through a consideration of the steady-state equation, which in turn is incorporated into the transient heat transfer equation, we obtain a Well-Balancing scheme that maintains steady-state solutions.

This scheme has been shown to effectively and efficiently obtain results for rectangular fin profiles - see [41, 36, 42]. In the work of Rusgara et al. [43], the Well-Balancing scheme has been used to solve a nonlinear partial differential equation modeling the temperature distribution in a triangular fin without requiring any additional assumptions or simplifications of the fin profile.

6.2 Numerical Approach

6.2.1 The Finite Volume Method and Numerical Balance Law

In this section, we introduce the finite volume method (FVM) and stipulate the advantages of this method within the context of the heat transfer problem posed in this thesis. In this scenario, the FVM reduces the order of the spatial derivative by one which motivates its use for the equation under consideration given the presence of the nonlinear source terms. We consider a partial differential equation of the form,

$$\frac{\partial \theta}{\partial \tau} - c(r)\frac{\partial}{\partial r}\Big(Q(r,\theta)\frac{\partial \theta}{\partial r}\Big) = R(\theta), \tag{6.2.1.1}$$

where $c(r)$ is a function of r and $Q(r,\theta)$ is a function of r and θ. According to the framework of the finite volume scheme, we divide the domain in space using a mesh $r_0, r_1, r_2, \dots, r_N$ and in time using a mesh $\tau_0, \tau_1, \tau_2, \dots, \tau_m$. In the following, we will assume, for simplicity, that all the cells have the same lengths $\Delta r = r_{i+\frac{1}{2}} - r_{i-\frac{1}{2}}$ for $i = 0, 1, \dots, N$ and $\Delta \tau = \tau_{j+\frac{1}{2}} - \tau_{j-\frac{1}{2}}$ for $j = 0, 1, \dots, m$.

In order to reduce the order of the spatial derivatives by one, we integrate Equation (6.2.1.1) over the grid cell $[r_{i-\frac{1}{2}}, r_{i+\frac{1}{2}}]$ to obtain,

$$\int_{r_{i-\frac{1}{2}}}^{r_{i+\frac{1}{2}}} \frac{\partial \theta}{\partial \tau} dr - \int_{r_{i-\frac{1}{2}}}^{r_{i+\frac{1}{2}}} c(r)\frac{\partial}{\partial r}\Big(Q(r,\theta)d(r)\frac{\partial \theta}{\partial r}\Big) dr = \int_{r_{i-\frac{1}{2}}}^{r_{i+\frac{1}{2}}} R(\theta) dr.$$

Implementing cell averaging, we have,

$$\Delta r_i \frac{d\tilde{\theta}_i(\tau)}{d\tau} - \int_{r_{i-\frac{1}{2}}}^{r_{i+\frac{1}{2}}} c(r)\frac{\partial}{\partial r}\Big(Q(r,\theta)d(r)\frac{\partial \theta}{\partial r}\Big) dr = \int_{r_{i-\frac{1}{2}}}^{r_{i+\frac{1}{2}}} R(\theta) dr, \tag{6.2.1.2}$$

where,

$$\tilde{\theta}_i = \frac{1}{\Delta r_i} \int_{r_{i-\frac{1}{2}}}^{r_{i+\frac{1}{2}}} \theta dr, \tag{6.2.1.3}$$

is the cell-averaged quantity of θ over the grid cell $[r_{i-\frac{1}{2}}, r_{i+\frac{1}{2}}]$. Based on the above, it can be seen that the order of the partial differential equation has been reduced by one.

6.2.2 Implementation of the Well-Balancing Scheme

In this section, we employ the numerical approach mentioned above for Equation (2.13) in order to construct a numerical balance law of (6.2.1.2). In this fashion, we are able to obtain a Well-Balancing scheme which preserves specific non-trivial steady state solutions and reduces some of the oscillations that occur around steady state solutions [69]. Hence, for a more general equation (6.2.1.1), the Well-Balancing scheme will provide a solution that must satisfy for steady states,

$$c(r)\frac{\partial}{\partial r}\Big(Q(r,\theta)\frac{\partial \theta}{\partial r}\Big) = R(\theta),$$

where $c(r) = \frac{1}{(r(r^*-1)+1)(r^*-1)^2}$ and $Q(r,\theta) = (r(r^*-1)+1)$ is a function of r only in our case with $R(\theta) = -\mathcal{N}_c\theta^2 - \mathcal{N}_r((\theta+\theta_a)^4 - \theta_a^4)$ the nonlinear source term. Furthermore, it should be noted that this methodology may be extended for higher order equations.

Based on the equation under consideration (2.13), we rewrite our scheme in the form of the one dimensional steady state,

$$\frac{1}{(r(r^*-1)+1)(r^*-1)}\frac{d}{dr}\Big(\frac{r(r^*-1)+1}{r^*-1}\frac{d\theta}{dr}\Big) = \mathcal{N}_c\theta^2 + \mathcal{N}_r((\theta+\theta_a)^4 - \theta_a^4)$$

$$\frac{d\theta}{dr}\Big|_{r=0} = 0, \qquad \theta(1) = 1, \qquad 0 < r < 1. \tag{6.2.2.4}$$

matching the form of Equation 6.2.1.1. Integrating over the grid cell $[0, r+\frac{\Delta r}{2}]$ with the use of the Finite Volume Method, as mentioned in the previous section, we obtain,

$$\int_0^{r+\frac{\Delta r}{2}} \frac{1}{(r(r^*-1)+1)(r^*-1)^2} \frac{d}{dr}\Big((r(r^*-1)+1)\frac{d\theta}{dr}\Big) dr$$

$$= \mathcal{N}_c \int_0^{r+\frac{\Delta r}{2}} \theta^2 dr + \mathcal{N}_r \int_0^{r+\frac{\Delta r}{2}} ((\theta+\theta_a)^4 - \theta_a^4) dr, \qquad 0 < r < 1.$$

which is equivalent to,

$$\frac{1+\mathrm{Log}((r+\frac{\Delta r}{2})(r^*-1)+1)}{(r^*-1)^2} \frac{d\theta(r+\frac{\Delta r}{2})}{dr} = \mathcal{N}_c \int_0^{r+\frac{\Delta r}{2}} \theta^2 dr + \mathcal{N}_r \int_0^{r+\frac{\Delta r}{2}} ((\theta+\theta_a)^4 - \theta_a^4) dr, \tag{6.2.2.5}$$

for $0 < r < 1$. Similarly, by integrating over the grid cell $[0, r-\frac{\Delta r}{2}]$,

$$\frac{1+\mathrm{Log}((r-\frac{\Delta r}{2})(r^*-1)+1)}{(r^*-1)^2} \frac{d\theta(r-\frac{\Delta r}{2})}{dr} = \mathcal{N}_c \int_0^{r-\frac{\Delta r}{2}} \theta^2 dr + \mathcal{N}_r \int_0^{r-\frac{\Delta r}{2}} ((\theta+\theta_a)^4 - \theta_a^4) dr, \tag{6.2.2.6}$$

for $0 < r < 1$. Based on the Mean Value theorem, we have,

$$\mathcal{N}_c \int_0^{r+\frac{\Delta r}{2}} \theta^2 dr + \mathcal{N}_r \int_0^{r+\frac{\Delta r}{2}} ((\theta+\theta_a)^4 - \theta_a^4) dr = \Big(r + \frac{\Delta r}{2}\Big)\Big(\mathcal{N}_c\theta^2(\varphi) + \mathcal{N}_r(\theta(\varphi)+\theta_a)^4 - \theta_a^4\Big), \tag{6.2.2.7}$$

For $0 < \varphi < r + \frac{\Delta r}{2}$. Next, a Taylor series approximation of $\theta^2(\varphi)$ and $(\theta(\varphi)+\theta_a)^4 - \theta_a^4$ around r provides,

$$\theta^2(\varphi) = \theta^2(r) + 2(\varphi - r)\theta(r)\frac{d\theta}{dr} + O((\varphi-r)^2),$$

$$\begin{aligned}(\theta(\varphi)+\theta_a)^4 - \theta_a^4 \;&=\; \theta^4(r) + 4(\varphi-r)\theta^3(r)\theta_a\frac{d\theta}{dr} + 6(\varphi-r)^2\theta^2(r)\theta_a^2\frac{d^2\theta}{dr^2} + 4(\varphi-r)^3\theta(r)\theta_a^3\frac{d^3\theta}{dr^3} \\ &\quad + (\varphi-r)^4\theta_a^4\frac{d^4\theta}{dr^4} - \theta_a^4 + O((\varphi-r)^4),\end{aligned} \tag{6.2.2.8}$$

where $O((\varphi - r)^2)$ and $O((\varphi - r)^4)$ are the error terms.

For $0 < \varphi < r + \frac{\Delta r}{2}$ we have,

$$\begin{aligned}
&\mathcal{N}_c \int_0^{r+\frac{\Delta r}{2}} \theta^2 dr + \mathcal{N}_r \int_0^{r+\frac{\Delta r}{2}} ((\theta + \theta_a)^4 - \theta_a^4) dr \\
&= \left(r + \frac{\Delta r}{2}\right)\Big[\mathcal{N}_c\Big(\theta^2(r) + \Delta r\theta(r)\frac{d\theta}{dr}\Big) + \mathcal{N}_r\Big(\theta^4(r) + 2\Delta r\theta^3(r)\theta_a\frac{d\theta}{dr} + \frac{3}{2}\Delta r^2\theta^2(r)\theta_a^2\frac{d^2\theta}{dr^2} \\
&+ \frac{1}{2}\Delta r^3\theta(r)\theta_a^3\frac{d^3\theta}{dr^3} + \left(\frac{\Delta r}{2}\right)^4\theta_a^4\frac{d^4\theta}{dr^4} - \theta_a^4 + O(\Delta r)^4\Big)\Big].
\end{aligned} \tag{6.2.2.9}$$

Similarly, for $0 < \varphi < r - \frac{\Delta r}{2}$ we obtain,

$$\begin{aligned}
&\mathcal{N}_c \int_0^{r-\frac{\Delta r}{2}} \theta^2 dr + \mathcal{N}_r \int_0^{r-\frac{\Delta r}{2}} ((\theta + \theta_a)^4 - \theta_a^4) dr \\
&= \left(r - \frac{\Delta r}{2}\right)\Big[\mathcal{N}_c\Big(\theta^2(r) - \Delta r\theta(r)\frac{d\theta}{dr}\Big) + \mathcal{N}_r\Big(\theta^4(r) - 2\Delta r\theta^3(r)\theta_a\frac{d\theta}{dr} + \frac{3}{2}\Delta r^2\theta^2(r)\theta_a^2\frac{d^2\theta}{dr^2} \\
&- \frac{1}{2}\Delta r^3\theta(r)\theta_a^3\frac{d^3\theta}{dr^3} + \left(\frac{\Delta r}{2}\right)^4\theta_a^4\frac{d^4\theta}{dr^4} - \theta_a^4 + O(\Delta r)^4\Big)\Big].
\end{aligned} \tag{6.2.2.10}$$

From Equations (6.2.2.9) and (6.2.2.10), the series can be written as,

$$\begin{aligned}
&\mathcal{N}_c \int_{r-\frac{\Delta r}{2}}^{r+\frac{\Delta r}{2}} \theta^2 dr + \mathcal{N}_r \int_{r-\frac{\Delta r}{2}}^{r+\frac{\Delta r}{2}} ((\theta + \theta_a)^4 - \theta_a^4) dr \\
&= 2\mathcal{N}_r r\theta^4(r) + 2\mathcal{N}_r\theta_a\Delta r^2\theta^3(r)\frac{d\theta}{dr} + r\theta^2(r)\Big(2\mathcal{N}_c + 3\mathcal{N}_r\theta_a^2\Delta r^2\frac{d^2\theta}{dr^2}\Big) \\
&+ \theta(r)\Big(\mathcal{N}_c\Delta \mathrm{r}^2\frac{d\theta}{dr} + \frac{1}{2}\mathcal{N}_r\theta_a^3\Delta r^4\frac{d^3\theta}{dr^3}\Big) + \frac{1}{8}\mathcal{N}_r r\theta_a^4\Big(\Delta \mathrm{r}^4\frac{d^4\theta}{dr^4} - 16\Big)
\end{aligned} \tag{6.2.2.11}$$

6.2.3 Balance Law

As mentioned in the previous subsection, we have

$$\int_0^{r+\frac{\Delta r}{2}} \frac{1}{(r(r^*-1)+1)(r^*-1)^2}\frac{d}{dr}\Big((r(r^*-1)+1)\frac{d\theta}{dr}\Big)dr$$

$$= \mathcal{N}_c \int_0^{r+\frac{\Delta r}{2}} \theta^2 dr + \mathcal{N}_r \int_0^{r+\frac{\Delta r}{2}} ((\theta+\theta_a)^4 - \theta_a^4) dr,$$

which is equivalent to,

$$\frac{1+\mathrm{Log}(r(r^*-1)+1)}{(r^*-1)^2}\frac{d\theta(r)}{dr} = \mathcal{N}_c \int_0^{r+\frac{\Delta r}{2}} \theta^2 dr - \mathcal{N}_r \int_0^{r+\frac{\Delta r}{2}} ((\theta+\theta_a)^4 - \theta_a^4) dr. \quad (6.2.3.12)$$

By the Mean Value Theorem and Taylor series expansion we have,

$$\begin{aligned}\frac{1+\mathrm{Log}(r(r^*-1)+1)}{(r^*-1)^2}\frac{d\theta(r)}{dr} &= \mathcal{N}_c r\Big(\theta^2(r) + 2(\varphi-r)\theta(r)\frac{d\theta}{dr} + O((\varphi-r)^2)\Big) + \mathcal{N}_r r\Big(\theta^4(r) \\ &+ 4(\varphi-r)\theta^3(r)\theta_a\frac{d\theta}{dr} + 6(\varphi-r)^2\theta^2(r)\theta_a^2\frac{d^2\theta}{dr^2} + 4(\varphi-r)^3\theta(r)\theta_a^3\frac{d^3\theta}{dr^3} \\ &+ (\varphi-r)^4\theta_a^4\frac{d^4\theta}{dr^4} - \theta_a^4 + O((\varphi-r)^4)\Big).\end{aligned} \quad (6.2.3.13)$$

For $0 < \varphi < r - \frac{\Delta r}{2}$ and Δr we have,

$$\begin{aligned}\frac{1+\mathrm{Log}(r(r^*-1)+1)}{(r^*-1)^2}\frac{d\theta(r)}{dr} &= \Big(r - \frac{\Delta r}{2}\Big)\Big[\mathcal{N}_c\Big(\theta^2(r) - \Delta r\theta(r)\frac{d\theta}{dr}\Big) + \mathcal{N}_r\Big(\theta^4(r) \\ &- 2\Delta r\theta^3(r)\theta_a\frac{d\theta}{dr} + \frac{3}{2}\Delta r^2\theta^2(r)\theta_a^2\frac{d^2\theta}{dr^2} - \frac{1}{2}\Delta r^3\theta(r)\theta_a^3\frac{d^3\theta}{dr^3} \\ &+ \Big(\frac{\Delta r}{2}\Big)^4\theta_a^4\frac{d^4\theta}{dr^4} - \theta_a^4 + O(\Delta r)^4\Big)\Big].\end{aligned} \quad (6.2.3.14)$$

After re-arranging terms, Equation (6.2.3.14) can be written as,

$$\begin{aligned}&\frac{d\theta}{dr}\Big[\frac{1+\mathrm{Log}(r(r^*-1)+1)}{(r^*-1)^2} + \Big(r-\frac{\Delta r}{2}\Big)\Big(\Delta r\mathcal{N}_c\theta(r) + 2\Delta r\mathcal{N}_r\theta^3(r)\theta_a\Big)\Big] \\ &= \Big(r-\frac{\Delta r}{2}\Big)\Big(\mathcal{N}_c\theta^2(r) + \mathcal{N}_r\Big(\theta^4(r) + \frac{3}{2}\Delta r^2\theta^2(r)\theta_a^2\frac{d^2\theta}{dr^2} - \frac{1}{2}\Delta r^3\theta(r)\theta_a^3\frac{d^3\theta}{dr^3} + \Big(\frac{\Delta r}{2}\Big)^4\theta_a^4\frac{d^4\theta}{dr^4} \\ &- \theta_a^4 + O(\Delta r)^4\Big).\end{aligned} \quad (6.2.3.15)$$

After simplification, we obtain

$$\begin{aligned}\frac{d\theta}{dr} =& (r^*-1)^2(2r-\Delta r) + O(\Delta r)^4 \\ &\times \frac{(16\mathcal{N}_r\theta^4(r) + 8\theta^2(r)(2\mathcal{N}_c + 3\mathcal{N}_r\theta_a^2\Delta r^2\frac{d^2\theta}{dr^2}) - 8\mathcal{N}_r\theta_a^3\Delta r^3\theta(r)\frac{d^3\theta}{dr^3}) + \mathcal{N}_r\theta_a^4(\Delta r^4\frac{d^4\theta}{dr^4} - 16)}{32(1+\mathrm{Log}(1+r(r^*-1))) - 16(r^*-1)^2(2r-\Delta r)\Delta r\theta(r)(\mathcal{N}_c + 2\mathcal{N}_r\theta_a\theta^2(r))}.\end{aligned} \quad (6.2.3.16)$$

Substituting Equation (6.2.3.16) into Equation (6.2.2.11), the source term for the balance law can be established as follows,

$$
\begin{aligned}
&\mathcal{N}_c \int_{r-\frac{\Delta r}{2}}^{r+\frac{\Delta r}{2}} \theta^2 dr + \mathcal{N}_r \int_{r-\frac{\Delta r}{2}}^{r+\frac{\Delta r}{2}} ((\theta+\theta_a)^4 - \theta_a^4) dr \\
&= 2\mathcal{N}_r r\theta^4(r) + r\theta^2(r)\Big(2\mathcal{N}_c + 3\mathcal{N}_r\theta_a^2\Delta r^2\frac{d^2\theta}{dr^2}\Big) + \frac{r}{8}\mathcal{N}_r\theta_a^4\Big(\Delta r^4\frac{d^4\theta}{dr^4} - 16\Big) \\
&- \Delta r^2\theta^3(r)\theta_a\mathcal{N}_r(r^*-1)^2(2r-\Delta r) \\
&\times \Big[\frac{16\mathcal{N}_r\theta^4(r) + 8\theta^2(r)(2\mathcal{N}_c + 3\mathcal{N}_r\theta_a^2\Delta r^2\frac{d^2\theta}{dr^2}) - 8\mathcal{N}_r\theta_a^3\Delta r^3\theta(r)\frac{d^3\theta}{dr^3} + \mathcal{N}_r\theta_a^4(\Delta r^4\frac{d^4\theta}{dr^4} - 16)}{16(1+\mathrm{Log}(1+r(r^*-1))) - 8(r^*-1)^2(2r-\Delta r)\Delta r\theta(r)(\mathcal{N}_c + 2\mathcal{N}_r\theta_a\theta^2(r))}\Big] \\
&- \mathcal{N}_c\theta(r)(r^*-1)^2(2r-\Delta r)\Delta r^2 \\
&\times \Big[\frac{16\mathcal{N}_r\theta^4(r) + 8\theta^2(r)(2\mathcal{N}_c + 3\mathcal{N}_r\theta_a^2\Delta r^2\frac{d^2\theta}{dr^2}) - 8\mathcal{N}_r\theta_a^3\Delta r^3\theta(r)\frac{d^3\theta}{dr^3} + \mathcal{N}_r\theta_a^4(\Delta r^4\frac{d^4\theta}{dr^4} - 16)}{32(1+\mathrm{Log}(1+r(r^*-1))) - 16(r^*-1)^2(2r-\Delta r)\Delta r\theta(r)(\mathcal{N}_c + 2\mathcal{N}_r\theta_a\theta^2(r))}\Big] \\
&+ \frac{1}{2}\theta(r)\mathcal{N}_r\theta_a^3\Delta r^4\frac{d^3\theta}{dr^3}.
\end{aligned}
\tag{6.2.3.17}
$$

Hence, integrating over the grid cell $[r+\frac{\Delta r}{2}, r-\frac{\Delta r}{2}]$ and incorporating Equation (6.2.3.17) we obtain,

$$
\begin{aligned}
\frac{\partial\theta}{\partial\tau} &= \frac{1}{(r^*-1)^2}\Big[\mathrm{Log}((r+\frac{\Delta r}{2})(r^*-1)+1)\frac{d\theta(r+\frac{\Delta r}{2})}{dr} - \mathrm{Log}((r-\frac{\Delta r}{2})(r^*-1)+1)\frac{d\theta(r-\frac{\Delta r}{2})}{dr}\Big] \\
&+ 2\mathcal{N}_r r\theta^4(r) + r\theta^2(r)\Big(2\mathcal{N}_c + 3\mathcal{N}_r\theta_a^2\Delta r^2\frac{d^2\theta}{dr^2}\Big) + \frac{r}{8}\mathcal{N}_r\theta_a^4\Big(\Delta r^4\frac{d^4\theta}{dr^4} - 16\Big) \\
&- \Delta r^2\theta^3(r)\theta_a\mathcal{N}_r(r^*-1)^2(2r-\Delta r) \\
&\times \Big[\frac{16\mathcal{N}_r\theta^4(r) + 8\theta^2(r)(2\mathcal{N}_c + 3\mathcal{N}_r\theta_a^2\Delta r^2\frac{d^2\theta}{dr^2}) - 8\mathcal{N}_r\theta_a^3\Delta r^3\theta(r)\frac{d^3\theta}{dr^3} + \mathcal{N}_r\theta_a^4(\Delta r^4\frac{d^4\theta}{dr^4} - 16)}{16(1+\mathrm{Log}(1+r(r^*-1))) - 8(r^*-1)^2(2r-\Delta r)\Delta r\theta(r)(\mathcal{N}_c + 2\mathcal{N}_r\theta_a\theta^2(r))}\Big] \\
&- \mathcal{N}_c\theta(r)(r^*-1)^2(2r-\Delta r)\Delta r^2 \\
&\times \Big[\frac{16\mathcal{N}_r\theta^4(r) + 8\theta^2(r)(2\mathcal{N}_c + 3\mathcal{N}_r\theta_a^2\Delta r^2\frac{d^2\theta}{dr^2}) - 8\mathcal{N}_r\theta_a^3\Delta r^3\theta(r)\frac{d^3\theta}{dr^3} + \mathcal{N}_r\theta_a^4(\Delta r^4\frac{d^4\theta}{dr^4} - 16)}{32(1+\mathrm{Log}(1+r(r^*-1))) - 16(r^*-1)^2(2r-\Delta r)\Delta r\theta(r)(\mathcal{N}_c + 2\mathcal{N}_r\theta_a\theta^2(r))}\Big] \\
&+ \frac{1}{2}\theta(r)\mathcal{N}_r\theta_a^3\Delta r^4\frac{d^3\theta}{dr^3}.
\end{aligned}
\tag{6.2.3.18}
$$

Next we substitute the finite difference approximations for a particular time t_j and for the spatial domain $r \in [r - \frac{\Delta r}{2}, r + \frac{\Delta r}{2}]$ giving,

$$\frac{\partial \theta}{\partial \tau} |_i \approx \frac{\theta_i^{j+1} - \theta_i^j}{\Delta t},$$

$$\frac{\partial \theta(r + \frac{\Delta r}{2})}{\partial r} |_j \approx \frac{\theta_{i+1}^j - \theta_i^j}{\Delta r}, \quad \frac{\partial \theta(r - \frac{\Delta r}{2})}{\partial r} |_j \approx \frac{\theta_i^j - \theta_{i-1}^j}{\Delta r},$$

$$\frac{\partial^2 \theta(r + \frac{\Delta r}{2})}{\partial r^2} |_j \approx \frac{\theta_{i+2}^j - 2\theta_{i+1}^j + \theta_i^j}{\Delta r}, \quad \frac{\partial^2 \theta(r - \frac{\Delta r}{2})}{\partial r^2} |_j \approx \frac{\theta_i^j - 2\theta_{i-1}^j + \theta_{i-2}^j}{\Delta r}, \quad (6.2.3.19)$$

$$\frac{\partial^3 \theta(r + \frac{\Delta r}{2})}{\partial r^3} |_j \approx \frac{\theta_{i+3}^j - 3\theta_{i+2}^j + 3\theta_{i+1}^j - \theta_i^j}{\Delta r}, \quad \frac{\partial^3 \theta(r - \frac{\Delta r}{2})}{\partial r^3} |_j \approx \frac{\theta_i^j - 3\theta_{i-1}^j + 3\theta_{i-2}^j - \theta_{i-3}^j}{\Delta r},$$

$$\frac{\partial^4 \theta(r + \frac{\Delta r}{2})}{\partial r^4} |_j \approx \frac{\theta_{i+4}^j - 4\theta_{i+3}^j + 6\theta_{i+2}^j - 4\theta_{i+1}^j + \theta_i^j}{\Delta r}, \quad \text{and}$$

$$\frac{\partial^4 \theta(r - \frac{\Delta r}{2})}{\partial r^4} |_j \approx \frac{\theta_i^j - 4\theta_{i-1}^j + 6\theta_{i-2}^j - 4\theta_{i-3}^j + \theta_{i-4}^j}{\Delta r},$$

Hence, our Well-Balancing scheme is given by,

$$\begin{aligned}
\theta_i^{j+1} &= \theta_i^j + \frac{\Delta t \Delta r}{(r^* - 1)^2} \Big[\text{Log}(r_{i+\frac{1}{2}}(r^* - 1) + 1)(\theta_{i+1}^j - \theta_i^j) - \text{Log}(r_{i-\frac{1}{2}}(r^* - 1) + 1)(\theta_i^j - \theta_{i-1}^j) \Big] \\
&+ 2r\Delta t \mathcal{N}_r (\theta_i^j)^4 + r\Delta t (\theta_i^j)^2 \Big(2\mathcal{N}_c + 3\mathcal{N}_r \theta_a^2 \Delta r^2 \frac{d^2\theta}{dr^2} \Big) + \frac{r\Delta t}{8} \mathcal{N}_r \theta_a^4 \Big(\Delta r^4 \frac{d^4\theta}{dr^4} - 16 \Big) \\
&- \frac{\Delta t \Delta r (\theta_i^j)^3 \theta_a \mathcal{N}_r (r^* - 1)^2 (2r - \Delta r)}{16(1 + \text{Log}(1 + r(r^* - 1))) - 8(r^* - 1)^2 (2r - \Delta r)\theta_i^j \Delta r (\mathcal{N}_c + 2\mathcal{N}_r \theta_a (\theta_i^j)^2)} \\
&\times \Big[16\mathcal{N}_r (\theta_i^j)^4 + 8(\theta_i^j)^2 (2\mathcal{N}_c + 3\mathcal{N}_r \theta_a^2 \Delta r^2 (\theta_{i+2}^j - 2\theta_{i+1}^j + 2\theta_{i-1}^j - \theta_{i-2}^j)) \\
&- 8\mathcal{N}_r \theta_i^j \theta_a^3 \Delta r^3 (\theta_{i+3}^j - 3\theta_{i+2}^j + 3\theta_{i+1}^j - 2\theta_i^j + 3\theta_{i-1}^j - 3\theta_{i-2}^j + \theta_{i-3}^j) \\
&+ \mathcal{N}_r \theta_a^4 \Delta r^4 (\theta_{i+4}^j - 4\theta_{i+3}^j + 6\theta_{i+2}^j - 4\theta_{i+1}^j + 4\theta_{i-1}^j - 6\theta_{i-2}^j + 4\theta_{i-3}^j - \theta_{i-4}^j) - 16\Delta r^4 \Big]
\end{aligned}$$

$$
\begin{aligned}
& - \frac{\Delta t \mathcal{N}_c (r^* - 1)^2 \theta_i^j (2r - \Delta r)\Delta r}{32(1 + \mathrm{Log}(1 + r(r^* - 1))) - 16(r^* - 1)^2 (2r - \Delta r)\Delta r \theta_i^j (\mathcal{N}_c + 2\mathcal{N}_r \theta_a (\theta_i^j)^2)} \\
& \times \Big[16\mathcal{N}_r (\theta_i^j)^4 + 8(\theta_i^j)^2 (2\mathcal{N}_c + 3\mathcal{N}_r \theta_a^2 \Delta r^2 (\theta_{i+2}^j - 2\theta_{i+1}^j + 2\theta_{i-1}^j - \theta_{i-2}^j)) \\
& - 8\mathcal{N}_r \theta_i^j \theta_a^3 \Delta r^3 (\theta_{i+3}^j - 3\theta_{i+2}^j + 3\theta_{i+1}^j - 2\theta_i^j + 3\theta_{i-1}^j - 3\theta_{i-2}^j + \theta_{i-3}^j) \\
& + \mathcal{N}_r \theta_a^4 \Delta r^4 (\theta_{i+4}^j - 4\theta_{i+3}^j + 6\theta_{i+2}^j - 4\theta_{i+1}^j + 4\theta_{i-1}^j - 6\theta_{i-2}^j + 4\theta_{i-3}^j - \theta_{i-4}^j) - 16\Delta r^4 \Big] \\
& + \frac{1}{2}\mathcal{N}_r \theta_i^j \Delta t \Delta r^4 \theta_a^3 (\theta_{i+3}^j - 3\theta_{i+2}^j + 3\theta_{i+1}^j - 2\theta_i^j + 3\theta_{i-1}^j - 3\theta_{i-2}^j + \theta_{i-3}^j),
\end{aligned}
\tag{6.2.3.20}
$$

where a linear interpolation is used to determine $r_{i+\frac{1}{2}}$ and $r_{i-\frac{1}{2}}$.

No-flux at the origin

In order to implement our Well-Balancing numerical scheme, we need to incorporate the boundary conditions. As per the work of Kraus et al. [70], it is noted that some fin's shapes need to be interpreted in a specific manner and cannot be characterized by linear transformation. As such, since the fin profile at the tip has zero thickness, we shall have no-flux at the fin tip. Due to the physical relevance placed on the fin tip as well as the dynamics of the fin tip profile as discussed in Section 4.3 where $r = 0$ we have at the origin,

$$
\frac{1}{(r(r^* - 1) + 1)(r^* - 1)^2} \frac{\partial}{\partial r}\left(r(r^* - 1) + 1 \frac{\partial \theta}{\partial r} \right)\Bigg|_{r=0} = 0,
$$

$$
\implies \frac{\partial}{\partial r}\left(r(r^* - 1) + 1 \frac{\partial \theta}{\partial r} \right)\Bigg|_{r=0} = 0. \tag{6.2.3.21}
$$

Implementing a time forward discretisation at the origin and employing the no-flux condition given by (6.2.3.21), we have

$$
\theta_i^{j+1} = \theta_i^j + \Delta t \mathcal{N}_c (\theta_i^j)^2 + \Delta t \mathcal{N}_r ((\theta_i^j + \theta_a)^4 - \theta_a^4). \tag{6.2.3.22}
$$

As per Equation (6.2.3.22), if we were to apply the no-flux condition based on the zero temperature initial condition, the temperature will always be zero which does not make sense. As such the dynamics at the fin tip can again be considered to be unstable under certain circumstances. In order to address this concern, we employ the Well-Balancing principle at the origin i.e. $i = 0$ by incorporating θ_0^j into Equation (6.2.3.22). Thus, the steady state solution can be established as follows,

$$\int_{r_0}^{r_0+\frac{\Delta r}{2}} \frac{1}{(r(r^*-1)+1)(r^*-1)^2} \frac{d}{dr}\Big(r(r^*-1)+1\frac{d\theta}{dr}\Big) dr = \frac{\Delta r}{2}\Big(\mathcal{N}_c\theta^2(r_0)+\mathcal{N}_r((\theta(r_0)+\theta_a)^4-\theta_a^4)\Big),$$

$$\implies \frac{1}{(r^*-1)^2}\Big(\text{Log}((r_0+\frac{\Delta r}{2})(r^*-1)+1)\frac{d\theta(r_0+\frac{\Delta r}{2})}{dr} - \text{Log}((r_0(r^*-1)+1)\frac{d\theta(r_0)}{dr}\Big)$$
$$= \frac{\Delta r}{2}\Big(\mathcal{N}_c\theta^2(r_0)+\mathcal{N}_r((\theta(r_0)+\theta_a)^4-\theta_a^4)\Big).$$

Since $\frac{d\theta}{dr}(r_0) = 0$, the solution simplifies as follows,

$$\frac{\text{Log}((r_0+\frac{\Delta r}{2})(r^*-1)+1)}{(r^*-1)^2}\frac{d\theta(r_0+\frac{\Delta r}{2})}{dr} = \frac{\Delta r}{2}\Big(\mathcal{N}_c\theta^2(r_0)+\mathcal{N}_r((\theta(r_0)+\theta_a)^4-\theta_a^4)\Big).$$

Through the use of the central difference approximation we obtain,

$$\theta_0^j = \theta_1^j - \frac{\Delta r(r^*-1)^2}{2\text{Log}(r_{\frac{1}{2}}(r^*-1)+1)}\mathcal{N}_c(\theta_0^j)^2 + \mathcal{N}_r(\theta_0^j+\theta_a)^4 - \theta_a^4). \tag{6.2.3.23}$$

Equation (6.2.3.22) and (6.2.3.23) provide a numerical Well-Balancing scheme for the fin profile at the origin.

Flux at the origin

The flux at the origin for the fin is non-zero and are governed by the boundary conditions adiabatic (i.e. a process that occurs without the transfer of heat/matter between the system and its surroundings). At the origin,

$$\frac{\partial\theta}{\partial\tau} - \frac{1}{(r^*-1)^2}\frac{\partial^2\theta}{\partial r^2} - \frac{1}{(r(r^*-1)+1)(r^*-1)}\frac{\partial\theta}{\partial r} + \mathcal{N}_c\theta^2 + \mathcal{N}_r((\theta+\theta_a)^4 - \theta_a^4)\bigg|_{r=0} = 0.$$

Since $\frac{1}{(r(r^*-1)+1)(r^*-1)}\frac{\partial\theta}{\partial r}(r_0) = 0$ we have,

$$\frac{\partial\theta}{\partial\tau} - \frac{1}{(r^*-1)^2}\frac{\partial^2\theta}{\partial r^2} + \mathcal{N}_c\theta^2 + \mathcal{N}_r((\theta+\theta_a)^4 - \theta_a^4)\bigg|_{r=0} = 0.$$

Implementing the forward difference and central difference approximation for time and space respectively, we have

$$\theta_0^{j+1} = \theta_0^j - \frac{2\Delta t}{\Delta r^2(r^*-1)^2}(\theta_1^j - \theta_0^j) + \Delta t\mathcal{N}_c(\theta_0^j)^2 + \Delta t\mathcal{N}_r((\theta_0^j+\theta_a)^4 - \theta_a^4). \quad (6.2.3.24)$$

Similarly, for the steady state equation of the fin we obtain,

$$\theta_0^j = \theta_1^j - \frac{\Delta r(r^*-1)^2}{2\mathrm{Log}(r_0(r^*-1)+1)}\mathcal{N}_c(\theta_0^j)^2 + \mathcal{N}_r(\theta_0^j+\theta_a)^4 - \theta_a^4). \quad (6.2.3.25)$$

The discretisation at the origin of the profile is given by Equation (6.2.3.24) and (6.2.3.25).

6.3 Results

In Section 6.3.1, we compare the results we obtained via the Well-Balancing scheme (WBS) and our two numerical methods i.e. the Crank-Nicolson scheme (CN) and the Crank-Nicolson scheme incorporating the Newton-Raphson predictor corrector and Usmani method (CN^{NR}). The results obtained via these numerical schemes are also compared to the solution obtained as per the work of Darvishi et al. [1] and the Differential Transformation Method discussed in Section 6.3.2.

6.3.1 Comparison of numerical schemes

The Well-Balancing scheme in comparison matches the shape and behaviour of the solutions observed in Darvishi et al. [1]. Similarly, to make a comparison between the numerical schemes we have employed, we allow our numerical schemes to iterate for large time T in order for convergence to a steady state. We find that convergence has occurred for the Well-Balancing scheme and Crank-Nicolson scheme at $T = 1$. As previously mentioned, this is not the case for the Crank-Nicolson method with predictor corrector. Once again, to maintain our CFL number as less than one for stability purposes, we choose $\triangle r = 0.1$ and $\triangle t = 0.0001$.

As seen in Tables 6.1 - 6.4, the numerical schemes produce solutions similar in shape and behaviour as solutions observed in Darvishi et al.[1]. However, there are discrepancies when we consider the errors between the methods. The temperature at the origin, i.e. $\theta(0)$, is often not the same across the methods. In terms of the solutions for the Well-Balancing scheme and the Crank-Nicolson scheme agrees to the third decimal for the same value of θ_0 for set parameter values as well as converge at the same rate. However, for the Crank-Nicolson method with the predictor corrector method, we find that the solutions do not converge to the same value for θ_0 for set parameter values, nor does the solution converge at the same rate. Due to the speed with which the Well-Balancing scheme is able to reach convergence, and its accuracy upon comparison with the work by Darvishi et al. [1] and the Crank-Nicolson, as seen in Section 5.4.1, we illustrate the solutions obtained in the figures to follow.

In Table 6.1 we observe a similar trend to the Crank-Nicolson scheme which may be misleading; that is, an increase in the dimensionless ambient temperature leads to a decrease in the tip temperature. As mentioned, in this work we altered our nondimensionalisation to define the ratio θ_a as $\frac{T_a}{T_b - T_a}$ which impacts the behaviour observed by

Table 6.1: *Temperature at $r = 0$ for varied values of θ_a.*

θ_a	θ_0^{WBS}	θ_0^{CN}	θ_0^{NR}
0.2	0.54424	0.54482	0.67327
0.4	0.51898	0.51860	0.64891
0.6	0.48011	0.48088	0.61438
0.8	0.43374	0.43321	0.57044
Parameter values: $\mathcal{N}_c = 10$	$\mathcal{N}_r = 1$	$r^* = \frac{1}{1.75}$	$T = 1$

the solution with regards to changes in the value of θ_a. Instead of a linear relationship between T_a and θ_a we have a nonlinear one given by $T_a = \frac{\theta_a T_b}{1+\theta_a}$, such that the behaviour inversely corresponds to that of Darvishi et al. [1]. Once again, our results are consistent with the physical dynamics of the problem.

Table 6.2: *Maximum error computed between the respective numerical solutions obtained, where $\mathcal{E}_{CN}^{WBS} = Max\,|WBS_{sol} - CN_{sol}|$, $\mathcal{E}_{NR}^{WBS} = Max\,|WBS_{sol} - CN_{sol}^{NR}|$ and their respective temperatures at the tip of the fin for varied values of $\mathcal{N}_c$.*

$\mathcal{N}_c$	$\mathcal{E}_{CN}^{WBS}$	$\mathcal{E}_{NR}^{WBS}$	θ_0^{WBS}	θ_0^{CN}	θ_0^{NR}
1	0.00012	-0.07605	0.79992	0.79980	0.87604
10	0.00329	-0.12516	0.54811	0.54482	0.67327
50	0.00242	-0.1121	0.27487	0.27244	0.38697
Parameter values: $\theta_a = 0.2$	$\mathcal{N}_r = 1$	$r^* = \frac{1}{1.75}$	$T = 1$		

Table 6.2 illustrates the effect of the buoyancy or natural convection parameter ($\mathcal{N}_c$) on the temperature distribution in the fin for varied values. As the buoyancy effect increases, i.e. $\mathcal{N}_c$, the local temperature in the fin θ decreases.

Table 6.3: *Maximum error computed between the respective numerical solutions obtained, where $\mathcal{E}_{CN}^{WBS} = Max\,|WBS_{sol} - CN_{sol}|$, $\mathcal{E}_{NR}^{WBS} = Max\,|WBS_{sol} - CN_{sol}^{NR}|$ and their respective temperatures at the tip of the fin for varied values of $\mathcal{N}_r$.*

$\mathcal{N}_r$	$\mathcal{E}_{CN}^{WBS}$	$\mathcal{E}_{NR}^{WBS}$	θ_0^{WBS}	θ_0^{CN}	θ_0^{NR}
5	0.00519	-0.09798	0.62863	0.62343	0.72661
10	0.00224	-0.10474	0.5291	0.52686	0.63384
50	0.00046	-0.09445	0.30537	0.3049	0.39982
Parameter values: $\theta_a = 0.2$	$r^* = \frac{1}{1.75}$	$\mathcal{N}_c = 1$	$T = 100$		

For Table 6.3, we look at the effect of the radiation parameter $\mathcal{N}_r$ on the fin temperature. An increase in the surface radiative heat transfer from the fin to the ambient fluid, leads to a decrease in the local fin temperature θ. This is representative of the effect of natural convective heat loss on the temperature distribution in the fin when there is a loss of radiation heat. However, the environment temperature and the ratio between the inner and outer radius are kept constant. As previously mentioned, we see that the buoyancy force $(\mathcal{N}_c)$ which is principally a macro scale effect influences the velocity and temperature fields where as the radiation parameter $(\mathcal{N}_r)$ influences the temperature field by increasing the heat transfer rates from the surface. Once again, we find that when the convection parameter $(\mathcal{N}_c)$ and the radiation parameter $(\mathcal{N}_r)$ are allowed to vary, the local fin temperature decreases because of the increasing strength of radiative heat exchange between the exposed surface of the fin and the ambient [1].

Table 6.4: *Maximum error computed between the respective numerical solutions obtained, where* $\mathcal{E}_{CN}^{WBS} = Max\,|WBS_{sol} - CN_{sol}|$, $\mathcal{E}_{NR}^{WBS} = Max\,\left|WBS_{sol} - CN_{sol}^{NR}\right|$, *and their respective temperatures at the tip of the fin, given as* θ_0, *for varied values of* r^*.

r^*	$\mathcal{E}_{CN}^{WBS}$	$\mathcal{E}_{NR}^{WBS}$	θ_0^{WBS}	θ_0^{CN}	θ_0^{NR}
0.2	0.00108	-0.1074	0.28012	0.27903	0.38752
0.4	0.00067	-0.12684	0.40156	0.40088	0.5284
0.6	0.00453	-0.12163	0.57835	0.57382	0.69998
0.8	0.00028	-0.07407	0.81972	0.81944	0.89379
Parameter values: $\theta_a = 0.2$	$\mathcal{N}_r = 1$	$\mathcal{N}_c = 10$	$T = 1$		

Table 6.4 presents the heat transfer rates versus the ambient temperature with the ratio of the tip radius to base radius (r^*) as a parameter. We observe that with increasing (r^*), the heat transfer increases. This is due to the increased heat transfer area as (r^*) increases. Furthermore, it should be noted that as the ambient temperature increases, the heat transfer rate decreases. This is expected as the driving force for the heat transfer decreases as θ_a increases.

6.3.2 Comparison of the Well-Balancing scheme to the semi-analytical solution

In this section, we compare the results we obtained via the Well-Balancing scheme against the series solution obtained for the steady state. As previously stated, we used the calculated polynomial of degree $n = 10$ obtained via the DTM, and also consider the work in [1] as a benchmark. We observe that the Well-Balancing scheme performs as accurately and efficiently as required. It can be seen in Table 6.5, that an

Table 6.5: *Numerical solutions obtained for DTM and the maximum error computed between the DTM solution and the Well-Balancing scheme solution obtained, where* $\mathcal{E}^{WBS} = Max\,|WBS_{sol} - DTM_{sol}|$ *for varied values of* θ_a.

θ_a	$\mathcal{E}^{WBS}$
0.2	0.01301
0.4	0.02139
0.6	0.03741
0.8	0.05974
Parameter values: $\mathcal{N}_c = 10$ $\quad \mathcal{N}_r = 1$ $\quad r^* = \frac{1}{1.75}$	$T = 5$

increase in the dimensionless ambient temperature θ_a, leads to an increase in the error produced between the DTM and the Well-Balancing scheme. In this case, we have a linear relationship between T_a and θ_a and the behaviour corresponds to that of Darvishi et al. [1].

Table 6.6: *Numerical solutions obtained for DTM and the maximum error computed between the DTM solution and the Well-Balancing scheme solution obtained, where* $\mathcal{E}^{WBS} = Max\,|WBS_{sol} - DTM_{sol}|$ *for varied values of* $\mathcal{N}_c$.

$\mathcal{N}_c$	$\mathcal{E}^{WBS}$
1	0.01623
10	0.00914
50	0.00259
Parameter values: $\theta_a = 0.2$ $\quad \mathcal{N}_r = 1$ $\quad r^* = \frac{1}{1.75}$	$T = 5$

Tables 6.6 indicates that for increasing values of $\mathcal{N}_c$, the error between the DTM solution

Table 6.7: *Numerical solutions obtained for DTM and the maximum error computed between the DTM solution and the Well-Balancing scheme solution obtained, where* $\mathcal{E}^{WBS} = Max\,|WBS_{sol} - DTM_{sol}|$ *for varied values of* $\mathcal{N}_r$*.*

$\mathcal{N}_r$	$\mathcal{E}^{WBS}$
1	0.01752
5	0.04083
10	0.08506
Parameter values: $\theta_a = 0.2$ $\quad r^* = \frac{1}{1.75}$	$\mathcal{N}_c = 1$ $\quad T = 100$

and the Well-Balancing scheme decreases when $T = 5$; in turn Table 6.7 indicates that for increasing values of $\mathcal{N}_r$ at $T = 100$ we obtain an increase in the error. As mentioned in the previous section, we see that when the convection parameter ($\mathcal{N}_c$) and the radiation parameter ($\mathcal{N}_r$) are allowed to vary, the local fin temperature decreases because of the increasing strength of radiative heat exchange between the exposed surface of the fin and the ambient [1].

Table 6.8: *Numerical solutions obtained for DTM and the maximum error computed between the DTM solution and the Well-Balancing scheme solution obtained, where* $\mathcal{E}^{WBS} = Max\,|WBS_{sol} - DTM_{sol}|$ *for varied values of* r^**.*

r^*	$\mathcal{E}^{WBS}$
0.2	0.02026
0.4	0.01687
0.6	0.00692
0.8	0.00314
Parameter values: $\theta_a = 0.2$ $\quad \mathcal{N}_r = 1$	$\mathcal{N}_c = 10$ $\quad T = 100$

It can be seen in Table 6.8 that as the ambient temperature ratio of the tip radius to base radius r^* increases, the DTM solution increases, but the error produced between the DTM and the Well-Balancing scheme decreases. As previously mentioned, this is expected as the driving force for the heat transfer decreases as θ_a increases.

6.4 Conclusion

We employed the numerical Well-Balancing scheme to solve a model describing the heat transfer in a porous radial fin. We compared the results we obtained from the Well-Balancing scheme to the two numerical schemes i.e. the Crank-Nicolson method and the Crank-Nicolson method incorporating the Newton-Raphson and Usmani method as well as compared it to the steady state solution. We show that the results obtained from the Well-Balancing scheme only match the shape and behaviour of those solutions in the work by Darvishi et al.[1]. Furthermore, we show that the Well-Balancing scheme solutions match the solutions produced by the Crank-Nicolson scheme; agreement is up to three decimal places. However, the Well-Balancing scheme does not match the results obtained by the Crank-Nicolson method with the Newton-Raphson predictor corrector.

As previously stated, given the solutions obtained in Darvishi et al. [1] the error we obtained when comparing our numerical solutions to the DTM may be due to a poor approximation of this series solution. Due to computational limitations we are able to obtain a limited number of terms before a lack of memory becomes an issue; $n = 10$ are very few terms if one considers the work of other authors such as Darvishi et al. [1] and Aziz et al. [27] for instance.

Chapter 7

Conclusion

A time dependent nonlinear partial differential equation modeling heat transfer in a porous radial fin was considered for its extensive practical applications [1, 27]. The equation comprises of two nonlinear terms of which the first nonlinear term $\mathcal{N}_c$ refers to the buoyancy or natural convection transport of energy by the infiltrate and the second nonlinear term $\mathcal{N}_r$ refers to the surface radiative heat transfer from the fin to the ambient fluid. These terms play a crucial part in this thesis as it has an impact on the schemes stability. In an attempt to overcome the model's sensitivity to the initial condition as well as cater for the nonlinear terms we have employed the Lie group method which proves as a useful tool for obtaining an initial condition [51].

The Differential Transformation (DTM) was useful in obtaining semi-analytical steady state solutions which provide a guide for the numerical solutions obtained [27]. In this work, we have employed a polynomial of order $n = 10$ as our steady state solution. We are, via this methodology, able to obtain a polynomial of degree $n = 16$ which compares well to the sufficiently accurate solution produced with $n = 15$ as per the work of Aziz et al. [27]. We note that in order to obtain the relevant accuracy for this method a large number of terms would need to be employed (as per the work by Darvishi et al. [1] and Aziz et al. [27]); however the required memory to do so becomes a limiting factor.

As per the literature [37, 39, 43], we employed the Crank-Nicolson method with and without the Newton-Raphson predictor-corrector (employing Usmani's method for the former) and the Well-Balancing scheme to solve a model describing the heat transfer in a porous radial fin. We show that the results obtained via the Crank-Nicolson scheme and the Well-Balancing scheme match well in comparison to the results obtained in the work by Darvishi et al. [1]; the Crank-Nicolson method, incorporating the Newton-Raphson and Usmani method, and the DTM do not match these results even though the behaviour observed is appropriate and comparable. The accuracy of the Crank-Nicolson scheme and the Well-Balancing scheme when compared to the work by Darvishi et al. [1] meant that they were the most appropriate methods to consider in terms of an analysis of the scheme's stability and the dynamics of the steady state system.

The presence of nonlinear sink terms necessitated an investigation into the impact they may have on the stability of the scheme and hence the validity of the solutions obtained. We find that the only manner in which the linearisation of the system of first-order ordinary differential equations (obtained from the steady state equation) is able to describe the dynamics of the nonlinear system is if $\mathcal{N}_c$ and $\mathcal{N}_r$ approximate zero, that is, are very small [4]. Thus, we conclude that the higher order terms (and hence nonlinear sink terms) have an influence on the stability of the system and cannot be ignored.

Furthermore, via our computational investigations, we could ascertain the impact of $\mathcal{N}_c$ and $\mathcal{N}_r$, showing that as they tend to infinity, erratic and unstable behaviour may be observed at the equilibrium point which represents the fin tip ($\theta \to 0$, $\theta'(0) = 0$). More interestingly, we were able to show that the convection parameter $\mathcal{N}_c$ has a more prominent impact on the stability of the solutions obtained via the Crank-Nicolson scheme, whereas the radiative parameter $\mathcal{N}_r$ and the ambient temperature impact more severely on the stability of the Crank-Nicolson scheme with Newton-Raphson method. This behaviour is sensible given the nature of these sink terms. Hence, the dynamics at the fin tip can be said to be stable in general since an instance where the parameters would obtain such values leading to a case where the equilibrium point is representative of the values of the necessary temperature and temperature gradient is rare [4].

We also compared the dynamics between the nondimensionalised equation introduced here and that considered in [1]. Considering the second form of nondimensionalisation, the equilibrium point $(\theta_a, 0)$ is found to be unstable stable point corresponding to the saddle point obtained for the equilibrium point $(0, 0)$ for the previous nondimensionalisation. This case would correspond to an instance where the tip temperature is equated to the ambient temperature. As such the dynamics at the fin tip can again be considered to be unstable under certain circumstances; our numerical solutions i.e. the Crank-Nicolson scheme and Well-Balancing scheme confirmed this and displayed the intricate interactions between the relevant parameters. We found that the buoyancy force had a more dominant role to play in the schemes' ability to obtain solutions [4]. This seems reasonable given the nature of the higher order terms obtained.

The interesting additional insight with regard to the latter nondimensionalisation was that for larger values of $\mathcal{N}_c$ and $\mathcal{N}_r$ we find that $\theta_1 = \theta > 0$, which provided a second physically relevant equilibrium point. The dynamical analysis conducted assisted us in confirming that the boundary dynamics at the fin tip, that is, for $0 < \theta < 1$ and $\theta' = 0$, are indeed stable. Given the other equilibrium point (4.5.22), it would seem however that for cases where $\theta = \theta_a$ we would revert to unstable behaviour at the fin tip. An interesting point to note is that since in the latter nondimensionalised equation θ_a engages with both the buoyancy force/convection parameter and the radiation parameter in the equation, the dynamics are more intricate. As the convection increases, small values of the radiation parameter lead to no solution. Then as the latter increases the solution will achieve the ambient temperature at the fin tip. For both nondimensionalised equations we discovered that under certain circumstances there could be unstable behaviour at the fin tip; the convection and radiation parameters as well as the ambient temperature have a role to play regarding the stability and effectiveness of the numerical scheme employed. In general, this is a concern as the fin efficiency can drop drastically which cannot be economically justified.

Bibliography

[1] M. Darvishi, R. Gorla, F. Khani, and A. Aziz, "Thermal performance of a porus radial fin with natural convection and radiative heat losses," *Int J Therm Sci*, vol. 19, no. 2, pp. 669–678, 2015.

[2] A. Rameshkumar and K. Nandha, "Heat transfer analysis of engine cylinder fin by varying extension geometry," 2016.

[3] H. Truong and R. Mancuso, "Performance predictions of radiating annular fins of various profile shapes," in *American Society of Mechanical Engineers and American Institute of Chemical Engineers, Joint National Heat Transfer Conference*, vol. 1, 1980.

[4] M. Iqbal and S. Sikka, "Temperature distribution and effectiveness of a two-dimensional radiating and convecting circular fin," *AIAA Journal*, vol. 8, no. 1, pp. 101–106, 1970.

[5] H. Keller and E. Holdredge, "Radiation heat transfer for annular fins of trapezoidal profile," *J Heat Transf*, vol. 92, no. 1, pp. 113–116, 1970.

[6] P. Smith and J. Sucec, "Efficiency of circular fins of triangular profile," *J Heat Transf*, vol. 91, no. 1, pp. 181–182, 1969.

[7] R. Chambers and E. Somers, "Radiation fin efficiency for one-dimensional heat flow in a circular fin," *J Heat Transf (US)*, vol. 81, 1959.

[8] M. Yovanovich, J. Culham, and T. Lemczyk, “Simplified solutions to circular annular fins with contact resistance and end cooling,” *J Thermophys Heat Transfer*, vol. 2, no. 2, pp. 152–157, 1988.

[9] S. Kiwan and O. Zeitoun, “Natural convection in a horizontal cylindrical annulus using porous fins,” *Int J Numer Methods*, vol. 18, no. 5, pp. 618–634, 2008.

[10] S. Kiwan, “Thermal analysis of natural convection porous fins,” *Transport Porous Med*, vol. 67, no. 1, pp. 17–29, 2007.

[11] B. A. Abu-Hijleh, “Enhanced forced convection heal transfer from a cylinder using permeable fins,” *J Heat Transf*, vol. 125, no. 5, pp. 804–811, 2003.

[12] M. Darvishi, F. Kani, and R. Gorla, “Natural convection and radiation in a radial porous fin with variable thermal conductivity,” *Int J Appl Mech Eng*, vol. 19, no. 1, pp. 27–37, 2014.

[13] A. Aziz and M. Rahman, “Thermal performance of a functionally graded radial fin,” *Int J Thermophysics*, vol. 30, no. 5, pp. 1637–1648, 2009.

[14] L. Yu and C. Chen, “Application of the taylor transformation to the transient temperature response of an annular fin,” *J Heat Transf*, vol. 20, no. 1, pp. 78–87, 1999.

[15] L. Yu and C. Chen, “Application of taylor transformation to the thermal stresses in isotropic annular fins,” *J Therm Stress*, vol. 21, no. 8, pp. 781–809, 1998.

[16] J. Zhou, “Differential transformation and its applications for electrical circuits,” 1986.

[17] Z. Odibat, “Differential transform method for solving volterra integral equation with separable kernels,”

[18] M. Torabi and H. Yaghoobi, "Accurate solution for acceleration motion of a vertically falling spherical particle in incompressible newtonian media," *Can J of Chem Eng*, vol. 91, no. 2, pp. 376–381, 2013.

[19] H. Yaghoobi and M. Torabi, "Analytical solution for settling of non-spherical particles in incompressible newtonian media," *Powder Technol*, vol. 221, pp. 453–463, 2012.

[20] H. Yaghoobi, P. Khoshnevisrad, and A. Fereidoon, "Application of the differential transformation method to a modified van der pol oscillator," *Nonlinear Sci Letts A*, vol. 2, no. 4, pp. 171–180, 2011.

[21] B. Jang, "Solving linear and nonlinear initial value problems by the projected differential transform method," *Comput Phys Commun*, vol. 181, no. 5, pp. 848–854, 2010.

[22] H. Yalcin, A. Arikoglu, and I. Ozkol, "Free vibration analysis of circular plates by differential transformation method," *App Math Comput*, vol. 212, no. 2, pp. 377–386, 2009.

[23] A. Ravi Kanth and K. Aruna, "Solution of singular two-point boundary value problems using differential transformation method," *Phys Lett A*, vol. 372, no. 26, pp. 4671–4673, 2008.

[24] H. Hassan and I. Abdel, "Application to differential transformation method for solving systems of differential equations," *Appl Math Model*, vol. 32, no. 12, pp. 2552–2559, 2008.

[25] M. Torabi, H. Yaghoobi, A. Colantoni, P. Biondi, and K. Boubaker, "Analysis of radiative radial fin with temperature-dependent thermal conductivity using nonlinear differential transformation methods," *Chinese J Eng*, vol. 2013, 2013.

[26] P. Ndlovu and R. Moitsheki, "Application of the two-dimensional differential transform method to heat conduction problem for heat transfer in longitudinal rectangular and convex parabolic fins," *Commun Nonlinear Sci Numer Simulat*, vol. 18, no. 10, pp. 2689–2698, 2013.

[27] A. Aziz, M. Torabi, and Z. K, "Convection-radiative radial fins with convection base heating and convection-radiative tip cooling: homogenous and functionally graded materials," *ECM*, vol. 74, pp. 366–376, 2013.

[28] R. Moitsheki and B. Bradshaw-Hajek, "Symmetry analysis of a heat conduction model for heat transfer in a longitudinal rectangular fin of a heterogeneous material," *Commun Nonlinear Sci Numer Simul*, vol. 18, no. 9, pp. 2374–2387, 2013.

[29] R. Moitsheki, "Steady heat transfer through a radial fin with rectangular and hyperbolic profiles," *Nonlinear Anal Real World Appl*, vol. 12, no. 2, pp. 867–874, 2011.

[30] R. Moitsheki, "Steady one-dimensional heat flow in a longitudinal triangular and parabolic fin," *Commun Nonlinear Sci Numer Simul*, vol. 16, no. 10, pp. 3971–3980, 2011.

[31] O. Vaneeva, A. Johnpillai, R. Popovych, and C. Sophocleous, "Group analysis of nonlinear fin equations," *Appl Math Lett*, vol. 21, no. 3, pp. 248–253, 2008.

[32] R. Popovych, C. Sophocleous, and O. Vaneeva, "Exact solutions of a remarkable fin equation," *Appl Math Lett*, vol. 21, no. 3, pp. 209–214, 2008.

[33] K. Moleofane, *Classical symmetry reductions of steady nonlinear one-dimensional heat transfer models*. PhD thesis, Faculty of Science, University of the Witwatersrand, 2014.

[34] P. Ndlovu and R. Moitsheki, “Conservation laws and associated lie point symmetries admitted by the transient heat conduction problem for heat transfer in straight fins,” *Open Phys.*, vol. 11, no. 8, pp. 984–994, 2013.

[35] R. Moitsheki and C. Harley, “Steady thermal analysis of two-dimensional cylindrical pin fin with a nonconstant base temperature,” *Math. probl. eng.*, vol. 2011, 2011.

[36] R. Moitsheki and C. Harley, “Transient heat transfer in longitudinal fins of various profiles with temperature-dependent thermal conductivity and heat transfer coefficient,” *Pramana*, vol. 77, no. 3, pp. 519–532, 2011.

[37] J. Crank and P. Nicolson, “A practical method for numerical evaluation of solutions of partial differential equations of the heat-conduction type,” *Math. Proc. Camb. Philos. Soc.*, vol. 43, no. 1, pp. 50–67, 1947.

[38] R. Gorla and A. Bakier, “Thermal analysis of natural convection and radiation in porous fins,” *Int Commun Heat Mass Transfer*, no. 5, pp. 638–645, 2011.

[39] H. Janssen, B. Blocken, and J. Carmeliet, “Conservative modelling of the moisture and heat transfer in building components under atmospheric excitation,” *Int J Heat Mass*, vol. 50, no. 5, pp. 1128–1140, 2007.

[40] Z. Qin, P. Berliner, and A. Karnieli, “Numerical solution of a complete surface energy balance model for simulation of heat fluxes and surface temperature under bare soil environment,” *Appl Math Comp*, vol. 130, no. 1, pp. 171–200, 2002.

[41] M. Turkyilmazoglu, “Exact solutions to heat transfer in straight fins of varying exponential shape having temperature dependent properties,” *INT J Therm Sci*, vol. 55, pp. 69–75, 2012.

[42] N. Suryanarayana, “Transient response of straight fins,” vol. 97, no. 3, pp. 417–423, 1975.

[43] I. Rusagara and C. Harley, "A numerical well-balanced scheme for one-dimensional heat transfer in longitudinal triangular fins," *Math. probl. eng.*, vol. 2013, 2013.

[44] S. Marsili-Libelli, *Environmental Systems Analysis with MATLAB®*. CRC Press, 2018.

[45] R. Moitsheki and C. Harley, "Numerical investigation of the temperature profile in a rectangular longitudinal fin," *Nonlinear Anal-Real*, vol. 13, no. 5, pp. 2343–2351, 2012.

[46] C. Harley, "Asymptotic and dynamical analyses of heat transfer through a rectangular longitudinal fin," *J Appl Math*, 2013.

[47] R. Jooma and C. Harley, "Heat transfer in a porous radial fin: Analysis of numerically obtained solutions," *Adv Math Phys.*, vol. 2017, 2017.

[48] A. Batiha and B. Batiha, "Differential transformation method for a reliable treatment of nonlinear biochemical reaction model," *Adv Stud Bio*, vol. 3, no. 8, pp. 355–360, 2011.

[49] S. Ghasemi, P. Valipour, M. Hatami, and D. Ganji, "Heat transfer study on solid and porous convection fins with temperature-dependent heat generation using efficient analytical method," *J Cent South Univ*, vol. 21, no. 12, pp. 4592–4598, 2014.

[50] M. Fidanoglu, G. Komurgoz, and E. Ozkol, "Heat transfer analysis of fins with spine geometry using differential transformation method," *IJMERR*, vol. 5, no. 1, pp. 67–71, 2016.

[51] E. Vorob'ev, "Symmetry analysis of nonlinear differential equations with the *Mathematica* program *SYMMAN*," *Mathl Comput Modelling*, vol. 25, no. 8/9, pp. 141–152, 1997.

[52] R. Moitsheki and M. Mhlongo, "Classical lie point symmetry analysis of a nonlinear one-dimensional fin problem," *J Appl Math*, vol. 2012, 2012.

[53] S. Ali, A. Bokhari, and F. Zamaan, "A lie symmetry classification of a nonlinear fin equation in cylindrical coordinates," *Abstr Appl Anal*, vol. 2014, 2014.

[54] C. Ferreira, J. Lòpez, and N. Mainar, E adn Temme, *Asymptotic approximations of integrals: An introduction, with recent developments and applications to orthogonal polynomials*, vol. 19. Electronic Transactions on Numerical Analysis., 2005.

[55] S. Kimura and A. Okajima, "Natural convection heat transfer in an anisotropic porous cavity heated from the side: Part 1. theory," *Heat Trans Asian Res*, vol. 29, no. 5, pp. 373–3884, 2000.

[56] Z. Yang, J. Cui, Y. Sun, and J. Ge, "Multiscale computation for transient heat conduction problem with radiative boundary condition in porous materials," *Finite Elem Anal Des*, vol. 102, pp. 7–18, 2015.

[57] M. Charrier-Mojtabi, B. Elhajjar, and A. Mojtabi, "Analytical and numerical stability analysis of soret-driven convection in a horizontal porous layer," *Phys Fluid (1994-present)*, vol. 19, no. 12, 2007.

[58] T. Patel and R. Meher, "Adomian decomposition sumudu transform method for solving a solid and porous fin with temperature dependent internal heat generation," *SpringerPlus*, vol. 5, no. 1, p. 1, 2016.

[59] A. Nayfeh and B. Balachandran, *Applied Nonlinear Dynamics: analytical, computational and experimental methods*. John Wiley & Sons, 2008.

[60] J. Hedrick and A. Girard, "Control of nonlinear dynamic systems: Theory and applications," *Controllability and observability of Nonlinear Systems*, p. 48, 2005.

[61] J. Sanders, F. Verhulst, and J. Murdock, *Averaging methods in nonlinear dynamical systems*, vol. 59. Springer, 2007.

[62] E. Coddington and N. Levinson, *Theory of ordinary differential equations.* Tata McGraw-Hill Education, 1955.

[63] R. Kouhia, "On the solution of non-linear diffusion equation," *J Struct Mech*, vol. 46, no. 4, pp. 116–130, 2013.

[64] M. Habibi, M. Oloumi, H. Hosseinkhani, and S. Magidi, "Numerical investigation into highly nonlinear heat transfer equation with bremsstrahlung emission in the inertial confinement fusion plasmas," *Contrib Plasm Phys*, vol. 55, no. 9, pp. 667–684, 2015.

[65] W. Press, S. Teukolsky, W. Vetterling, and B. Flannery, "Numerical recipes in fortran (cambridge)," 1992.

[66] D. Britz, R. Baronas, E. Gaidamauskaite, and F. Ivanauskas, "Further comparisons of finite difference schemes for computational modelling of biosensors," *Nonlinear Anal Model Control*, vol. 14, pp. 419–433, 2009.

[67] D. Britz, J. Strutwolf, and O. "Ø"sterby, "Digital simulation of thermal reactions," *Appl Math Comp*, vol. 218, no. 4, pp. 1280–1290, 2011.

[68] R. Usmani, "Inversion of jacobi's tridiagonal matrix," *Computers Math Applic*, vol. 27, no. 8, pp. 59–66, 1994.

[69] W. Wang, H. Yee, B. Sjögreen, T. Magin, and C. Shu, "Construction of low dissipative high-order well-balanced filter schemes for non-equilibrium flows," *Journal of Computational Physics*, vol. 230, no. 11, pp. 4316 – 4335, 2011.

[70] A. Kraus, A. Aziz, and J. Welty, *Extended Surface Heat Transfer.* 2001.